Modelling Icing on Structures for Wind Power Applications

Pedersen, Marie Cecilie

Publication date:
2018

Document Version
Publisher's PDF, also known as Version of record

MODELLING ICING ON STRUCTURES FOR WIND POWER APPLICATIONS

BY
MARIE CECILIE PEDERSEN

DISSERTATION SUBMITTED 2018

AALBORG UNIVERSITY
DENMARK

Modelling Icing on Structures for Wind Power Applications

Ph.D. Dissertation

Marie Cecilie Pedersen

Dissertation submitted June 2018

Dissertation submitted:	June 2018
PhD supervisor:	Assoc. Prof. Henrik Sørensen Aalborg University
Assistant PhD supervisors	Assoc. Prof. Thomas Condra Aalborg University
	Benjamin Martinez, Senior R&D Eng. Vattenfall Vindkraft A/S
PhD committee:	Professor Søren Knudsen Kær (Chairman) Aalborg University
	Professor Lars Roer Sætran, NTNU
	Mark Zagar Vestas Wind Systems A/S
PhD Series:	Faculty of Engineering and Science, Aalborg University
Department:	Department of Energy Technology

ISSN (online): 2446-1636
ISBN (online): 978-87-7210-218-4

Published by:
Aalborg University Press
Langagervej 2
DK – 9220 Aalborg Ø
Phone: +45 99407140
aauf@forlag.aau.dk
forlag.aau.dk

Printed in Denmark by Rosendahls, 2018

Abstract

Wind turbines located in cold climate regions are exposed to icing during the wintertime, which can lead to several icing induced problems, such as production losses, blade fatigue and safety issues. Despite this, wind power located in cold climate regions is very attractive due to the combination of favourable weather conditions and that the sites are onshore, remote and sparsely populated. To circumvent the challenges related to icing, empirical models are used to understand and predict the severity of icing at a given site, but since wind turbine icing is a very complex phenomenon the industry needs strong reliable tools for ice prediction and production loss assessment.

Using Computational Fluid Dynamics (CFD) a 2D model to simulate icing over time has been developed. The CFD Icing Model is developed based on the demand to improve the currently used production loss assessment framework. The CFD Icing Model is developed by implementing know theory in a commercial CFD software by user defined functions and available macros. In-cloud icing conditions and rime ice accretion is the modelling target for the model and ice accretion is modelled using an impingement model and customised surface boundary conditions for the object exposed to icing. The shape of the object exposed to icing is changes according to the calculated mass of ice every timestep.

Ice accretion is a dynamic process, controlled by the atmospheric conditions given to the model as the inlet boundary conditions. Thus, for modelling icing over time and for validation purposes, on-site measurements are used to compile a dataset consisting of inlet boundary conditions and validation data, obtained using image analysis. The results of modelling icing over time using the CFD Icing Model, corresponds very well to the results of the maximum ice thickness obtained from image analysis. The study presents a unique methodology for modelling icing over time using the CFD Icing Model developed and on-site data, which are most often available to the wind turbine owner and/or operator.

Resumé

Vindmøller placeret i koldt klima er ofte udsat for isdannelse om vinteren, som kan medføre flere problemer, så som tab af produktion, materialeudmattelse og problemer i forbindelse med sikkerhed. Til trods for dette er vindenergi i koldt klima meget attraktivt, hvilket skyldes kombinationen af gunstige vejrforhold, at placeringen er på land, samt øde, og oftest meget sparsomt befolket. I forsøget på at håndtere udfordringerne, benyttes empiriske modeller til at forstå og forudsige problemets omfang. Men da isdannelse er et meget komplekst fænomen har vindmølleindustrien brug for stærke og pålidelige værktøjer til at forudsige isdannelsen og til at vurdere produktionstabene på et givent sted.

En 2D model til at simulere isopbygning over tid er blevet udviklet ved hjælp af "Computational Fluid Dynamics" (CFD). Den såkalde "CFD Icing Model" er udviklet ud fra ønsket om at forbedre den eksisterende ramme, som, på nuværende tidspunkt, benyttes til at vurdere produktionstab i forbindelse med isdannelse. Modellen er udviklet ved at implementere allerede kendt teori i et kommercielt software ved hjælp af bruger-specificerede-funktioner og tilgængelige makroer. Modellering af "in-cloud icing" og opbygningen af rim-is er målet for modellen, og dette udføres ved hjælp af en kollisionsmodel og specialdesignede overflade randbetingelser for objektet der er udsat for isopbygning. Formen på objektet ændres i overensstemmelse med den beregnede masse af is, som ligeledes beregnes hvert tidsskridt.

Opbygning af is er en dynamisk process, som kontrolleres af de atmosfæriske forhold. Sådanne data gives til modellen, som inløbsrandbetingelser. I dette studie benyttes målinger til at samle et komplet dataset til simulering af isdannelse, hvilket består af inløbsrandbetingelser samt data til valideringsformål. Valideringsdata er fremskaffet ved at analysere billeder fra lokationen. De modellerede resultater stemmer rigitg godt overens med valideringsdataene fra billedanalysen. Dette studie præsenterer en unik metode, som benyttes til at simulere isens opbyging over tid ved hjælp af den udviklede "CFD Icing Model" og målinger fra koldt klima, som oftest vil være tilgængelige for vindmølleindehaveren eller operatøren.

Preface

This dissertation is submitted to the Doctoral School of Engineering and Science in Aalborg University in partial fulfillment of the requirements for the Danish Ph.D. degree. It covers research work in the Institute of Energy Technology in Aalborg University from the period January 2014 to September 2017, including a three-month research stay at the research center of TechnoCentre éolien, Gaspé, Québec, Canada. The objectives of the project were industry-oriented, and thus insights from both the industry and academia were included in the work. The work was co-funded by Vattenfall Vindkraft A/S and the Innovation Fund Denmark as part of the Danish Industrial PhD program (no.1355-00120B).

Dissertation Structure

The topic of the dissertation is wind turbine icing and modelling of icing for wind power applications. Because of the nature of the topic, the dissertation presents a *multidisciplinary* study, which involves many branches of engineering. The purpose of the work was to develop an icing model based on computational fluid dynamics. The model is to be used in the future for, amongst other things, site assessments and supplementing methods currently in use. The project is motivated through the experience of the utility company, Vattenfall, with icing issues from cold climate sites in Sweden.

The dissertation consists of two parts; Part I, which is a summary of the topic and the work carried out and Part II, which contains the papers published as a part of the dissertation. Part I introduces the subject of wind turbine icing and modelling icing over time using computational fluid dynamics and on-site measurements. The modelling methodology is outlined, and the results and future work are discussed. In Part II the papers are reprinted in full to facilitate the reader. A summary of each Paper is found in Section 1.8. Paper A, Paper B and Paper C were published by Elsevier and general permission to reprint the articles in the dissertation is explicitly given by Elsevier. Per-

mission for reprint of Paper D was given by the AIAA (American Inst of Aeronautics and Astronautics) copyright clearance center, for Paper E it was given by WinRen, SE by email correspondence and likewise by email correspondence for Paper F. The papers are listed under the Dissertation Details on page ix.

Acknowledgement

I gratefully acknowledge Vattenfall Vindkraft A/S and the Innovation Fund Denmark for their financial support. A special gratitude is owed to Vattenfall R&D and the Turbine Icing Program. I would like to thank Lars Olesen and Jens Ingeman Madsen for your support, guidance and the technical discussions. I would like to thank Benjamin Martinez for his expertise and supervision within the field of wind turbine icing and for the trips to cold climate sites. I would also like to thank Anders Bech Borchersen for being my very best room-mate, colleague and Python expert. At Aalborg University I would like to thank my supervisors Henrik Sørensen and Thomas Condra. I am very thankful for your positive mindset and excellent expertise. Henrik Sørensen for your great ideas, constructive feedback during model development and in general for the time spent on my work. Thanks to Thomas Condra for your great support, your excellent feedback on my written work and for all the great stories. I would also like to thank my colleagues Anna Lyhne Jensen, Jakob Hærvig and Anders Schou Simonsen at Aalborg University for laughing of most of my jokes in the office, for discussion academic topics and for all the post cards and great times. During the winter of 2015/2016 I had the pleasure of being a guest researcher at the TechnoCentre éolien, Gaspé, Québec, Canada. During the stay abroad, I was able to visit cold climate sites at the Gaspé Peninsula and get in touch with state-of-the-art experimental set-up for ice detection and site validation. I would like specially to thank Matthew Wadham-Gagnon, Nigel Swytink-Binnema for good collaboration and the great experience of visiting Gaspé. And a very special thanks to the lovely Darlene Eden for your great hospitality your kindness and a lot of great moments in your warm living room.

Finally, I would like to thank my family and Peter for your endless support and love and our daughter Solveig for being born during the project period.

Marie Cecilie Pedersen
Aalborg University, June 25, 2018

Dissertation Details

Dissertation Title:	Modelling Icing on Structures for Wind Power Applications
Ph.D. Student:	Marie Cecilie Pedersen
Supervisors:	Assoc. Prof. Henrik Sørensen, Aalborg University Assoc. Prof. Thomas Condra, Aalborg University Senior R&D Engineer, Benjamin Martinez, Vattenfall Vindkraft A/S

The dissertation is based on a collection of papers, three journal publications and three conference publications. The journal publications are:

[A] Marie Cecilie Pedersen, Henrik Sørensen, Nigel Swytink-Binnema, Benjamin Martinez and Thomas Condra "Measurements from Cold Climate Site in Canada: Boundary Conditions and Verification Methods for CFD Icing Models for Wind Turbines", Cold Regions Science and Technology, vol. 147, pp. 11-21, March 2018. https://doi.org/10.1016/j.coldregions. 2017.12.007.

[B] Marie Cecilie Pedersen, Henrik Sørensen, Nigel Swytink-Binnema and Thomas Condra "Computational Fluid Dynamics Analysis and Field Measurements on Ice Accretion on a Cup Anemometer Support Arm", Applied Thermal Engineering, vol. 135, pp. 530–536, May 2018. https://doi.org/10.1016/j.applthermaleng.2018.01.086.

[C] Marie Cecilie Pedersen and Chungen Yin "Preliminary Modelling Study of Ice Accretion on Wind Turbines", Energy Procedia, vol. 61, pp. 258-261, 2014. https://doi.org/10.1016/j.egypro.2014.11.1102.

The main body of the dissertation is based on journal Paper A and journal Paper B. The conference publications completed during the PhD period are:

[D] Marie Cecilie Pedersen, Benjamin Martinez and Chungen Yin, "Development of CFD-based Icing Model for Wind Turbines: A Case Study of Ice Sensor", Presented at the 33rd Wind Energy Symposium, AIAA SciTech Forum 2015, American Inst of Aeronautics & Astronautics, January 5-9, 2015, Kissimmee, Florida, USA. https://doi.org/10.2514/6.2015-1472.

[E] Marie Cecilie Pedersen, Henrik Sørensen, Benjamin Martinez and Thomas Condra, "Case Study of an Ice Sensor using Computational Fluid Dynamics, Measurements and Pictures - Boundary displacement", Presented at International Workshop on Atmospheric Icing on Structures, June 28-July 3, 2015, Uppsala, Sweden.

[F] Marie Cecilie Pedersen and Henrik Sørensen, "Towards a CFD Model for Prediction of Wind Turbine Power Losses due to Icing in Cold Climate", Presented at the International Symposium on Transport Phenomena and Dynamics of Rotating Machinery, April 9-15, 2016, Honolulu, Hawaii's O'ahu, USA.

Additionally, the following publications were co-authored during the PhD period.

[1] Jakob Hærvig, Anna Lyhne Jensen, Marie Cecilie Pedersen and Henrik Sørensen "General Observations of the Time-Dependent Flow Field Around Flat Plates in Free Fall," *ASME-JSME-KSME Joint Fluids Engineering Conference*, July 26-31, 2015, Seoul, Korea.
https://doi:10.1115/ AJKFluids2015-12708.

[2] Jakob Hærvig, Anna Lyhne Jensen, Marie Cecilie Pedersen and Henrik Sørensen "Numerical and Experimental Study of the Rotational Behaviour of Flat Plates Falling Freely with Periodic Oscillating Motion", *ASME 2017 Fluids Engineering Division Summer Meeting*, July 30-August 3, 2017, Hawaii's Big Island, USA.
https://doi:10.1115/FEDSM2017-69503.

Contents

Terminology

Abbreviations	Description
ALE	Arbitrary Eulerian Lagrangian
BEM	Blade Element Method
CC	Cold Climate
CFD	Computational Fluid Dynamics
H&S	Health & Safety
IEA	International Energy Agency
IC	Icing Climate
LTC	Low Temperature Climate
NWP	Numerical Weather Prediction
ROI	Region Of Interest
UDF	User Defined Function
URANS	Unsteady Reynolds-Averaged Navier Stokes
WRF	Weather Research and Forecasting

Icing Terms:	Description
Anti-icing:	Prevention of ice accretion on a surface
De-icing:	Removal of ice after it has accreted
Freezing rain/drizzle:	Precipitation formed by the melting of snow crystals by warm air, which afterwards passes a freezing layer of air near the ground
Glaze ice:	Transparent ice, with a high density
Hoar frost:	Icing/deposit of water vapor on structures
Ice accretion:	The build up of ice on an object
Ice ablation:	The removal of ice by ablation process: sublimation, melting and ice shedding
Ice intensity:	Icing rate, deposit of ice per time

Ice severity:	Ice load, *i.e.* amount of accreted ice mass per meter
In-cloud icing:	Icing by super-cooled water droplets in a cloud or fog
Intrumental icing:	Time periods with ice on instruments
Meteorological icing:	Time period with ice growth
Rime ice:	White ice, with a low density
Operational limits of standard wind turbine:	$-10°$C in operation and $-20°$C before shutdown

Latin Variables	Description	Units
$\mathbf{A}$	Face area vector	m^2
CBH	Cloud base height	m
cn	Calibration number	-
d	Diameter	m
e	Edge	m
H	Enthalpy	J/kg
h	Cell height	m
L	Ice thickness	m
MVD	Median Volumetric Diameter	μm
$\dot{m}$	Mass flux	kg/m^2s
m	Mass	kg/m
N_c	Droplet concentration	cm^{-3}
p	Power	kW
P	Presssure	Pa
RH	Relative Humidity	%
S	Source term	
T	Temperature	$°$C
u, v	Velocity	m/s
$\boldsymbol{u}, \boldsymbol{v}$	Velocity vector	m/s
V	Volume	m^3
W	Cloud liquid water content	kg/m^3
z	Reference height	m

Greek Variables	Description	Units
α	Volume fraction	-
β	Collection efficiency	-
δ	Adiabatic cloud water gradient	-
ϕ	Source variable	-
Γ	Diffusion coefficient	-
τ	Response time	s
ρ	Density	kg/m^3
θ	Wet bulb temperature	$^{\circ}C$

Subscripts	Description
C	continuity
c	continious phase
d	droplet
dew	dew point
E	energy
g	moving mesh
i	i^{th} entry
L	left
M	momentum
p	dispersed
q	secondary phase
R	right
v	vapour
vs	saturated vapour
w	wet bulb
x	x-direction
y	y-direction
z	z-direction

Part I

Summary

Chapter 1

Introduction to Wind Turbines in Cold Climates

This chapter motivates the topic of wind turbine icing. The chapter goes through the development of wind power in cold climates and its challenges. The phenomenon of atmospheric icing on structures, such as wind turbines and measurement equipment is introduced. The production loss assessment framework currently used, is presented to clarify the need for the research presented in the dissertation. Finally, the potential of implementing the research is sketched followed by a brief outline of the modelling approach chosen.

1.1 Motivation

Wind power in cold climates is a growing business, which has evolved to become a natural part of the modern world of wind energy. This is primarily due to the attractive weather conditions that cold climate sites have to offer. The sites are dominated by a favorable combination of high wind speeds and high air densities, because of the low air temperatures. Besides the weather conditions, the expansion of wind power into cold climate areas has been motivated, especially in Europe, by the fact, that the easier accessible sites are already occupied [1]. Additionally, an advantage of expanding wind power to remote cold climate sites is the elimination of issues and regulations related to the proximity of human neighbours, industry or roads. However, operating wind turbines in cold climates is not unproblematic and the wind farms are challenged by several issues related to icing primarily during the wintertime. In general, as presented below, the icing issues can be divided into three main categories:

1. Production losses: Ice can be accreted on the wind turbine blade during operation, which will degrade the aerodynamic performance of the wind turbine or, worst-case, lead to periods of standstill.

2. Blade fatigue: Ice on the blade induces an additional load, which can lead to blade fatigue. The additional load can also lead to additional maintenance costs and mechanical failures of the turbine [2], [3].

3. Safety issues: Safety issue are related to ice being thrown off the wind turbine blade during operation or stand-still. The phenomenon is in general referred to as ice shedding and it can give rise to serious risks for passers-by, service personal and nearby buildings. A straightforward approach to gather information about the severity of ice shedding on a site is by inspection and collecting ice fragments [4]. Ice throw models also exists such as, for example, that presented by Biswas et al. [5]. It was shown, that an ice-fragment of 1 kg will travel up to 200 meters and if the fragment is rather flat, the lift force will increase the distance up to 350 meters. Another ice throw model was presented by Bredesen et al.(2015) [6], who used numerical weather prediction (NWP) models and collected pieces of ice to develop a statistical model, applicable for wind turbines and other tall structures. From the statistical results, risk zones and safety zones could be identified. In some parts of northern Sweden, Norway and Finland the indigenous people might pass by the wind turbines with herds of reindeers and so ice shedding can be a great risk for both people and animals, if they are not warned. Some wind farm owners, for example Vattenfall, have put in-place a texting-system, which helps reduce the risks for the indigenous people [7].

The severity of each topic at a site depends on the local weather conditions, but the loss of production is typically the dominating problem, with the largest economic impact. Unfortunately, the present knowledge, of the wind power community, is insufficient to solve the icing issues, which still challenges the advancement of wind power in cold climate.

1.1.1 The Expansion of Wind Power in Cold Climates

Despite the challenges faced by wind turbine owner and operators in cold climates, the installed capacity has been growing over the past 20 years. In 2002 the IEA (International Energy Agency) Wind program established the IEA Task 19, which is a task group dedicated to gather information and provide recommendations for the development of wind energy in cold climates. At that point in time the installed capacity was around 0.5 GW [8], see Figure 1.1. Ten years later, in 2013, the first BTM world market update was published [9], which showed an installed capacity of around 70 GW in 2012. The

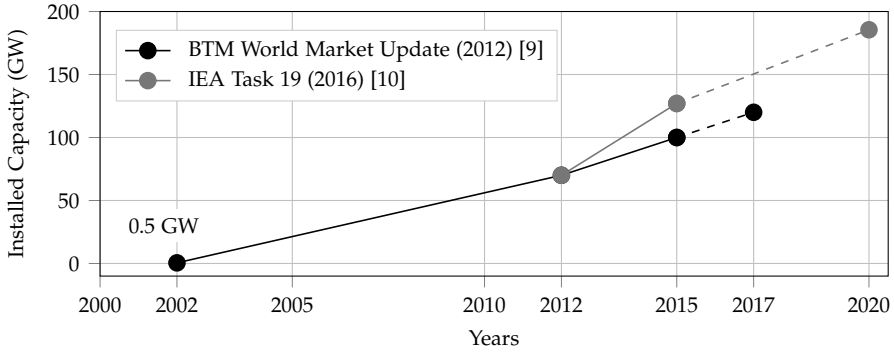

Figure 1.1: Cumulation of installed capacity of wind power in cold climate in GW. In 2002 the installed capacity was around 0.5 GW. In 2012 an installed capacity of 70 GW was found, and the dotted black line shows forecast by BTM World Market Update for 2015 and towards 2017 [9]. The IEA Task 19 showed an installed capacity of 127 GW by 2015 and the dotted grey line shows the forecast towards 2020 of 185.5 GW [11].

report said, that 100 GW would be installed in cold climate sites by 2015 and that by 2017 a further 20 GW would also be installed [9], see Figure 1.1. Three years after the published BTM world market update, the IEA Task 19 studied the installed capacity and published a new market update on the installed capacity in cold climates [11]. The study was based on the BTM World Market Update value for 2012 (70 GW) and a global cold climate map, where wind turbine sites were categorised according to the IEA ice class standards. The classification was developed by the IEA Task 19 to help developers identify the icing severity and the potential icing issues at a site [12]. An example of an icing map can be seen in Paper A, Figure A.2 where the ice class(1-5) and the corresponding percentage loss of the annual energy production (AEP) is seen. In this way, all global on-shore sites could be identified and classified, and the total installed capacity could be determined. The new market update by the IEA Task 19 showed a cumulative installed capacity of 127 GW by the end of 2015 and a forecast for the end of 2020 of 185.5 GW. The installed capacity for 2015 turned out to be 27 GW higher than first predicted by the BTM world market update [9], and what is interesting is, that it corresponds to approximately 30% of the total global installed wind power capacity. In addition, a growth rate per year of 11.7 GW was forecast [11]. For comparison this is around three times the annual rate of off-shore wind power and it leaves wind power in cold climates as one of the largest "non-standard" wind energy markets [10].

As exhibited implicitly by the numbers, wind power in cold climates is an important part of the modern energy marked and it will continue to be so. Already after the first market update, research related to wind turbine

icing has experienced a significant growth. Dedicated conference and seminars such as, amongst others, the annual Winterwind conference [13], the annual seminar "Optimizing Wind Power in Cold Climates" by WindPower Monthly's [14] have arisen to disseminate knowledge of the newest research. Also, task forces compounded from a mixture of experts from academia and the industry, such as the COST Action 727 working group [15], IEA Task 19 [8] and others, were established to help the development of wind power in cold climate regions.

1.1.2 Icing Issues at Swedish Wind Farm

The icing issues experienced at Stor-Rotliden wind farm operated by Vattenfall and Vattenfall's wish to expand wind power in cold climate regions in Sweden, have been the driving force that initiated this project. Stor-Rotliden wind farm consists of 40 Vestas V90 2.0 MW turbines and is located at a severe icing site in the province of Västerbotten in northern Sweden - see the location in Figure 1.2. During the wintertime, winds from the east bring wet cold air in over the land from the Baltic sea, that creates the perfect conditions for ice growth. An example of a wind turbine blade exposed to icing conditions in Stor-Rotliden wind farm is seen in Figure 1.3.

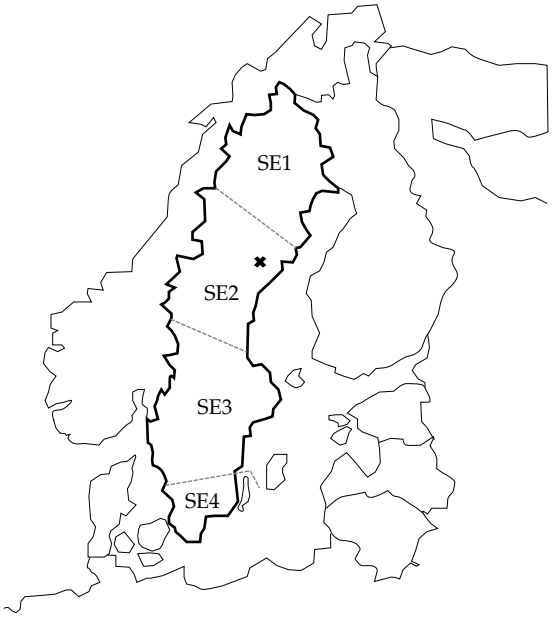

Figure 1.2: Location of Stor-Rotliden wind farm in Middle Norrland in Sweden. The location is marked by the **x**. The areas named SE1, SE2, SE3 and SE4 indicate the power flow sectors in Sweden [16].

Figure 1.3: The pictures are taken from the hub and looking towards the tip of the blade. Left, the blade is heavily covered by ice and forced in standstill until the conditions change and the ice can melt. Right, the blade is covered by a layer of rime ice and is still in operation. The pictures from Stor-Rotliden wind farm were kindly provided by Vattenfall's Turbine Icing Program [7].

To the left in Figure 1.3, extreme conditions are seen, where the blade is completely covered by a thick layer of ice and not rotating. To the right in Figure 1.3, less severe conditions are seen, where the blade is covered by a thinner layer of ice but still rotating. At this wind farm, the annual power losses due to icing of around is estimated to be around 8 % - 9 % of the total annual production, since the farm was put into operation in 2011 [7]. The expected losses were based on a set of data measured at the site in the winter of 2009-2010, but the losses experienced when the wind farm came into operation in 2011 far exceeded the expected values. In the dynamic European energy market, with low energy prices, losses of this magnitude have a tremendous influence on the competitive performance of wind power in cold climates. The spot-prices for electricity from 2013-2015 from the area (SE2), where the wind farm is located, are shown in Figure 1.4. For wind power in cold climates to be attractive, it is essential to have a sustainable and reliable business case in the extremely competitive market.

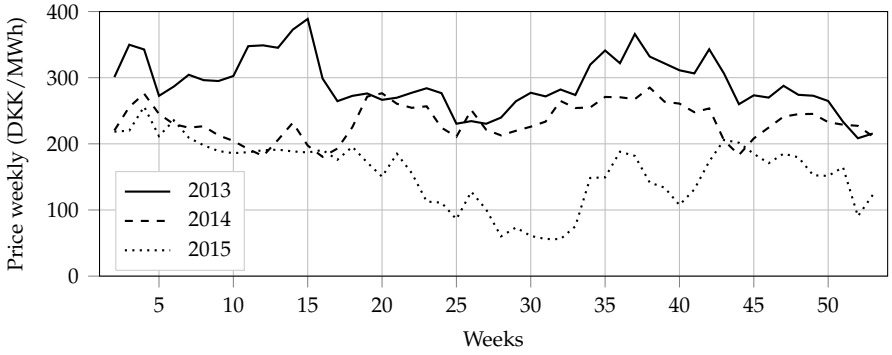

Figure 1.4: The spot-prices for electricity per week from 2013-2015 in Sweden for the power flow sector SE2, where the wind farm is located [17].

To understand the losses experienced at the wind farm, production data from the winters of 2011, 2012 and 2013 were analysed - see Figure 1.5 and 1.6. The actual power produced from the reference turbine was analysed to identify power losses due to icing in kW. The power losses were found as the difference between the maximum possible power obtainable and the actual power produced, see Figure 1.5. The maximum obtainable power was based on the measured wind speed. Figure 1.5 shows, that the actual power produced lies

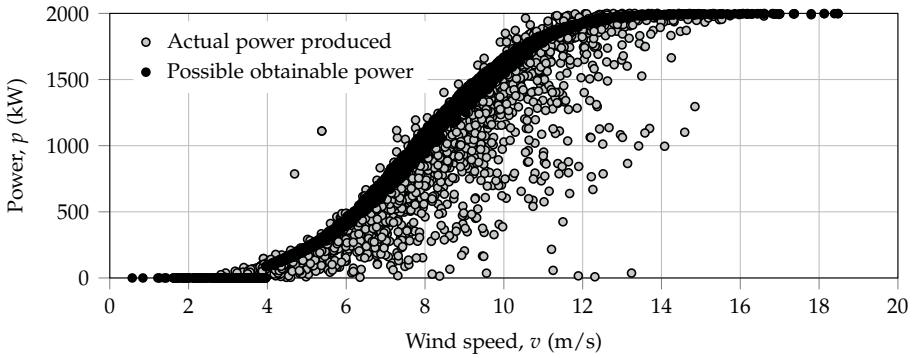

Figure 1.5: Production data from the winters of 2010-2011 and 2011-2012 (October - March) from reference turbine at Swedish wind farm. The possible production is compared to the actual production, which provides a visual overview of the loss of production in kW. The difference of the possible power and the actual power gives the loss of production. Every 24 hours consists of 135 samplings. The data was kindly provided by Vattenfall's Turbine Icing Program [7].

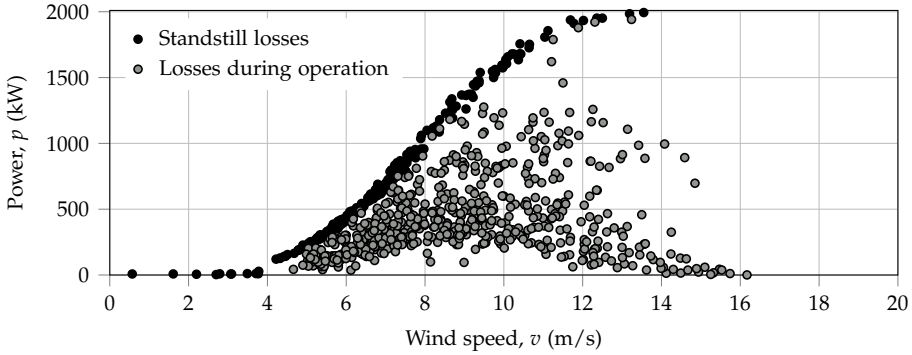

Figure 1.6: Classification of the loss of production into standstill losses and operational losses, based on data from the winters of 2010-2011 and 2011-2012 (October - March) from reference turbine at Swedish wind farm. Every 24 hours consists of 135 samplings. The data was kindly provided by Vattenfall's Turbine Icing Program [7].

scattered below the possible power. Figure 1.6 shows the total losses, which are divided into standstill losses and operational losses. During standstill, the ice load on the blades is so high, that the wind turbine is forced to stop

operating. Thus, during standstill the losses are equal to the possible production and the profit is, at best, zero. Operational losses occur when, the wind turbine keeps operating but the aerodynamic performance is reduced due to ice loading. It was calculated as the difference between the possible power and the actual power. Figure 1.3 to the left corresponds to a standstill situation and Figure 1.3 to the right corresponds to a case of operational losses.

Because of the challenges experienced at Stor-Rotliden wind farm, Vattenfall installed 9 Siemens 3.2 MW wind turbines with de-icing systems at the wind farm in Juktan, Sweden. The profitability of operating the wind turbines with de-icing systems is still being tested [7]. Under development for the upcoming year is a major investment in two large wind farms with a total installed capacity of 353 MW corresponding to 1.1 TWh per year. The capacity will be shared amongst the two wind farms, one located at Fåbodberget about 20 km from Stor-Rotliden wind farm and the other located at Blakliden further north in Sweden, in the province of Västerbotten [18]. To ensure a sustainable expansion and development of wind power in cold climate regions, reliable predictions of the production and the production losses due to icing is extremely important. Such predictions can be based upon experience from already existing wind farms, such as Stor-Rotliden and Juktan, forecasting models or a combination of the two. Nevertheless, it is fundamental to get a good understanding of the atmospheric conditions at the wind farms, which are causing the icing issues; production losses, blade fatigue and safety issues. The phenomenon of atmospheric icing is the cause of all icing issues experienced by wind turbines and is the dominating reason for production losses due to icing for wind power in cold climate regions. The following section introduces the topic of atmospheric icing and ice detection.

1.2 Wind Power Sites in Cold Climate

In the wind power business, and as defined by the IEA Task 19 [12], the term Cold Climate (CC) refers to sites, which experience severe periods of icing events and/or temperatures below the operation limits of a standard wind turbine [19]. Areas with temperatures below the operation limits are defined as a Low Temperature Climate (LTC) and areas with icing events and atmospheric icing are defined as an Icing Climate (IC) [12]. Some sites might only belong to one category, whilst others are a combination of the two, as illustrated in Figure 1.7. Common for the sites is the presence of atmospheric icing during the wintertime. Cold Climate sites are primarily found in the northern regions of Europe, such as Sweden, Norway, Finland and Germany, in the mountainous regions of Europe, such as Switzerland and in Canada [4, 19, 20].

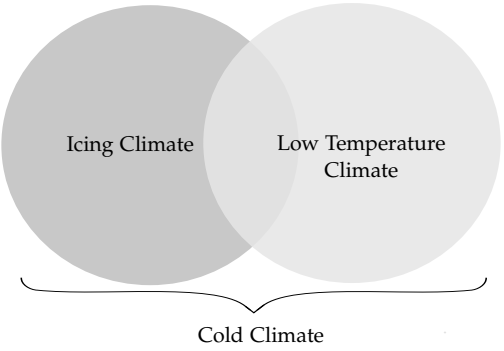

Figure 1.7: Cold Climate is a term describing the weather conditions at a site and can be divided into two categories; Low Temperature Climate (LTC) and Icing Climate (IC). LTC is defined as areas having more than 9 days per year with an air temperature below -20 °C and an average annual temperature below 0 °C. IC is defined by the number of icing events and by having Instrumental Icing more than 1 % of the year and meteorological icing more than 0.5 % of the year [12]. See Section 1.2.2 for the definition of instrumental icing and meteorological icing.

1.2.1 Atmospheric Icing

According to the ISO Standard 12494:2001 [21], atmospheric icing can be defined as any process of ice buildup and snow accretion on the surface of an object exposed to the atmosphere. It covers all processes in the atmosphere where drifting or falling water droplets, rain, drizzle or wet snow will stick or freeze to an object. Atmospheric icing is normally divided into two processes, which are defined by the meteorological conditions. Table 1.1 provides an overview of the processes, the types of accreted ice and the conditions of the air and droplets. In continuation hereof, Table 1.2 provides more details on the accreted icing types. Since in-cloud icing is the dominating process for wind turbine icing in Sweden most emphasis is put on this topic. As mentioned, wet and cold air is blown from the Baltic sea in over land, to where the wind farm is located. The wind turbines get shrouded in the clouds or the heavy fog, which means, that they are operating under the so-called; in-cloud conditions. Depending on the cloud depth and elevation above ground level, some turbines might be more shrouded than others and thereby more exposed to ice accretion. Ice accretion starts as soon as the mixture of air and droplets hit the surface of the wind turbine blade.

Figure 1.8 provides an estimate of the relationship between temperature and wind speed for in-cloud icing conditions. It is seen, from the Figure, that rime ice is the dominating ice type for in-cloud icing. In comparison with Table 1.1, Figure 1.8 implicitly provides information about droplet size and the cloud liquid water content. However, a high liquid water content will shift the curves to the left and extending the regions of glaze ice. From Table 1.1,

Meteorological conditions for atmospheric icing

Process	Definition	Icing Types	Cloud liquid water	Droplet
Precipitation icing	Ice accretion by freezing rain, drizzle and wet-snow, typical temperature range; $\{T \mid -10°C \leq T \leq +3°C\}$	- Glaze - Wet snow	medium very high	large flakes
In-cloud icing	Ice accretion, by a cloud/fog containing super-cooled droplets, which meet an object and freeze upon contact, typical temperature range; $\{T \mid -20°C \leq T < 0°C\}$	- Glaze - Hard rime - Soft rime	high medium low	medium medium small

Table 1.1: Overview of the meteorological conditions, controlling atmospheric icing [21]. Typical values for in-cloud icing, varies from 5 µm - 50 µm for the droplet size and varies from 0.05 kg/m^3 - 0.5 kg/m^3 for the cloud water content. As the temperature approached -20°C and below the cloud liquid water most often goes towards zero, resulting in no ice accretion. Having such periods after a period of ice growth, can leave the wind turbine or structure iced-up for many hours or even days.

Properties of accreted atmospheric icing

	Soft rime	Hard rime	Glaze	Wet Snow
Density	200-600 kg/m^3	600-900 kg/m^3	300-600 kg/m^3	900 kg/m^3
Color	white	opaque	transparent	white
Shape	cone/elliptic	cone, elliptic	smooth, ice-horns or icicles	smooth, eccentric

Table 1.2: Properties of ice accreted because of atmospheric icing [21]. For wind turbine icing, it is interesting to differentiate the ice type by density, appearance and shape.

Table 1.2 and Figure 1.8 it is important to notice, that it is the temperature (T), the cloud liquid water content (W), the wind speed (v) and the droplet size, which are the dominating and all-important parameters for atmospheric icing.

The process of ice accretion on an object exposed to in-cloud icing conditions is illustrated in Figure 1.9. The process of rime ice accretion is shown to the left and this process is characterised by being both cold and dry and is often referred to as dry ice accretion. To the right, the process of glaze ice accretion is shown. This wet condition is characterised as being less cold and is often referred to as wet ice accretion. Under dry ice accretion (Figure 1.9 left) the droplets freeze instantaneously, which typically results in an elliptic/cone shape around the impact area and, as is illustrated, the shape tends

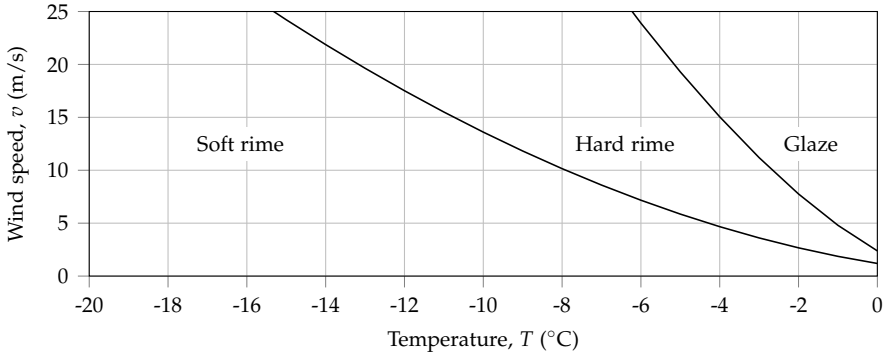

Figure 1.8: The relationship between wind speed, air temperature and the ice type for in-cloud icing [21].

to approximate a triangular form for small objects. During wet ice accretion (Figure 1.9 right) only parts of the droplet will freeze by impact and the remaining part of the droplet will create a liquid water film at the surface of the object. Because of wind and gravity, the liquid water will move and freeze further downstream, away from the impact area. Sometimes the water can run all the way to the shadow side of the object. The conditions result in an even and smooth shape, but it can also, under special conditions, result in ice icicles or ice horns. The development of severe ice horns is typically seen

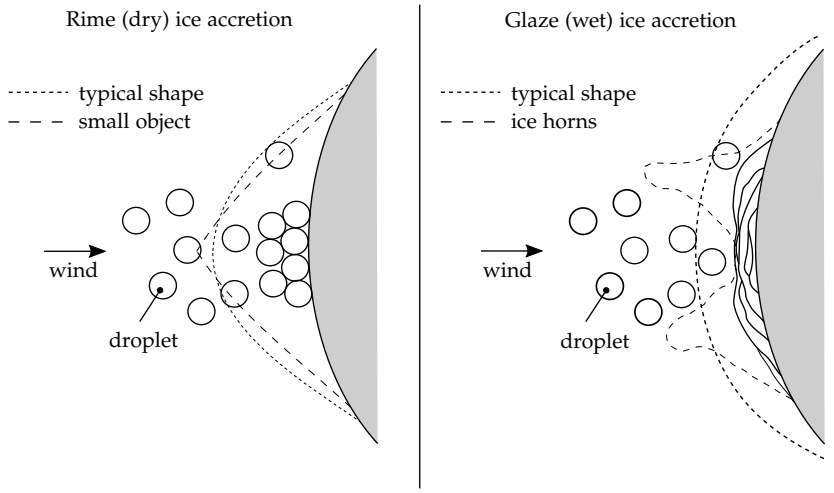

Figure 1.9: The process of ice accretion during in-cloud icing. Rime ice accretion is shown to the left and glaze ice accretion to the right. Left; the dotted line illustrates the typical cone shape of rime ice accretion and the expected triangular shape for small objects. Right, the dotted lines illustrate the typical smooth shape of glaze ice accretion and the growth of ice horns.

with aircraft icing, in climatic wind tunnel experiments [22] or from modelled results [23]. These ice horns are less likely to develop on a rotating wind turbine.

1.2.2 Ice Detection

The way to identify atmospheric icing at a site is by ice detection. When operating wind turbines in cold climate areas it is crucial to be able to detect when the ice is accreting on the turbine blade and for how long it will stay on the blade. Wind turbines, with de-icing systems equipment, also rely on good ice detection, especially if the turbine is to be stopped while de-icing occurs. Detecting the ice too late or too early can add additional costs and in the worst case it can eliminate the benefit of the system. In the field of wind turbine icing, ice detection is the way to measure the phases of icing. It starts from the establishment of the meteorological conditions to the process of ice accretion followed by a period when ice is present on the blade or structure and when it starts ablating. The combination of phases is referred to as an *icing event*. Since ice detection is still rather immature and often not always reliable [24], different instruments and methods are often combined to obtain the best possible picture of an icing event. Figure 1.10, shows pictures from a meteorological mast (met mast) located at the location called Granliden, which is approximately 20 km from the Stor-Rotliden wind farm (Figure 1.2). The instruments are placed at an elevation of approximately 100 m, and consists of the instruments described in Table 1.3. The pictures provide a clear indication of the severity of icing at the site.

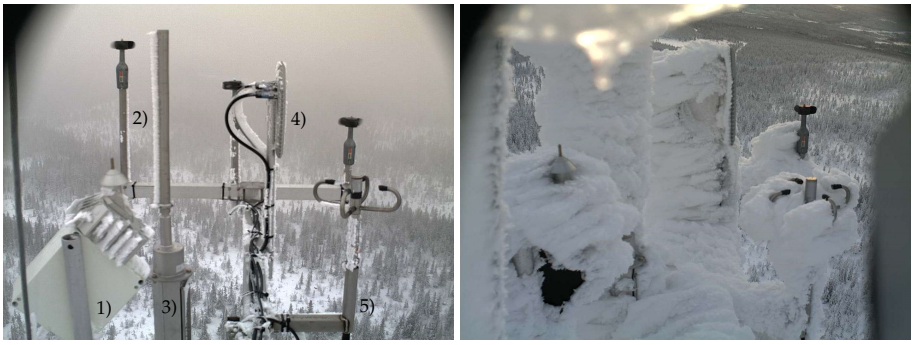

Figure 1.10: Pictures from a met mast located at Granliden, Sweden. To the left, light icing conditions are shown and to the right, heavy icing conditions are seen. Instruments seen on the pictures are: 1) Goodrich 0872F1 ice detection system, 2) 3NRG ice detection system, 3) SAAB Combitech IceMonitor, 4) LID-3300IP ice detector and 5) HoloOptics T44. The pictures were kindly provided by Vattenfall's Turbine Icing Program [7].

Wickman (2013) [24] analysed data from six wind turbines at Stor-Rotliden

Instruments seen in Figure 1.10.

No.	Name	Functionality
1)	Goodrich 0872F1	Metrological icing is measured by a vibrating probe with a heating system. When ice accretes on the probe its natural frequency is changed, which is transformed to an ice thickness on the surface [25]
2)	3NRG	Three sensor are combined for ice detection [24]
3)	SAAB Combitech, IceMonitor	Ice load is measured on a freely rotating cylinder, following the ISO 12494:2001 standard [21]. The cylinder is lifted by a spring, which is kept ice free, by a heating system [26]
4)	LID-3300IP, Labkotec	Meteorological icing is measured by a vibrating wire with a heating system. A ultrasonic signal is weakend when ice accumulates on it [27]
5)	HoloOptics T44	Uses IR to measure icing rates of all types of atmospheric ice on a vertical cylinder probe [28]

Table 1.3: Description of the instruments installed at the met mast at Grandliden, Sweden, seen in Figure 1.10.

wind farm, and from three met masts at the locations of Granliden, Blakliden and Fåbodberget in the province of Västerbotten Sweden, to identify trigger levels, limitations, reliability and accuracy of the instruments. The study revealed a poor performance of most instruments during icing conditions and a low accuracy especially during severe icing conditions. Camera photos and ice detector outputs were shown to be of great value and during light icing conditions, the combination of different ice detectors helped provide a more reliable picture of the icing event. Wickman (2013) [24] concluded that the instruments could not quantify the icing processes reliably nor indicate the production losses experienced. Another study analysing data from met masts, was presented two years later by Wadham-Gagnon et. al (2015) [29]. The study compared 9 different ice detection methods, to analyse three icing events during a measurement campaign from the Site Nordique Expérimental en Éolien Corus (SNEEC), Riviére-au-Renard, Quebec, Canada (see more about the experimental setup in Paper A). From the ice detection methods, it was possible to detect the number of hours of both meteorological and instrumental icing. These two parameters are important factors for the utility to classify a site, as mentioned in Section 1.1. In 2006, the COST Action 727 working group called "Measurements and data collection on icing" [15], defined the period of icing on structures, and later for wind turbines [12] as follows:

- Meteorological Icing: The period where ice accretion happens because of the meteorological conditions. It covers the time from the presence

of the meteorological conditions until accretions begins.

- Instrumental Icing: The period where ice is present and visible on the structure/instrument. It covers, the persistence of ice after ice accretion and until the ice starts ablating. Ice might be removed during the persistence period by erosion, sublimation or ice shedding.

The possibility of detecting instrumental icing and meteorological icing directly is one of the pressing needs from the industry, but it is, however, still not possible [10]. It was concluded from Section 1.2.1, that the ice specific parameters, such as the cloud liquid water content (W) and the droplet size and droplet distribution are the very important parameters for atmospheric icing. Unfortunately, they are also still a challenge to measure, because of a rather immature technology [2, 10, 29]. Currently this is a problem because, amongst others ice models strongly rely on those inputs. It also makes it difficult to evaluate the modelled values of the cloud liquid water content and the droplet size generated from Numerical Weather Prediction Models (NWP), which are widely used and accepted within the industry. Section A.2.1 in Paper A discusses the difficulties of modelling icing, when there are uncertainties related to the boundary conditions, *i.e* the icing specific atmospheric variables.

As stated in Section 1.1.2 this work was motivated by the need for reliable predictions of the expected production at a cold climate site. The following Section presents the production loss assessment framework currently used and how this work can be a part of improving the approach to obtain more reliable predictions for wind farms located at cold climate sites.

1.3 Site Assessment in Cold Climate Regions

For the operation of wind power in cold climate, it is important to assess the expected production in the planning phase of a wind farm, but it also essential to assess the expected production losses of a wind farm in operation. Figure A.1 in Paper A shows the modelling framework currently used for estimating the expected production in a cold climate site or the expected production losses due to icing. This framework is currently the most accepted approach within the community. At present, the modelling framework consists of three overall steps, which are explained briefly in the following:

1. Obtain atmospheric weather conditions as input boundary conditions for an icing model. Atmospheric data can be modelled by mesoscale NWP Models, as for example the Weather Research and Forecast model (WRF) [30], or the Coupled Ocean/Atmosphere Mesoscale Prediction

System (COAMPS) [31][1]. The WRF model is often used for wind turbine icing applications and is a next-generation mesoscale numerical weather prediction system, used for forecasting applications and research [30]. The atmospheric conditions modelled typically include: wind speed, temperature, relative humidity and the distribution of the liquid water content. The concentration of droplets and the droplet size distribution is based on the cloud liquid water content and is often derived according to the scheme by Thompson (2009) [33]. NWP models can provide time series of atmospheric data, with a standard output time-step of 1 hour. However, some NWP models have special ice features, with grid resolutions $\leq$ 3 km, which can provide outputs with smaller time steps.

2. Obtain ice load: The NWP output variables are used as inputs to an empirical ice load model, which is often based on Makkonen's ice model [34]. The ice load is often validation using definitions of standard icing from the ISO standard 12494:2001 [21]. Standard icing is defined as ice accretion on a freely rotating rod with a diameter of 0.03 meters and a length of 0.5 meters, such as the SAAB Combitech IceMonitor - see instrument marked by 3) in Figure 1.10. More details on the model by Makkonen is given in Section 2.1.

3. Statistical model: As seen from Figure A.1 in Paper A, a typical target is to predict the expected aggregated production or the aggregated production losses of a wind farm. The NWP variables and the predicted ice load act as predictors to the statistical model. Furthermore, production data is used to train the statistical model, and these are typically obtained by using SCADA data and the standardised power curve method defined by the IEA Task 19 in 2016 [10]. Other approaches used to train the model, were presented by Byrkedal et. al (2015) [35], who estimated the power production by a three-dimensional power curve based on the ice load. Finally, Davis (2014) [36, 37] developed a power loss approach based on different forecast models, which is widely used today.

[1]The NWP modelling concept can briefly be described as follow: "The basic concept behind a numerical meteorological model is based on a set of conservation criteria that form a set of coupled nonlinear partial differential equations that must be fulfilled simultaneously. The coupled set of equations is known as the primitive equations, covering the conservation of mass, conservation of heat, conservation of momentum, conservation of water and any other scalar such as passive tracers. Analytical solutions to these equations exist for a limited number of highly idealized situations covered by the primitive set of equations, but no methods exist to solve the general set of equations and numerical methods have to be used [32]." The domain of interest is discritized horizontally and vertically. The physical processes not explictly predicted by the forecast model are parameterized, and initial conditions and boundary conditions of the model are typically obtained by historical data and/or measurements.

The modelling framework is very effective, since it can provide production losses over a large time scale and has a relatively low processing time. However, as discussed in Paper A and by Davis et al. (2014) [37], small scale effects are not included in the setup currently, which uses the empirical ice load model and NWP input variables. In this work, it is suggested, that the framework can be improved by including new predictors, which add information about ice shape, ice thickness and aerodynamic performance (see the column called "Potential (new)" to the right under "Predictors" in Figure A.1 in Paper A). It is a hypothesis of this project and a cornerstone of the project motivation, that additional predictors, for the production site assessment, can be deveopled.

1.4 Potential Impacts of Adding New Ice Predictors

The approach for obtaining the ice predictors used in the currently used modelling framework explained in Section 1.3 (illustrated by Figure A.1 in Paper A), can be categorised as phenomenological [38]. The work presented in the dissertation goes bottom-up and addresses ice prediction from the physical perspective. The idea is, that by doing so, both perspectives of ice prediction (phenomenological and physical) can be included in the framework, which should improve the model outputs. Figure 1.11 illustrates thise line of thinking. How to predict icing using the Physical approach is outlined in Section 1.5 and more details on numerical icing models are given in Chapter 2.

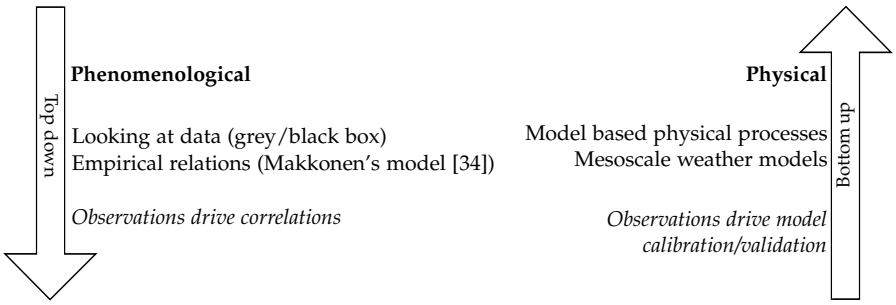

Figure 1.11: Generalised sketch of the approaches to predict icing, inspired by J. I. Madsen (2014) [38]. The phenomenological approach uses models based on empirical correlations and black/grey-box data, *i.e.* top down. The physical approach however, models the actual physical processes of icing in small scale and uses observations for model validation and/or calibration.

1.5 Project Objectives

Numerical modelling of ice accretion on structures or wind turbine blades requires the simulation of 1) the mixture of air and droplets, 2) modelling of droplet impingement on the object exposed to icing and 3) modelling of ice growth and the new shape of the object exposed to icing. As presented in Section 1.3, Section 1.4 and Paper A, there is a need for simulating icing using an advanced numerical icing model. Existing numerical icing models, primarily developed for aeronautic applications (see Chapter 2) are mainly based potential flow solvers, but more recently interfaces with Computational Fluid Dynamics (CFD) solvers have been included to obtain improved flow solutions and the possibility to study the aerodynamic degradation due to icing. Some scepticism still exists in the field of wind turbine icing towards advanced icing models using CFD, because of the computational time required and the limitation of using steady state meteorological conditions [15], [36], [10]. However, this study aims to develop an icing model based on CFD with focus on the application and the needs from the wind power industry.

The project objectives are elaborated by the following research questions:

1. Development of a CFD icing model using ANSYS-Fluent:
    a. What is the required functionality?
    b. How can the deformation of the object exposed to icing be incorporated?
    c. How to enable the flow solution to take this deformation into account in a dynamic manner?
2. Determination of inlet boundary conditions for the CFD-based icing model:
    a. How can the boundary conditions for modelling of icing using a CFD-based icing model be established?
    b. What are the challenges related to boundary conditions for modelling of icing?
3. Simulation of icing over time by a CFD-based icing model:
    a. How can a basis for validation of the simulations be created?
    b. How can periods of ice accretion or an icing event be modelled in a dynamic manner?
    c. Is it possible to use non-stationary boundary conditions?

1.6 Methodology

The dissertation centres on *application* and is industry-oriented. The steps used to reach the objectives are described in the following and summarised in Table 1.4.

Development of a CFD Icing Model using ANSYS Fluent
The overall functionality of the model is to generate ice predictors, which were defined in Section 1.4. The structure of the CFD Icing Model will be developed following the general steps of a numerical icing model, as described in Section 2.2. Droplet impingement, calculating the mass flux of ice and the generation of the new surface of the object are to be implemented into ANSYS Fluent through User Defined Functions (UDFs). Known theory will be used to calculate the collection efficiency, ice mass flux from droplet impingement and displacement vectors [39–41]. To obtain a new surface and domain mesh, the Dynamic Mesh package and associated macros will be used with UDFs.

Determination of inlet boundary conditions for the CFD-based icing model
As presented in Section 1.2.1 it is the atmospheric conditions, which control ice accretion and thereby icing events. Thus, modelling icing is strongly connected to the atmospheric conditions given to the model. These conditions will be referred to as the inlet *boundary conditions* of the icing model. The boundary conditions will be established using on-site measurements in combinations with methods by Mazin (1995) [42] and Gjessing (1990) [43] to estimate the cloud liquid water content (W). Uncertainties related to boundary conditions for icing models is a key topic to discuss, which is seen in Paper A focusing on the atmospheric conditions and in Chapter 4 focusing on experimental setups and numerical models.

Simulation of icing over time by a CFD-based icing model:
Icing will be simulated over time by the CFD Icing model developed with the established inlet boundary conditions. Validation data is established from camera pictures using image analysis. Using this method the maximum ice thickness of the cross section of the object exposed to icing can be validated.

1.7 Outline of Summary Report

The structure of the dissertation is illustrated by Figure 1.12. Three overall categories define the work; Atmospheric Conditions, Advanced Icing Models and Simulating Ice Accretion, which are also the categories covered in the Pa-

For modelling icing

Model	Methods	Software
Multiphase flow:	FVM, URANS	ANSYS Fluent
CFD Icing Model:	User defined functions (UDFs)	ANSYS Fluent

For simulating and validating icing

Data	Methods	Source of raw data
Boundary conditions:	On-site measurements	Met-mast data
	Estimated from measurements	Met-mast data
Validation data:	Image analysis	Camera pictures

Table 1.4: Overview of the modelling methodology used in the dissertation.

pers. A brief outline of each chapter is given in the following and an outline of the papers is given in Section 1.8:

Chapter 1:
Introduces the topic of wind turbines in cold climate regions and the fundamentals of atmospheric icing is presented. The general motivation of the project is given together with the motivation for developing an ice model based on CFD for wind power applications.

Chapter 2:
Provides a detailed literature review of existing icing models within aircraft icing and wind turbine icing. The pros and cons of numerical modelling of icing are presented and discussed. The literature review forms the basis of the approach used in Chapter 3 to develop the CFD Icing Model for wind power applications. Answers to research question 1.a.

Chapter 3:
Goes through the CFD Icing Model developed using Paper B and additional Papers C, D, E and F. The details of the sub models are explained to illustrate the implementation of icing theory into ANSYS Fluent and the capabilities of the model and contributions to the field. A list of the macros and UDFs used are given. Answers to research question 1.b, 1.c, 2.b, 3.b and 3.c.

Chapter 4:
Presents the methodology developed for simulating icing over time. The methodology uses on-site measurements to create a unique set of data, which consists of; inlet boundary conditions for the CFD Icing Model and validation data (Paper A). The validation and application of the CFD icing model is shown by modelling of icing over one hour using the dataset (Paper B). Answers to research questions 2.a, 2.b and 3.a and 3.b.

Chapter 5:
Closes the dissertation. The Chapter presents the final remarks, the perspective and suggestions to the future work. Discussion of an improvement strategy for the currently used modelling framework for production loss and production assessment for wind farms in cold climate and the work in general.

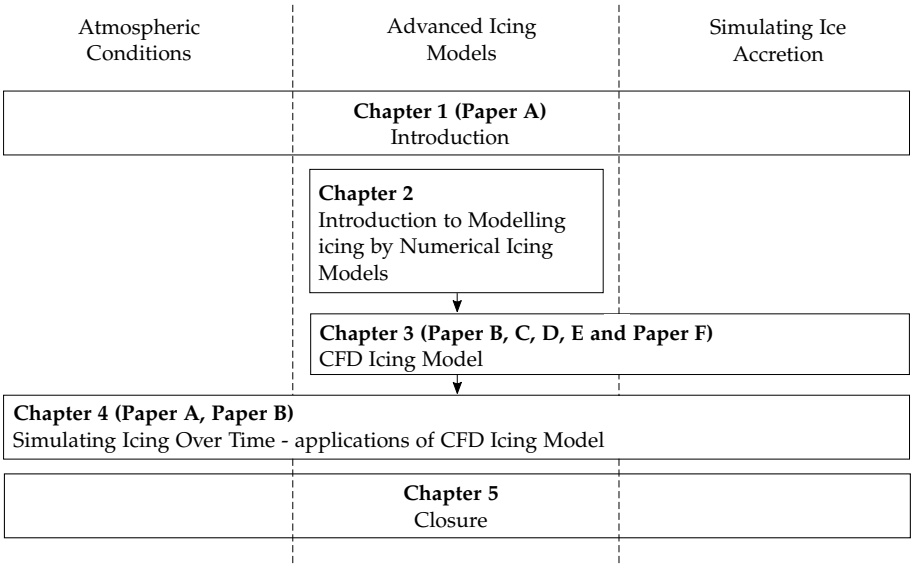

Figure 1.12: Diagram illustrating the structure of the summary report. The work is divided into the three main topics; Atmospheric Conditions, Advanced Icing Models and Simulating Ice Accretion by the columns separated by the dashed lines, which are present in the Chapters as illustrated by the lines.

1.8 Outline of Papers

As described, the dissertation is based on a collection of papers, which are all reprinted in Part II of the Dissertation. Paper A and Paper B compose the main contributions of the Dissertation, but additional research papers were also published during the study. Those papers are Paper C, Paper D, Paper E and Paper F and they are mainly related to the development of the CFD Icing Model, presented in Chapter 3. In the following, an outline of the context of each paper is given and in Part II the papers are reprinted.

Paper A: Measurements from Cold Climate Site in Canada: Boundary Conditions and Verification Methods for CFD Icing Models for Wind Turbines:
The purpose of this work was to analyse on-site measurements from a cold climate site to establish a dataset containing boundary conditions for modelling of icing using a CFD-based icing model. Emphasis is put on estimating the liquid water content and the droplet size for in-cloud icing conditions. Furthermore, validation data of ice load, ice thickness and ice mass rate are found in the measurements by image analysis. The main conclusions from the paper are the establishment of a complete dataset for modelling and validating ice accretion over time.

Paper B: Computational Fluid Dynamics Analysis and Field Measurements on Ice Accretion on a Cup Anemometer Support Arm:
A method to model ice accretion on the cross section of a cup-anemometer support arm is presented. The CFD Icing Model was developed in ANSYS Fluent using existing theory and UDFs. The main purpose of the work was to 1) simulate ice accretion over 1 hour using measurements from a cold climate site, analysed in Paper A and 2) verify the modelled results using experimental data. The main ain and conclusion of the work was to show the functionality of the CFD Icing Model and that the modelled maximum ice thickness compared very well with the validation data.

Paper C: Preliminary Modelling Study of Ice Accretion on Wind Turbines:
A new methodology for simulating icing for wind power applications is presented. The purpose of the paper was to present preliminary icing simulations performed by modelling of in-cloud icing conditions on a NACA63-3-418 profile using ANSYS Fluent and an Euler-Euler model. The choice of turbulence model was elaborated and it was shown that, that the k-ω SST model was the most favourable for the application.

Paper D: Development of CFD-based Icing Model for Wind Turbines: A Case Study of Ice Sensor:
A case study of an ice sensor exposed to icing is presented. The ice sensor is the SAAB IceMonitor, located on a met-mast in a Swedish wind farm owned by Vattenfall. The main purpose of this case study was to introduce an impingement model and a surface generation model to the CFD Icing Model, which is under development. Preliminary results from the mesh displacement method is presented and discussed. Furthermore, the study discussed the likelihood of ice accretion on both the windward and the leeward side of the object exposed to icing.

Paper E: Case Study of an Ice Sensor using Computational Fluid Dynamics, Measurements and Pictures - Boundary Displacement:
The main purpose of this work is to present the surface boundary displacement model, which is to be implemented in the CFD Icing Model, which is under development. Icing conditions are simulated on a cylinder, corresponding to the cross-section of the SAAB IceMonitor. The C-grid topology with a structured inner part and an unstructured outer part was used. The main conclusions were, that the surface boundary displacement model developed showed promising robust results for the case study presented.

Paper F: Towards a CFD Model for Prediction of Wind Turbine Power Losses due to Icing in Cold Climate:
The focus of this work was to apply the CFD Icing Model, which is under development for modelling icing on an airfoil. Icing was simulated on a NACA64-618 profile for different ambient conditions for icing period of 20 minutes using the current version of the CFD icing model. The effects of taking the surface roughness into account was shown and when varying the droplet size and the liquid water content, showed an increase in the accreted mass of ice which was in agreement with the literature.

Chapter 2

Introduction to Modelling Icing by Numerical Icing Models

This chapter explains and discusses the process of modelling icing using numerical icing models. The chapter is opened by a literature review of the development of icing models, followed by a review of the most commonly seen numerical icing models. The possibilities and advantages of using a CFD based icing model is presented.

2.1 Introduction to Ice Models

Ice models exist in various forms. In the field of wind energy, icing models have a relatively short history, whereas ice models have been studied for decades within the aircraft industry, where icing is important exclusively due to safety. Ice accretion before takeoff or during takeoff disturbs the control system of the airplane, leading to miscalculation of the stall angle, which can lead to emergency landings or at worse, plane crashes. The ice can also loosen and get ingested by the engines, which for example was the case in 1991 for a McDonnell Douglas DC-9-81, operated by SAS [44]. The aircraft was supposed to fly from Stockholm to Copenhagen one early morning in December but only managed to be airborne for a few minutes due to engine failure caused by fire due to ingestion of glaze ice into the engines. The flight emergency landed at 121 knots and the fuselage broke into three pieces, luckily leaving all passengers unharmed [44]. In-flight icing event is also an issue for the aeronautics and in 1953 B.L. Messinger [45] published the paper called; "Equilibrium Temperature of an Unheated Icing Surface as a Function of Air Speed". The work was initiated by the wish to exchange an

anti-icing method using constant thermal system, to a cyclic thermal de-icing method. B.L. Messinger [45] described the energy balance of an unheated surface under icing conditions, as a function of air speed, altitude, ambient temperature and the liquid water content. An equilibrium temperature was defined for the insulated, unheated surface exposed to icing and more importantly was the introduction of the freezing-fraction. B.L Messinger defined, that the actual surface temperature, would depend on the energy balance on the surface during icing conditions. At a temperature $T < 0^{\circ}C$ all impinging liquid (droplets) were assumed to solidify and the energy balance would consist of heat lost by convection, sublimation and warming of droplets and heat gained by the release of the latent heat of fusion, viscous/frictional heating and by kinetic energy heat release at droplet impact. At a temperature $T = 0^{\circ}C$ a freezing fraction (n) was introduced in the expression of heat gained by latent heat of fusion, which basically means, that not all impinging liquid would solidify, and some would also leave the surface by so-called blow-off or run-off.

Most icing models seen today, in the aircraft industry and within wind power, have been based on the fundamental work by B.L. Messinger. The aircraft industry has inspired the development of icing models for wind power applications, and some aircraft models have been shown to have a functionality well fitted for wind power applications. However, one significant difference exists between icing models for aircraft icing applications and wind energy applications, and that is the time needed to be simulated (modelled). For aircraft icing, only the ice accretion process is of interest, because the ice will be removed by some de-icing or continuous anti-icing system immediately, because of safety reasons. Thus, icing models for aircraft applications have a history of being advanced and including many details of the physics of the ice accretion process and the flow behavior of the droplets and the air. For wind energy applications, full icing events are typically modelled, and the information is typically needed over longer time periods of hours, and even on an annual basis for some applications. Because of this, empirical models with fast processing times have been widely used within the wind energy industry.

2.1.1 Empirical Icing Models

Makkonen's first icing model [46], was developed to model atmospheric icing on stationary structures, such as overhead power lines, masts, trees and measurement equipment. His work was inspired by the infrastructural problems faced during the wintertime in Finland and similar locations. The empirical model used today has been developed over the past 20 years, based on vast studies, of for example: icing on stationary cylinders shaped objects [46],

ice accretion on wires [47], relations related to heat transfer and roughness for cylinders [48], the collection efficiency of droplets on cylinders [49], wet snow on structures [50] and relations for obtaining the cloud liquid water content and droplet size from rotating cylinders and empirical models [51]. The model, as seen today, was presented by L. Makkonen (2001) as: "A model for the growth of rime, glaze, icicles wet snow on structures [34]". The model describes the growth of ice on a freely cylinder, by the product of the liquid water content, droplet velocity, cross sectional area of the object and three coefficients; the collection efficiency, the sticking efficiency and the accretion efficiency. The three coefficients are based on empirical correlations.

As mentioned in Section 1.3, Makkonens model is also referenced in the ISO 12494:2001 standard [21] and included as an appendix. Since the flow field is not solved the model is fast and within wind turbine icing, the model is most often used in combination with NWP boundary conditions to model icing over long time periods. This basically means, that the wind turbine is represented by a freely rotating cylinder and it is an open question, if that is desirable. Furthermore it is also a question, if it would be desirable to have information of the actual ice accretion, the ice shape and ice distribution on the blade. Because of this issue, N. Davis (2014) [36] developed the ice model "iceBlade" based on Makkonens model but used a 1 m long segment 85 % down the blade to represent the wind turbine blade. He also included an ice ablation equation in his model and showed promising results through the improvements. However, he did not take the change of shape of the cylinder into account which, as discussed in Section 1.3, might be very useful as input to the statistical model in the overall icing forecasting framework. N. Davis (2014) [36] discusses the topic and suggested, that a more detailed icing model, such a CFD based icing model, might improve the overall icing forecasting framework. The following section presents the process of modelling icing by advanced numerical icing models, such as a CFD based model.

2.2 Advanced Icing Models

As presented in the Chapter 1, and in detail in Section 1.2.1, many parameters must be, or can be, considered when modelling ice accretion. In numerical modelling of ice accretion, the process can be divided into three general parts starting from the calculation of the air flow, followed by water impingement calculations and finalised by ice shape calculations. The process is typically a continuous process as illustrated in Figure 2.1. The parts can be treated in very different ways, depending on the numerical approach used. Icing models, which solves the flow field and droplet impingement are often re-

ferred to as *advanced icing models* [10]. In the following subsection different advanced icing models are presented and discussed.

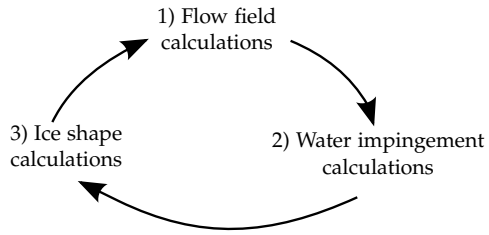

Figure 2.1: Schematic of the general parts of ice accretion numerical modelling.

2.2.1 Review of Existing Models

In general, the modelling strategy for the advanced icing models can be divided into two categories:

1. Models of airfoils exposed to icing using potential flow theory and discretisation using the panel method
2. 2D or 3D models based on Computational Fluid Dynamics (CFD)

Some models can be categorised as hybrids, meaning that the panel flow code can interface with a CFD flow solver. Common for the codes are, that they contain similar parts, see Figure 2.1, but they are handled differently; the flow field is solved in different ways, different droplets trajectory schemes are used, heat and mass transfer are solved differently and the prediction method of ice growth in between each time step varies. The list of bullets below provides an overview of the most well know and relevant advanced icing codes, which one would encounter within the field of wind turbine icing. Those models are the following: LEWICE, ONICE (ONERA), TRAJICE, TURBICE and FENSAP-ICE. The review is also included to provide an overview of the advanced icing models with sufficient details and references, which is missing within wind turbine icing and if available, often contains incorrect information and the lack of details. The models are described, in the order given, as follows.

- LEWICE: has been developed by The Icing Branch at the NASA Glenn Research Center, Ohio, USA for aeronautics. The NASA Lewis Ice Accretion Prediction Code (LEWICE) was released in its first version in

1990 [52] and LEWICE 3.2.2 is the newest version [53]. The code consists of three main parts: 1) the air flow is calculated based a Hess-Smith 2D potential flow panel method [54], 2) droplet trajectories and collection efficiency are calculated by a Lagrangian approach and 3) a thermodynamic model that solves for mass and energy in each control volume and obtains an ice profile. The energy balance is based on Messenger's model [45]. In LEWICE the new shape of the airfoil is calculated by a time-stepping approach and a new leading edge of the airfoil is calculated [55]. LEWICE is the most recognized and used icing code for aircraft icing applications, such ice shapes predictions, collections efficiencies, and anti-icing heat requirements. The code and the predicted ice shapes, has furthermore been validated against a wide variety of experimental conditions. The initial development (1986-1991) of LEWICE, ONICE (see below) and TRAJICE (see below) was a close collaboration, where research and experimental data were shared among the agencies of the U.S, the U.K and France [55]. Since the codes were developed by aircraft producing countries, advanced experimental setups were available; The NASA Lewis Icing Research Tunnel and the NASA Heat Transfer Tunnel in Cleveland (USA), the Artington Icing wind tunnel facility near Guilford in Surrey (England) and the engine icing facilities at CEPr (France). Even though LEWICE already has a long history, the code is always under development and the newest 3.5 version of LEWICE is currently being validated [56, 57]. The model has been extended to handle mixed phase and ice crystal conditions and a new capability to use results from unstructured grid flow solvers.

  - LEWICE3D: is a post processer, that utilizes the fluid flow simulated by a third-part CFD software to compute various parameters associated with icing risks. It can calculate; droplet trajectories, the collection efficiency and ice shape. LEWICE3D has also been very well validated [58], [56].

- ONICE(2D): has been developed by the Office National D'etudes Et de Recherches Aerospatiales (ONERA) of France for the aeronautics industry. The code can also be divided into three main parts: 1) a potential flow is solved in a C-grid using the finite element method taking compressibility into account, 2) droplet trajectories and calculated based on the drag force produced by the difference between the velocity of the droplets an the flow field surrounding it and 3) the heat transfer coefficient is calculated based on Makkonens correlation [47], and Messenger's model [45] was used to determine the local freezing fraction (n). And finally, a predictor-corrector approach is used to obtain the new ice shape [55].

  - ONICE3D: is an extension of ONICE2D, where the original set-up has been coupled with a boundary layer calculation to take the viscous effects into account, using a RANS solver [59]. ONICE3D was developed, with modules which can stand-alone, so that the user can interchange, for example, the CFD solver etc. [60].

- TRAJICE: has been developed by, at that time called, the Defense Research Agency (DRA), in the U.K for the aeronautics industry. The code is very similar to LEWICE in its construction, but a two-dimensional flow solver is applied and coupled with a two-dimensional droplet trajectory code to determine the mass flux impingement on the airfoil surface. The heat balance is also based on Messenger's equations, but the convection and evaporation are modified to take compressible effects into account [55].

- TURBICE: has been developed by the Technical Research Centre of Finland (VVT) for wind power applications. The first versions of the model were seen in 1992 by K. J. Finstad and L. Makkonen, and further improvements of the flow solver, the velocity range and range of angle of attack, ice density calculations and numerical stability was presented in 1996 by K. J. Finstad and L. Makkonen [61]. Makkonen et al. (2001) [61] presented the numerical model, which is the TURBICE model of today. The structure of TURBICE is very similar to the previously described potential flow models (LEWICE, ONICE and TRAJICE) and three main parts can be described briefly as follows; 1) a potential flow is solved using the panel method discretisation, 2) comparable to ONERA the droplet trajectories are found from the flow solutions and the droplet drag coefficients, here obtained from K.V. Beard (1969) and I. Langmuir (1946) [62, 63] and 3) energy and mass balances are solved on the surface of the airfoils, inspired by Messenger's models [45], and the local heat transfer coefficient is solved using the heat transfer model by Makkonen [48]. The local calculated ice thickness is added to the original surface to obtain the new ice shape. Time is represented by several icing layers at every finite calculation area. The ice layers are formed by the local ice thickness and the ice mass flux and ice density. A new flow solution and droplet solution are obtained after each simulated ice layer.

- FENSAP-ICE^{TM}: has been developed by Newmerical Technologies International (NTI), Quebec, Canada for aircraft applications. The code is an in-flight icing simulation tool, which applies Navier-Stokes like equations to model ice accretion [64]. The code is built upon 4 steps: 1) solve air flow field by CFD solver, 2) solve droplet flow and impingement (DROP3D), 3) calculate ice accretion and ice shape (ICE3D) [65]

and 4) mesh displacement. The ice model, called ICE3D, uses Messenger's description of icing on an unheated surface by a formulation using differential partial equations [39, 40]. FENSAP-ICE^{TM} calculates the flow solution once and feed this into DROP3D, which will solve the droplet flow by an Eulerian multiphase flow model and calculate the collection efficiency. ICE3D can now be run with; the collection efficiency and the droplet velocity from DROP3D and wall shear stress and the convective heat flux from the airflow solution, as inputs. The mesh will be displaced in the flow solver by an Arbitrary Lagrangian Eulerian (ALE) scheme, after the ice accretion time has finished [66], [67]. The new ice shape is calculated and, if needed, the mesh is updated. In the default structure of FENSAP-ICE^{TM} the flow field is not updated over time and ice accretion is based on the flow solution of the clean geometry. A multi-shot approach has been developed, where the flow and droplet will be solved more than once during the ice accretion time. FENSAP-ICE^{TM} models turbulence by the one-equation Spalart-Allmaras model (by default), which is widely used for airfoils and wind sections. However the two-equation k-ϵ can also be chosen [41]. More recently, it was possible to interface FENSAP-ICE^{TM} with ANSYS Fluent, probably allowing for an improved airflow solution for turbulence. And recently FENSAP-ICE^{TM} was bought by ANSYS but is not an integrated part of the ANSYS Fluent interphase package [68].

FENSAP-ICE^{TM} is currently the only complete CFD based icing model available, but it is a commercial software and is used for ice certification of aircrafts. After wind turbine industry began looking for more advanced icing models, studies were made to show the abilities of the code for wind turbine icing as well. Small studies were presented by T. Reid (2013) from NTI [69, 70] and D. Switchenko from NTI (2014) [23]. The publications by T. Reid consists of a Part I [69] and II [70], where ice was simulated with constant inlet boundary conditions over 1 hour on the NREL Phase VI rotor for five different cases, four glaze ice conditions and one rime ice condition. Performance degradation were studied by comparing the torque vs. wind speeds for Case II for three different times, *i.e.* 10 min, 20 and 60 minutes of ice accretion compared to the clean blade. The power loss vs. wind speed were found. Since the study uses constant inlet boundary conditions, T. Reid suggests that using varying inlet boundary conditions, might be important to study, since the solution might change. He suggests, that the multi-shot available in FENSAP-ICE^{TM}, could be used to change the inlet boundary conditions over time. In Part II [70] the required heating power along the span of the blade was presented, which is useful for de-icing

applications. Another wind power application of FENSAP-ICE^{TM} was shown by D. Switchenko [23], who simulated icing over an icing event of 17 hours and compared the power reduction to the power produced at site. Weather data from a site at the Gaspé Peninsula, (Québec), Canada and an industrial scale wind turbine, the WindPACT 1.5 MW was used. The cloud liquid water content and the MVD was not measured, so assumed constant values were used over the 17 hours. In the paper, the multi-shot approach was applied, and the mesh was updated every 30 minutes followed by an update of the inlet boundary conditions. To minimise the computational time, the blade was represented by nine blade sections, *i.e.* nine airfoils. The lift and drag coefficients was obtained by the CFD solution of the air flow and a Blade Element Method (BEM) code was used to evaluate the power reduction over time. Furthermore, the study showed, that large surface roughness, would increase the power reduction.

From the review of the development of the panel-based codes, it can be concluded that the demand for a stronger flow solver, which can take boundary layer effects into account, is sought by the users. In the original models of LEWICE and ONICE, the possibility to use a flow solution based on CFD was included. And, for FENSAP-ICE^{TM} the opportunity to use flow solutions, more advanced than the one provided by FENSAP-ICE^{TM}'s own airflow solver, has been included. Besides the wish to provide a better air flow solution to the panel-based models, there is another very essential reason, making it ideal for the panel-based codes to interface with a CFD flow solution. This is the need for analysing the aerodynamic degradation of the airfoil, wing or wind turbine blade after ice accretion. The panel-based codes can compute the ice shape of an airfoil exposed to a given set of constant meteorological icing conditions with a low computational effort and fast. This makes the panel-based codes very attractive. However, the ice shapes must be exported to some other flow software to study the aerodynamic degradation of the profile, for example in terms of a reduced lift force and an induced drag force. For aircraft icing, it is also very interesting to evaluate the flow characteristics close to and after stall [71].

Towards Models for Wind Turbine Icing

Aerodynamic degradation of a wing (aircraft or wind turbine) due to icing are typically studied using an ice shape, followed by an analysis using CFD to obtain the lift and drag coefficients, which for example can be used by a blade element momentum (BEM) code to obtain power and thrust coefficients. An example of using this approach for wind power applications, was presented by Etemaddar et al. (2014) [72]. Icing was studied on airfoils from

a 5 MW NREL (National Renewable Energy Laboratory) reference wind turbine [73] and ice shapes were generated using LEWICE. The lift and drag coefficients were obtained using ANSYS Fluent and power and thrust coefficients were obtained by the BEM code WT-Perf by NREL [72]. In the study, also the dynamic response of the wind turbine was also studied by the coupled servo aeroelastic simulation code HAW2C, by Risø National Laboratory, Denmark [74]. Another example of generating ice profiles along a turbine was presented by Hu et al. (2017) [75], who simulated ice on the NREL VI wind turbine using LEWICE. ANSYS Fluent was used to obtain lift and drag coefficients and the aero-hydro-servo-elastic tool FAST v8 by NREL was used to study the wind turbine dynamic response.

To solve the issue of having to combine an ice model based on a potential flow solver and a flow analysis, other studies worked on developing CFD based icing models, such as FENSAP-ICE, which can also provide the ice shape, and displace the mesh or remesh the domain. As illustrated in Figure 2.1 the second step towards such a model, is the droplet solution and modelling of the collection efficiency. Wirogo and Srirambhatla (2003) [76] presented an approach to calculate the collection efficiency using an Eulerian approach and a Lagrangian approach in FlUENT. For the Eulerian approach, the collection efficiency was obtained by using the user-defined-scaler-transport framework available in ANSYS Fluent. Wirogo and Srirambhatla (2003) [76] compared the results to simulations from FENSAP-ICE^{TM} and experiments and demonstrated the approach on a Boeing 737-700 nacelle scaled model and on a multi-element wing. A similar approach was presented recently by Hu et al. (2017) [77], who calculated the collection efficiency on the 3D S809 straight wind turbine blade.

The third step in Figure 2.1 is to obtain an ice shape, which requires the calculation of the ice mass and the ice height. As shown by Figure 1.9 in Section 1.2.1 the ice shape can either be accreted by a "dry" process or a "wet" process, *i.e.* rime ice accretion of glaze ice accretion. Coa et al. (2008) [78] presented an icing model developed in an in-house CFD code, capable of modelling rime ice accretion to obtain the volume of ice in each control volume and thereby generate the iced surface. Cao et al. (2011) [79] extended the model to include the Messinger's thermodynamic model [45], where equations of mass and energy were solved in every control volume of the surface of the object exposed to icing. Ice accretion on multi-element airfoil was studied [79], and later the model was extended for three-dimensional applications for aircraft wing applications [80], [81]. In the work by Cao et al. [78–81] focus was on the thermodynamics of the ice model for providing accurate estimates for anti-icing (de-icing) heating systems for aircraft, thus the ice shapes are generated but no mesh displacement was developed for the

numerical model. Another study, presenting the application of Messengers thermodynamic model is seen in [80], who developed an ice model comparable to the panel-based codes described above (LEWICE, TRAJICE, ONICE etc.). Villalpando et al. (2016) [82] also presented an interesting study, where icing was modelling using the Eulerian approach using ANSYS. Villalpando et al. (2016) [82] used a formulation of Messengers model given by Myers (2001) [83], where the evolution of the ice thickness is described by an ordinary differential equation (ODE) of the energy balance on the surface of the object exposed to icing. In this case the collection efficiency was calculated through a user defined function and used in a MATLAB script, which would solve the ODE over each grid element adjacent to the airfoil to create a new file with coordinates of the new surface of the object. The new surface coordinates were given to Gambit[1], which would generate a new mesh by a journal file. The new mesh of the iced airfoil could be read by ANSYS Fluent to start a new simulation. Ice was simulated on, amongst others, airfoils to study heating requirements for de-icing systems.

2.2.2 Conclusion from Review of Existing Icing Models

From the review and analysis presented in Section 2.2.1, the following conclusion can be drawn, which has formed the basis for the development of the CFD Icing Model, presented in Section 3.1:

- Advanced icing models are not easily accessible and very few has been developed for wind power applications.
- There is a need for a flow solution, which also takes the viscous effects into account, such as using a CFD solver.
- The wind power industry is interested in the application of advanced icing models, but they need simulations of longer time periods with constant or varying inlet boundary conditions [23].
- Ice accretion, ice shape generation (and mesh update/displacement) and analysis of the aerodynamic degradation are most often carried out by a combination of tools [82], [77].

From the points above it can be concluded, that there is a need for the development of a CFD based icing model for wind power applications. The model should work as one integrated composite unit. The design should be balanced between the need for accuracy and computational time and it must be able to simulate icing over time using varying inlet boundary conditions. The CFD Icing Model developed in the study based on these requirements are presented next, in Chapter 3.

[1]Gambit is the original meshing tool used by FLUENT Inc.

Chapter 3

CFD Icing Model

This chapter provides a review of the developed CFD Icing Model. The process of developing the model is presented by referencing to main Paper B and additionally to Papers C, D, E and F, while some topics will be further elaborated.

3.1 Review of the Developed CFD Icing Model

The CFD Icing Model was developed over a longer time period and the Papers C, D, E and F present different aspects of the model development process and in journal Paper B, the full model and validation of the results was presented. As a starting point, the model development was focused on icing on airfoils, as seen in Paper C entitled: "Preliminary Modelling Study of Ice Accretion on Wind Turbines". But because of the availability of experimental data, the model developed shifted to focus on ice accretion simulations on cylinders. However, the modelling framework was demonstrated on the NACA64618 airfoil profile in Paper F entitled: "Towards a CFD Model for Prediction of Wind Turbine Power Losses due to Icing in Cold Climate". Modelling ice accretion on a cylinder was initiated in Paper D entitled: "Development of CFD-based Icing Model for Wind Turbines: A Case Study of Ice Sensor", as seen by Figure D.1 and continued in Paper E entitled: "Case Study of an Ice Sensor using Computational Fluid Dynamics, Measurements and Pictures - Boundary displacement" and Paper B entitled: "Computational Fluid Dynamics Analysis and Field Measurements on Ice Accretion on a Cup Anemometer Support Arm". Since the model is described in the papers (see Table 3.1), this Chapter presents additional information to improve/clarify the description of the model and the choices made.

A flow diagram of the model is presented in Figure 3.1 and Table 3.1 provides an overview of the contributions of the papers to the model development.

Step 1 to step 4 of the flow diagram in Figure 3.1 are reviewed and presented

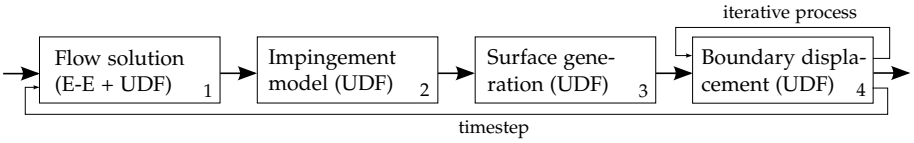

Figure 3.1: Flow diagram of the developed CFD Icing Model by four parts. In step 1 the multiphase flow is treated by the Euler-Euler model, available in ANSYS Fluent. The remaining, steps 1 to step 4, of the model were developed using macros and user defined functions (UDFs).

in the following sections 3.1.2 - 3.1.5, while referencing to the papers listed in Table 3.1. To support the content of the papers, the choice of multiphase flow model is further elaborated in Section 3.1.1. Besides this, a method to update the inlet boundary conditions over time is presented in Section 3.2; a method not presented in the papers (Table 3.1) but demanded by the Project Objectives (Section 1.5). A list of the macros and UDFs used is provided in Section 3.4 and the Chapter is closed by concluding remarks on the CFD Icing Model in Section 3.3.

		Steps of Fig. 3.1			
Paper	Description	1	2	3	4
C	Expressing in-cloud icing conditions	x			
D	Modelling impingement, new node locations		x	x	
E	Development of surface boundary disp. model			x	x
F	Test of modelling approach for airfoil	x	x		
B	Modelling icing over time by CFD Icing Model	x	x	x	x

Table 3.1: Contributions from Papers B, C, D and E to the development of the CFD Icing Model presented by the different parts in Figure 3.1. The order of the papers seen in the table follows the development order of the CFD Icing Model. Paper F was used to test the possibility of using the modelling approach on an airfoil with surface roughness and contributes indirectly to the overall goal of modelling icing for wind power applications.

3.1.1 Choice of Multiphase Flow Model

In-cloud icing conditions (see Section 1.2.1) can be described is a flow consisting of a mixture air and super-cooled droplets, *i.e.* a multiphase flow. As discussed in Section 2.2 the mixture of air and droplets can be represented by different approaches when modelling icing. For this study, the mixture is categorised as a dispersed dilute flow having a one-way coupling between the continuous phase and the particle phase. The particle-fluid interactions dominate the flow transport and the dispersed phase motion is affected by the continuous phase, not vice versa. For such a flow type, the numerical approach for the continuous phase/flow is typically based on an Eulerian

reference frame, while different approaches can be chosen for treating the particle phase; typically, a Lagrangian approach or an Eulerian approach [84], resulting in an Euler-Lagrangian or an Euler-Euler treatment of the two-phase flow [85]. For the standard in-cloud icing conditions, see Table 1.1, the flow has a low particulate loading, *i.e.* a low mass density ratio of the particle phase to continuous phase, and a Stokes Number, $St < 1$. Paper B presents the use of the Euler-Euler approach for modelling in-cloud icing with a separated fluid treatment. However, since both the Euler-Lagrangian and the Euler-Euler approach are appropriate for modelling in-cloud icing the fundamental differences of the two approaches are presented and discussed in the following.

In the Eulerian description of the particle phase, it is assumed that the particles characteristics can be described as a continuum. The assumption allows all phases to be treated with a consistent numerical scheme and numerical grid. The concentration of particle in the flow is described by a particle volume fraction α_p, which is basically the fraction of the computational volume containing of droplets. Correspondingly, the concentration of the continuous phase is described by a volume fraction α_c [84]. For modelling in-cloud icing, two phases are present in the flow, but the Eulerian formulation does, in general terms, allow for an unlimited number of secondary phases (q), typically only limited by convergence and/or computational power. In the Eulerian formulation the sum of all phases (q) must be equal to unity, as seen by Equation 3.1:

$$\sum_{q=1}^{n} \alpha_q = 1 \Rightarrow \alpha_p + \alpha_c = 1 \tag{3.1}$$

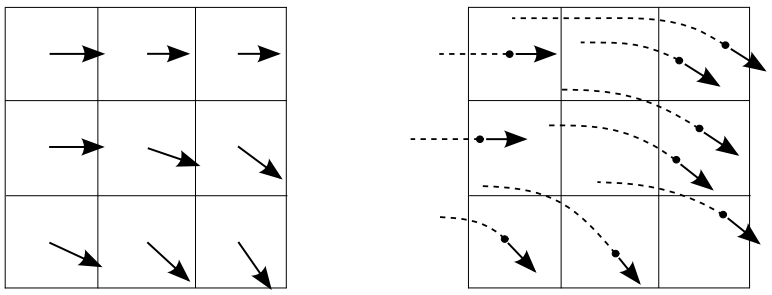

Figure 3.2: a) The particle velocity vector (cell based) in the Eulerian particle velocity field and b) the particle patch line in the Lagrangian particle velocity field. The illustration was inspired by Crowe (2006) [84].

As opposed to the Eulerian treatment, the Lagrangian approach assigns each particle (or group of particles) with an individual identity; therefore, it is often referred to as the discrete phase method. In the Lagrangian method the properties of the particle are calculated along the path of the particles, whilst the properties of the particles are averaged using the Eulerian method. These fundamental differences are illustrated in Figure 3.2, where the particle velocity vectors and particle path lines are seen for the Eulerian and the Lagrangian dispersed phase approach, respectively.

In terms of using either the Euler-Lagrangian or Euler-Eulerian approach to model in-cloud icing and as the reference frame of an CFD-based ice model, it is relevant to consider four topics: 1) particle impingement, 2) the collection efficiency, 3) the computational effort required and 4) the particle representation, as seen in the following:

1. Particle phase impingement:
    - **Lagrangian:** Particle seeding issues, especially for complex geometries. The upstream seeding of particle has a major influence on the impact of the particle on the object [76].
    - **Eulerian:** No seeding issues. Upstream conditions do not affect the particle impingement. Well suited for complex geometries and for 3D cases [76].
2. The collection efficiency, β:
    - **Lagrangian:** Boundary conditions well developed and straightforward. However, possible issues with inaccurate collection efficiency because of an insufficient number of particles released [39].
    - **Eulerian:** The collection efficiency can be calculated at all wall boundaries, since the volume fraction of droplets can be accessed everywhere in a computational domain [39]. However, the boundary conditions are not straightforward, and requires special attention, see Section 3.1.2.
3. Computational requirements:
    - **Lagrangian:** Governing equations are well developed. Expensive for 3D cases because of the need of many seeding locations [76].
    - **Eulerian:** Consistent computational schemes can be used for all phases [84], [39]. However, a partial differential equation is solved for each phase and it can be expensive for a droplet distribution [76], [86].
4. Particle phase representation:

- **Lagrangian:** Particle size and distribution can be specified directly.
- **Eulerian:** Solves for one droplet size at the time. To study the variation of ice mass flux or collection efficiency of an entire droplet size distribution might require multiple runs.

Based on the presented comparison and the literature review given in Chapter 2.2.1, the Eulerian treatment of the particle phase was chosen to represent in-cloud icing conditions in the CFD Icing Model. This was primarily due to the obvious advantages of the elimination of seeding issues and the calculation foundation of the collection efficiency.

3.1.2 Step 1: Flow Solution

When using the Eulerian description of the particle phase, either a mixture-fluid or a separated-fluid and point-force treatment can be used. In the mixture-fluid approach, the phases are assumed to be in local kinetic and thermal equilibrium and a strong coupling exists. Momentum, continuity and energy are solved for the mixture, volume fractions equations are solved for the secondary phases and typically algebraic equations are needed for the relative velocities. In the separated-fluid treatment, the momentum, continuity and energy equations are solved for each phase, since the continuous phase and the particle phase compose two separate continua. For the CFD Icing Model, the separated-fluid treatment was used, which in the ANSYS Fluent terminology corresponds to the Euler-Euler multiphase flow model [85]. The transport equations of the Euler-Euler formulation were presented in Paper B, equation B.2 and B.3. The system of coupled equation is closed by the source term, expressing the sum of the interphase momentum exchange coefficient K_{pq} times the relative velocity of the continuous phase and the particle phase, as described in equations B.4 - B.7 (Paper B). The interphase expression is part of the separated/fluid formulation [84]. In ANSYS Fluent 18.0 all interphase exchange coefficient models are empirically based, since this is what is available from the literature at present [85]. Turbulence was modelled using the k-ω SST model, which was found to be the best choice in Paper C, see page 135.

Surface Boundary Conditions

An important parameter to consider, when simulating icing using the Eulerian method, is the boundary conditions of the object exposed to icing. If the idea of letting the accumulated ice become part of the object exposed to icing is used, the droplets volume fraction must be absorbed at the surface of the object. This is not a default wall boundary condition in the Eulerian formulation and must be included to ensure mass conservation in the computational domain (see review Section 2.2.1). As presented in Paper B, the CFD

Icing Model prescribes a source term on the surface of the object exposed to icing as follows:

$$S_\phi = -(\boldsymbol{v}_\mathrm{d} \cdot \boldsymbol{A})\alpha_\mathrm{d}\rho_\mathrm{d}\phi \tag{3.2}$$

where ϕ is the dependent source variable, α_d the droplet volume fraction, ρ_d the droplet density and **A** the face area vector and $\boldsymbol{v}_\mathrm{d}$ the droplet impingement vector. To avoid instability in the system of equations, mass and energy must be balanced correctly. This is done by adding a source term to the equations of continuity, energy and momentum, as seen by Equations 3.3 - 3.6 as follows:

$$S_{\phi,\mathrm{C}} = -(\boldsymbol{v}_\mathrm{d} \cdot \boldsymbol{A})\alpha_\mathrm{d}\rho_\mathrm{d} \tag{3.3}$$

$$S_{\phi,\mathrm{E}} = -(\boldsymbol{v}_\mathrm{d} \cdot \boldsymbol{A})\alpha_\mathrm{d}\rho_\mathrm{d}H_\mathrm{d} \tag{3.4}$$

$$S_{\phi,\mathrm{M_x}} = -(\boldsymbol{v}_\mathrm{d} \cdot \boldsymbol{A})\alpha_\mathrm{d}\rho_\mathrm{d}u_\mathrm{d} \tag{3.5}$$

$$S_{\phi,\mathrm{M_y}} = -(\boldsymbol{v}_\mathrm{d} \cdot \boldsymbol{A})\alpha_\mathrm{d}\rho_\mathrm{d}v_\mathrm{d} \tag{3.6}$$

where H_d is the particle phase enthalpy of the cell, u_d is the x-direction particle phase velocity of the cell and v_d is the y-direction particle phase velocity of the cell. In ANSYS Fluent the macro; DEFINE_SOURCE can be used to

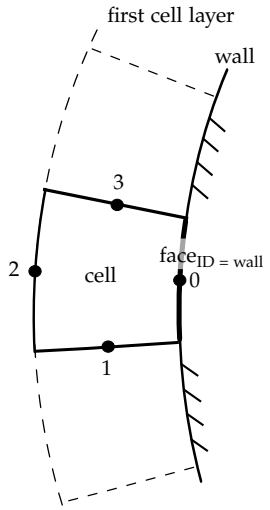

Figure 3.3: Finding face of cell with wall face ID corresponding to the ID of wall of the object exposed to icing.

customise sources [87] and has been applied to incorporate Equation 3.3 - 3.6 in the solution. The macro loops over all cells in the computational domain, but the source terms are only to be applied on the cells adjacent to the wall of

the object exposed to icing, as illustrated in Figure 3.3. Thus, the cell adjacent to the wall, is found by a cell face loop, looping over faces 0-3 of all the cells in the computational domain, as seen in Figure 3.3. The cells which have a face with a face zone identity corresponding the zone identity of the wall of the object exposed to icing must be identified. When the cells are found, the source terms are calculated. The macro works on a volumetric basis, so the source terms must be returned in a similar way as; S_ϕ / V_{cell}, where V_{cell} is the volume of the corresponding cell. The calculation of the source terms in every cell face, here illustrated as face$_1$ - face$_3$, on the wall surface is illustrated in Figure 3.4.

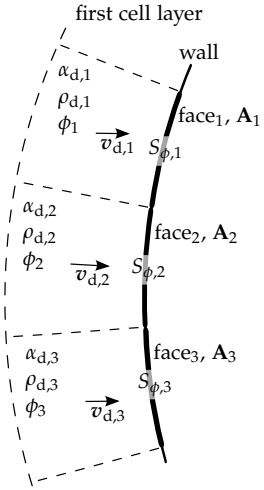

Figure 3.4: Illustration of the calculation of the source terms at the cell faces along the wall surface (face$_1$ - face$_3$) of the the object exposed to icing. The variables of the source term, seen in Equation 3.2, vary along the surface wall in every cell and each calculated source term $S_{\phi,i}$ are subtracted from the calculation every timestep.

3.1.3 Step 2: Impingement Model

Ice accretion was determined by the impingement of droplets, from where the mass flux of ice was calculated. It was assumed, that all impinging mass would freeze instantaneously and turn into ice and thereby the mass flux of impingement would be equal to the mass of ice, as illustrated in Equation D.5 (Paper D). The impingement of droplets is found by the collection efficiency, β, as presented in Equation B.10 (Paper B). Figure B.5 - Figure B.9 (page 121-page 123) show the collection efficiency and the impact of droplet size variations, inlet velocity variations and object size variations. The mass flux of ice is found as the product of collection efficiency (β), the liquid water content (W) and the free-stream velocity (v_∞), see Equation B.11 (Paper

B). As illustrated by Figure B.10 (Paper B) to the right, the impingement model runs as a face loop on the object exposed to icing and provides β and $\dot{m}_{\text{ice}}$ as face centre values. The impingement model was built into the DEFIINE_GRID_MOTION macro followed by step 3 and step 4, see Table 3.4 on page 47.

3.1.4 Step 3: Surface Generation

The new surface of ice was generated based on the calculated $\dot{m}_{\text{ice}}$, which was used to obtain ice accretion speed vectors, $\mathbf{v}_{\text{n,i}}$ Equation B.12 (Paper B), giving the new face center locations. By linear interpolation, illustrated to the left in Figure B.10 (Paper B), the corresponding new node locations were found, represented by node displacement vectors, $\mathbf{V}_{\text{n,i}}$, Equation B.13. Adding $\mathbf{V}_{\text{n,i}}$ to the current node locations, would provide the new surface and thereby the distance to be displaced. The new surface is implemented into the original mesh by the surface boundary displacement model. Paper D introduces the concept of the surface boundary displacement, which was further developed in Paper E. Finally, as referenced above, Paper B presents the final surface boundary displacement methodology by equations B.12 - B.14. Section 3.1.5 goes through the surface mesh and volume mesh displacement by dynamic meshing and user defined functions.

3.1.5 Step 4: Surface Boundary Displacement

The surface boundary displacement model was developed in the dynamic mesh environment in ANSYS Fluent and runs in the DEFINE_GRID_MOTION macro (see Table 3.4). The basic principles of the model are:

1. Describe/calculate the motion of the surface exposed to icing
2. Displace surface and update domain volume mesh

The motion of the surface is determined by the ice accretion (Section 3.1.4) and the displacement and mesh update were performed by using the dynamic mesh environment. When using dynamic meshing a generic transport equation is applied to all model equations to ensure conservation [85]. The equation can be described on an arbitrary control volume V, whose boundary is moving, by the integral form of the conservation equation for a general scaler ϕ as follows [85]:

$$\frac{d}{dt}\int_V \rho\phi dV + \int_{\partial V} \rho\phi(\boldsymbol{u} - \boldsymbol{u}_g)\cdot d\boldsymbol{A} = \int_{\partial V} \Gamma\nabla\phi \cdot d\boldsymbol{A} + \int_V S_\phi dV \tag{3.7}$$

where ρ is the fluid density, $\boldsymbol{u}$ is the flow velocity vector, $\boldsymbol{u}_g$ is the mesh velocity vector of the moving mesh, Γ the diffusion coefficient, S_ϕ the source term

and finally ∂V is used to represent the boundary of the control volume V. Moving the surface boundary, by the calculated motion, affects the remaining mesh of the computational domain. This is solved by letting the cells, close to the moving boundary, be either compressed or split according to some specified criteria such as a ratio based approach or height-based approach, as illustrated in Figure 3.5 (see more in Paper B page 125) [88]. This is called; mesh Layering and is performed in combination with mesh Smoothening [68, 85].

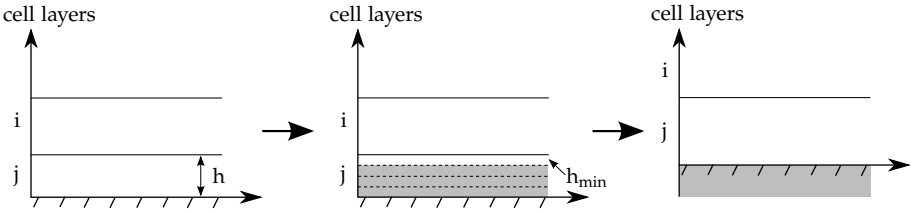

Figure 3.5: "Compression of cell layer j into cell later i, by allowing cell layer j to be compressed until the specified minimum cell height, h_{min}, is met. The ratio based option ensures that the mesh grading is retained, *i.e.* the first cell layer does not get larger than the second layer" [88].

Based on the experience from Paper E, F and Paper B, the optimum Dynamic Mesh settings used for the CFD Icing Model are given in Table 3.2.

Dynamic Mesh settings used for the CFD Icing Model		
Dynamic mesh zones:		UDF
Domain inlet:	Stationary	
Object wall:	User defined	Mesh motion

Mesh Methods:		Options
Smoothening:	Diffusion	Implicit Update
Layering:	Height based	

Table 3.2: Overview of the dynamic mesh settings for the boundary displacement model.

As seen in Table 3.2, two dynamic mesh zones were defined; the inlet boundary of the domain was specified as a stationary zone, and the wall of the object exposed to icing is a zone defined by user defined motions. The volume mesh is updated by using the two mesh methods; Smoothening and the diffusion-based approach and Layering and the height-based options. Finally, the mesh convergence options were controlled by the implicit update method.

3.2 Updating Boundary Conditions over Time

Section 3.1 goes through the four steps of the developed CFD Icing Model (flow diagram seen in Figure 3.1) and the development, application and va-

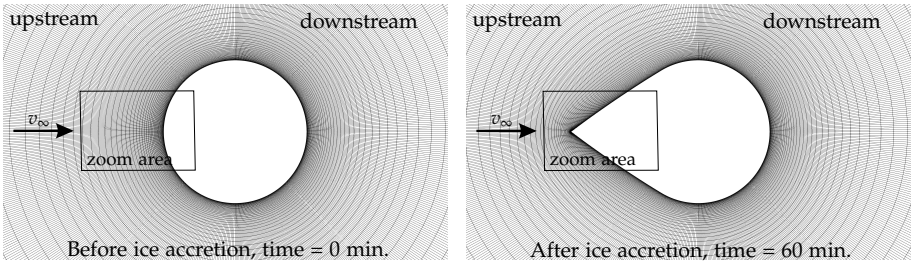

Figure 3.6: The cross section of the anemometer support arm, on which ice accretion was simulated over 60 minutes in Paper B. To the left, the mesh around the cross section of the anemoemeter support arm (a cylinder) is seen before ice accretion. The direction of the flow is marked by the black arrow and the area, which is used in Figure 3.7 to show the boundary displacement over time, is framed by the black rectangular. To the right, the mesh around the boundary of the cross section of the anemometer support arm is seen after 60 minutes of ice accretion. A rather pointy shape was developed, which was due to the nature of the multiphase flow of air and droplets and the small diameter of the cross section of 2.64 cm.

lidation of the model was shown by the papers listed in Table 3.1. A feature of the model not applied in the publications, is a step 5 presented in Figure 3.8. By step 5, it is possible to use nonstationary inlet boundary conditions when simulating icing over time. This is very interesting if for example simulating an icing event and if atmospheric measurements are available as inlet boundary conditions. This is discussed in Chapter 4.

3.2.1 Step 5: Update Atmospheric Conditions

A UDF was developed, which reads values in a look-up table and updates the boundary conditions at given simulation times. The look-up table could be arranged as illustrated by Table 3.3:

	Example of boundary variables in the look-up table					
Time (sec.)	X-velocity (m/s)	Y-velocity (m/s)	Temperature (K)	MVD (μm)	α_d (-)	Pressure kPa
600	8.869	-0.9326	268.15	25	$3{\cdot}10^{-7}$	1018.9
...	...	...	...	...	...	
...	...	...	...	...	...	
10800	9.967	0.872	265.15	23	$2.5{\cdot}10^{-7}$	1018.1

Table 3.3: Example of how a look-up table could look like. The first column contains the time at which the UDF should update the inlet boundary conditions of the model, and the remaining columns show example of variables, which would be relevant to update over time.

The variables in the look-up table are read using the DEFINE_ON_DEMAND macro. Next the inlet boundary conditions are defined by using the DEFINE_PROFILE macro, one profile for each variable. By a face loop inside each

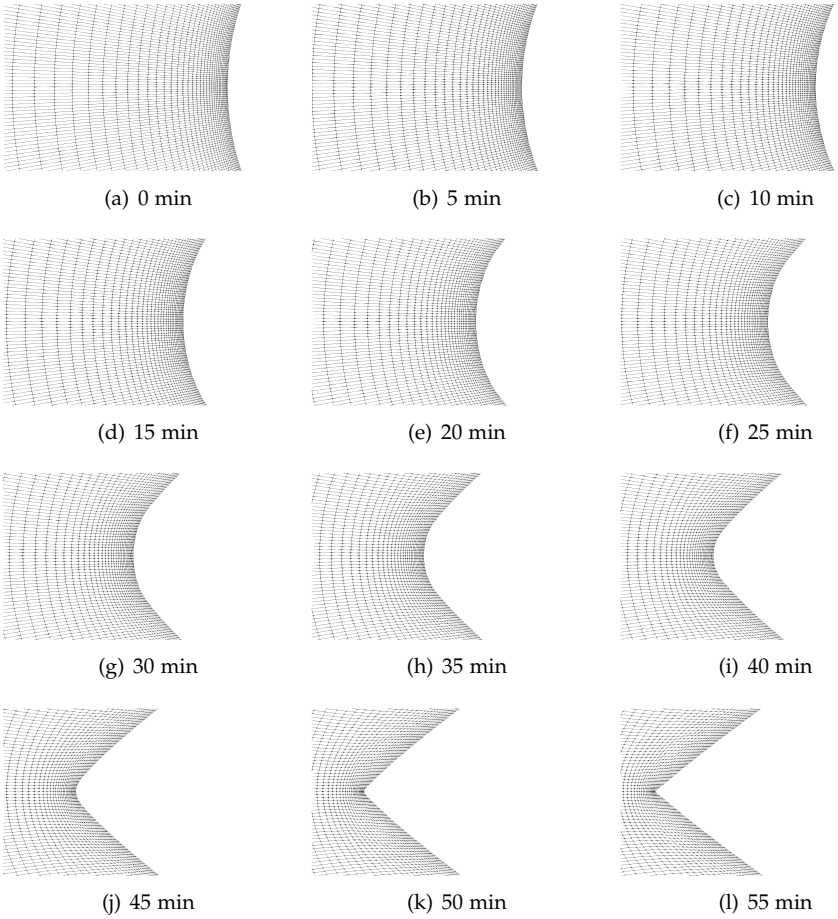

(a) 0 min (b) 5 min (c) 10 min

(d) 15 min (e) 20 min (f) 25 min

(g) 30 min (h) 35 min (i) 40 min

(j) 45 min (k) 50 min (l) 55 min

Figure 3.7: Deformation of the mesh over time, seen in the zoom area defined in Figure 3.6. The deformation is shown by an interval of 5 minutes, starting by the clean cylinder in figure (a) and showing 55 minutes of ice accretion in figure (f). The deformed object after 60 minutes of ice accretion is seen in Figure 3.6.

DEFINE_ PROFILE macro, the profiles of the inlet boundary conditions are updated at the given time. If updating the droplet size (MVD) over time, the variables are given to the computation by the DEFINE_PROPERTY macro. Updating the cloud liquid water content W affects the volume fraction of the particle phase (see relation in Equation B.8), and thus updating W over time, means updating the particle volume fraction α_p.

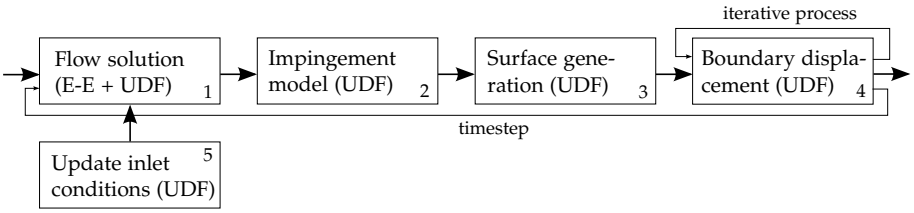

Figure 3.8: Flow diagram of the CFD Icing Model developed, showing the four steps seen in Figure 3.1 and an additional step 5. In step 5 a UDF is included to update the boundary conditions over time by loading values from a lookup table.

3.3 Concluding Remarks on CFD Icing Model

The Chapter reviewed the CFD Icing Model developed, by referencing to the published papers and by presenting a step 5 not presented in the publications. The model was developed based on the observations listed by the bullet points in Section 2.2.2 and the project objectives specified in Section 1.5. The following conclusions can be drawn from the work presented:

- A CFD Icing Model was developed and prepared for wind turbine icing. The model was developed as one integrated composite unit. In this way, all processes of simulating icing work in one transient unit; simulating in-cloud icing conditions, modelling ice accretion, updating the inlet boundary conditions, obtaining the new iced surface and displacing the surface boundary and the remaining boundary mesh.
  - The model was developed in 2D, which is found perfectly sufficient for wind power applications. Examples are the study of the aerodynamic degradation using a blade representation by airfoils and a BEM code or for de-icing applications.
- The CFD Icing Model can run using constant inlet boundary conditions or by updating the boundary conditions over time. The updating time and number of parameters to be updated can be customised to match the actual requirements.
- Paper B presented a setup for simulating icing over 1 hour, which corresponded to the measured values. The application towards airfoils was demonstrated in Paper F, while Paper C, Paper D, and Paper E presented the development of the CFD Icing Model.

Besides the functionality of the CFD Icing Model, the atmospheric conditions (inlet boundary conditions) given to the model are even more essential for simulating ice accretion. However, several significant challenges are related to the ice model boundary conditions. The following Chapter 4, discusses

those challenges using Paper A, and reviews the developed methodology for simulating icing over time using on-site measurements.

3.4 List of Macros and UDFs

Table 3.4 provides an overview of the used UDF macros for the CFD Icing Model, seen in Figure 3.1 (Figure 3.8).

For the source terms, step 1 in Figure 3.8:	
Name of Macro	Purpose
DEFINE_SOURCE	to add the calculations of the source to the simulation. Compiled and hooked under the cell zone conditions for the dispersed phase.
DEFINE_EXECUTE_AT_END	to display (intermediate) the result after each timestep. Compiled and hooked under UDFs hooks.
For the impingement model, step 2 in Figure 3.8:	
Name of Macro	Purpose
DEFINE_GRID_MOTION	to include the calculations of the collection efficiency used to obtain the ice mass flux. Compiled and hooked by the Dynamic Mesh tab, defining a user-defined wall under the Dynamic Mesh Zones.
For the surface generation and boundary displacement, step 3 + 4 in Figure 3.8:	
Name of Macro	Purpose
DEFINE_GRID_MOTION	to update the boundary nodes according to the new surface.
For updating the inlet boundary conditions over time, step 5 in Figure 3.8:	
Name of Macro	Purpose
DEFINE_ON_DEMAND	to read values in a look-table of x number of rows. Compiled and executed before the simulation starts.
DEFINE_PROFILE	to customise the inlet profiles, such as the inlet velocity. Compiled and hooked under the specified boundary conditions.
DEFINE_PROPERTIES	to customise material properties, such as droplet diameter or volume fractions. Compiled and hooked under the secondary phase properties or at velocity inlet boundary.

Table 3.4: Overview of the user defined functions (UDFs) and macros used by the CFD Icing Model.

Chapter 4

Simulating Icing Over Time

The chapter presents the methodology developed for simulating icing over time by the CFD Icing Model. The chapter presents how on-site measurements can be used as inlet boundary conditions for the CFD model. Furthermore, a validation methodology using on-site measurements is presented.

4.1 Methodology for Simulating Icing Over Time and Model Validation

A unique methodology for *simulating icing over time* was developed and the approach is illustrated in Figure 4.1.

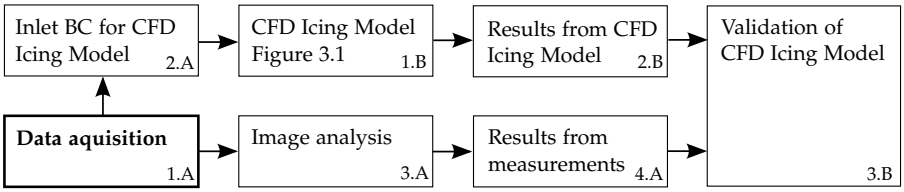

Figure 4.1: Flow diagram of the methodology for simulating icing over time using boundary conditions derived from on-site measurements and the CFD Icing Model developed. The diagram is combined based on the work conducted in Paper A (1.A - 4.A) and in Paper B (step 1.B - 3.B). The methodology starts with the data aquisition (1.A), from where the inlet boundary conditions,BCs, (2.A) and the validation data (3.A) were established. Icing was simulated using the inlet boundary conditions and the CFD Icing Model (1.B) and the model results of the ice thickness (2.B) and measurement results of the ice thickness (4.A) were used for the model validation, illustrated by the last box (3.B).

The methodology combines data acquisition, using on-site measurements, and the CFD Icing Model developed (presented in Chapter 3). Figure 4.1 was assembled around the work presented in Paper A titled: "Measurements from Cold Climate Site in Canada: Boundary Conditions and Verification Methods for CFD Icing Models for Wind Turbines" and in Paper B titled: "Computational Fluid Dynamics Analysis and Field Measurements on Ice Accretion on a Cup Anemometer Support Arm", as follows:

- Paper A: Presents the data aquisition and data analysis, corresponding to step 1.A to step 4.A. The main purpose of the work was to identify how to obtain boundary conditions and validation data for an ice model, such as the CFD Icing Model, and create a complete dataset for simulating icing over time.
- Paper B: Presents the simulation of icing using the CFD Icing Model and the validation of the modelled results using the data from image analysis, corresponding to step 1.B, 2.B and step 3.B. The main purpose of the work was to *apply* the CFD Icing Model for *simulating icing over time* by using the dataset.

Next, the methodlogy of Figure 4.1 is reviewed and elaborated on, while referencing to Paper A and Paper B. Emphasis is put on the sensitivity of the icing specific parameters on ice models and validation data. The Chapter is closed by concluding remarks, which leads to the Closure in Chapter 5.

4.1.1 Review of Method to Create Datasets from On-site Measurements (Paper A)

Simulating icing for wind power application is not straightforward. As presented in Chapter 2 and Chapter 3 the icing model is of great importance and should fit the application and needs of the user. Another very crucial parameter is the ice specific parameters, such as the cloud liquid water content, the droplet concentration and the droplet size. Those parameters are used, together with, amongst others, the wind speed and temperature, as inlet boundary conditions for ice models. Icing models either take modelled data, measured data or a combination of the two as inlet boundary conditions. Ice models are especially sensitive to the ice specific parameters because currently, there is no standard recognised way of obtaining the parameters [10]. As described in detail in Paper A page 85, the topic can be divided into two problems [89]:

1. There is no standardised way of measuring the cloud liquid water or droplet size for low-level clouds
2. There is no common standard for retrieving the cloud liquid water and thereby the droplet size from NWP models

As summarised in Section 1.3, a modelled dataset of atmospheric conditions obtained from NWP models is typically used as input for the empirical icing model[1]. The sensitivity of the modelled data is related to the choice of parameterization scheme [36,37,90] and the droplet concentration N_c used. Because of this uncertainty and because of the large time scale difference between the standard NWP values and CFD based icing models, an alternative approach is to obtain the liquid water using atmospheric measurements. In the aircraft industry a large bulk of data from airborne measurements exists and an approach derived by Mazin (1995) [42], based on 8 years of data, was used in this work to estimate the cloud liquid water content. However, the conditions close to the ground in the lower level of the atmosphere, where the wind turbine or met-mast is typically located, are different from those experienced during in-flight conditions. However, this is an immature topic within wind turbine icing and only a few studies can be found in the literature so far. For this work, it was found relevant to use an approach presented by Gjessing et al. (1990) [43], which is based on the vertical cloud visibility gradient, to estimate the cloud liquid water content. The two methods are described in detail in Section A.2.3 and Section A.2.4 and the results are found in Section A.3, Figure D.3. Appendix 2 provides additional information on how the wet-bulb temperature θ_w was obtained. Besides the inlet boundary conditions, validation data was obtained from image analysis, as briefly described in Section A.2.6. An alternative method for image analysis was included in Appendix 1, which can be used for future work and other similar images.

The results of using the two methods showed values of the W in a similar range, with a maximum of 0.1 g/m^3 for $T < 0$ °C, corresponding well to previous studies of the Gaspé Peninsula [91]. Since wind turbine icing during in-cloud icing conditions is the main interest of this work, the method by Gjessing et al. (1990) [43] was found more relevant, since it is based on measurements of the cloud base height (CBH). Using CBH provides information about the location of the wind turbine or met-mast inside the cloud. However, the method is sensitive to this distance from the reference height z to the cloud base, *i.e.* (z - CBH), and thereby the measurement of CBH. As mentioned earlier, the droplet concentration N_c is another parameter, which cannot be measured directly in the atmosphere, but is needed for the calculation of the droplet size. Figure A.10 on page 98 presented the theoretical droplet distributions of the median volumetric diameter MVD, as a function of the cloud liquid water content, while varying the droplet concentration N_c from 50 cm^{-3} to 1000 cm^{-3}. For the specific site, an N_c between 75 - 200 cm^{-3} approximately, would be considered reasonable, as illustrated by the

[1]This is because of the relatively low processing time and the high time step size. In Paper A, Section A.1 page 82 the approach is described in detail and in Section 1.3, page 15 under bullet point 1 and bullet point 2 a short review can be found.

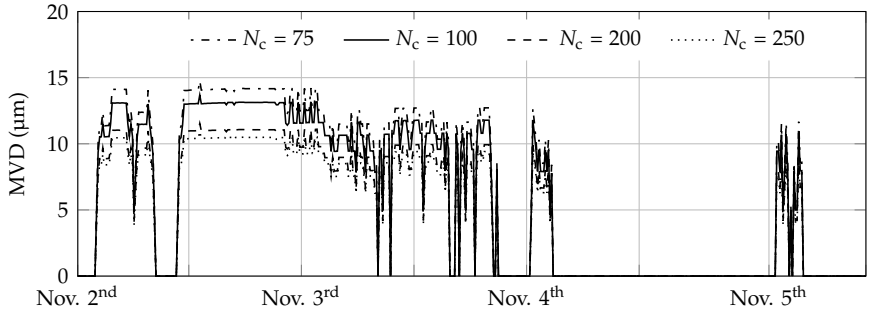

Figure 4.2: Calculated values of the median volumetric diameter MVD for droplet distrbutions from 75-250 cm^{-3} as a function of time using the estimated values of W_c, see Figure D.3 in Paper A.

grey area on Figure A.10. Figure 4.2 shows this variation, as a function of time using the estimated values of W_c.

The results from the study, is a complete dataset for simulating icing over time, as presented in Paper A, Figure A.16. In the following section, the application of the dataset is described and the ice specific parameters are further discussed in relation to the application in the CFD Icing Model developed.

4.1.2 Review of Applying the Dataset for Simulating Icing over Time (Paper B)

In Paper B icing was simulated over time using the CFD Icing Model developed and using the dataset, which corresponds to step 1.B, 2.B and 3.B in flow diagram of Figure 4.1. The developed CFD Icing Model was presented in Chapter 3 and the specific details of the set-up of the simulated cases, are described in Paper B when using the dataset and similar for the simulation carried out for the model development in Paper C, D, E and F.

In Paper B it was found, that the simulated maximum ice thickness, corresponded well to the results obtained from image analysis, as seen in Figure 4.3 [88]. "A difference in the maximum length of 11.9 % after 30 min, 1.8 % after 45 min and 4 % after 60 min of ice accretion are observed " [88]. Figure 4.4 shows a comparison of the simulated mass of accreted ice per unit length $m_{\text{ice - CFD}}$ to the value obtained from image analysis $m_{\text{ice - image}}$ as a function of time during one hour of ice accretion. The ice mass was calculated using the expression given in equations A.7 - A.9, page 92 in Paper A.

As discussed in the previous section and in Paper A, there will always be uncertainties related to ice model results and to the validation data. In this study

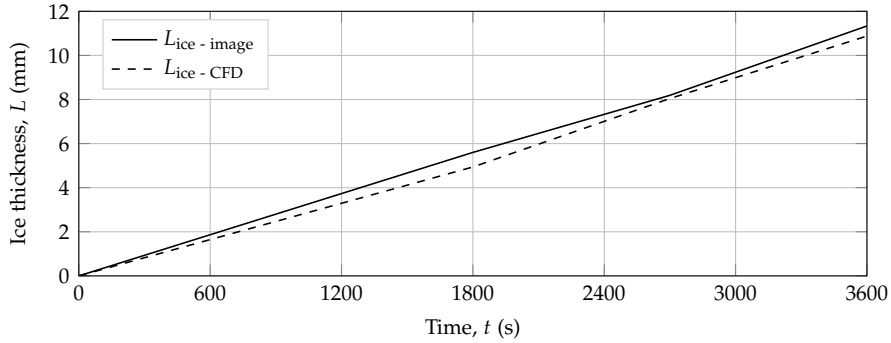

Figure 4.3: Comparison of the simulated ice thickness $L_{\text{ice - CFD}}$ and the ice thickness $L_{\text{ice - image}}$ obtained from image analysis found in [89] (Paper B).

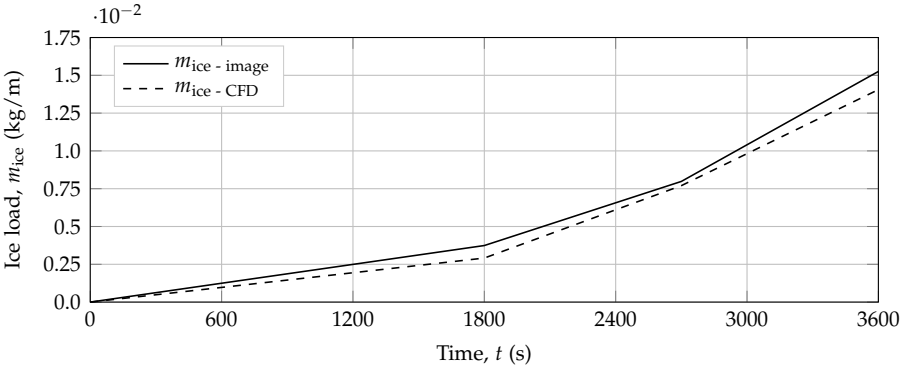

Figure 4.4: Comparison of the simulated mass of accreted ice $m_{\text{ice - CFD}}$ and the mass of accreted ice $m_{\text{ice - image}}$ obtained from image analysis as a function of time. The data of $m_{\text{ice - image}}$ was presented in [89] (Paper B).

it was desired to use data, which are most often available to the wind turbine owner/operator, such as the on-site measurements from met-masts and/or the wind turbine. The ice shapes and thickness were simulated using inlet boundary conditions based on on-site measurements and thus, the validation data should be created using the same meteorological conditions. And in this study image analysis was applied to find the maximum thickness. However, even though a method to update the inlet boundary conditions over time was established, as presented in Section 3.2 in Chapter 3, validation data have unfortunately not been available. Such validation data are pictures looking at the cross-section of the object exposed to icing. From such pictures, the ice shape could be extracted by image analysis. Thus, because of this fact, it was found reasonable to use constant inlet conditions and the validation by image

analysis as presented in Paper A and Paper B.

Discussion

Validation data could also have been obtained by experiments in climatic wind tunnels, from where the ice shape produced could be analysed in the lab and, amongst others, the cross-section of the ice shape and the maximum thickness would be available. Using that approach, the maximum thickness *and* the ice shape can be validated. Examples are also seen, for icing on airfoils, that the shapes are used to create solid geometries for wind tunnels for analysing of the aerodynamic changes in the lift and drag coefficients [92,93]. However, the problem of the ice specific parameters remains an issue. This was shown by A. Hudecz (2014) [93], who collected ice accretion profiles by performing experiments in a climatic wind tunnel facility at FORCE Technology in Kgs. Lyngby, Denmark[2] and by simulations using TURBICE, the panel-based code by VTT, described in Chapter 2.2.1 page 30. The simulated numerical results were compared directly to the experimental results with two purposes; 1) to validate the ice shapes and 2) to calibrate the wind tunnel parameters for liquid water content and MVD. The changes in lift and drag forces were obtained directly for the experimental obtained profiles by instruments in the wind tunnel and using ANSYS Fluent for the profiles obtained using TURBICE. However, as discussed, some ice specific parameters are still very difficult to measure directly, thus Hudecz (2014) wanted to calibrate those parameters by the numerical simulations of ice accretion. Rime, glaze and mixed ice were modelled in the wind tunnel, however since TURBICE uses constant input parameters, mixed ice, which implies a varying temperature, could not be simulated using the code. The comparison of numerical results by TURBICE and the wind tunnel results revealed that the numerical profiles were significantly smaller than the experimental. Thus, different combinations of the liquid water content and MVD were given to TURBICE with the aim to produce ice shapes like the experimental results. The study showed, that obtaining numerical results close to the experimental, required an increase in the liquid water content by 40 % and an increase by 42 % for MVD for rime ice accretion. Hudecz (2014) suggested, that MVD was larger than specified by the nozzle because of coalescence of droplets, and the vertical distribution of the liquid water content deviated because of deflection of droplets due to gravity because of the relatively low velocities of 5-10 m/s. This, furthermore, led to an increased ice deposit at the pressure side of the airfoils [93]. However, those differences might also be related to the difficulty of specifying and measuring cloud liquid water content W, MVD and N_c in a spray. The results from the study by Hudecz [93] and the

[2]The facility was established by a collaboration between the Technical University of Denmark (DTU) and FORCE Technology [93].

discussing in Section A.1 in Paper A is very interesting and clearly clarifies the importance of the defining a standard way of specifying the atmospheric and ice specific conditions for ice models for wind power applications.

4.2 Concluding Remarks on Simulating Icing Over Time

This Chapter reviewed the methodlogy developed for simulating icing over time by using on-site measurements. Furthermore the issues and uncertainties related to ice model boundary conditions were presented and dicussed. The dataset established and the proposed methodology were conducted based on the observations listed by the bullet points in Section 2.2.2 and the specified project objectives 2.a, 2.b and 3.a in Section 1.5. The following conclusions can be drawn from the work presented:

- A methodology was developed, which employs general data from a (wind farm) met-mast to construct a complete dataset of inlet boundary conditions and validation data for simulating icing over time. However, one must still pay attention to the uncertainties related to the prescribed droplet concentration N_c.
- Creating validation data using image analysis was shown to be (cost) effective, but pictures of the cross-section of the object exposed to icing would have been very useful, if using varying inlet boundary velocities over time.
- As a state-of-the-art, the methodology presented of simulating icing using on-site measurements and validating the ice thickness by ice thickness extracted from image analysis is unique and a very cost-effective approach for the wind farm owner to:
  - get a picture of the icing severity at a potential site
  - model the icing severity at an existing site
- By using the validated CFD Icing Model, presented in Paper B, new ice predictors can be obtained, which can be used as inputs to the production loss assessment framework described in Section 1.3 and seen in Figure A.1 in Paper A.

The use of cameras on the wind turbine itself to monitor icing, either by the wind turbine operator or the wind turbine manufacturer, is a growing trend. Thus, it is strongly believed by the author, that the methodology presented will also be applicable for simulating icing on the entire wind turbine blade or on a representative number of blade sections.

Chapter 5

Closure

This chapter summarises the main conclusion of the dissertation and an outlook is given with proposals for future work.

5.1 Conclusions

The contributions of this work are a CFD Icing Model and a methodology to simulate icing over time, which coupled together has the potential of improving the production loss assessment framework currently used (Section 1.3). The main contributions of the work were presented in Chapter 3 and 4 based on Paper A - F and are summarised as follows, in accordance with the project objectives and research questions (Section 1.5).

Development of a CFD icing model using ANSYS Fluent:
A 2D model CFD Icing Model was developed, where all processes of simulating icing work in an integrated composite unit. Known theory was implemented and available macros and User Defined Functions were used. It was concluded, that the best functionality was found by developing the model as a transient model where ice growth was calculated by the impingement model every timestep, from which the ice mass was converted to an ice thickness, which was added to the existing surface. The surface was moved by displacement vectors and the surface mesh was updated so that a good mesh quality was maintained. In this way, the actual flow field was considered in every time step. Thus, the collection efficiency is a function of the actual shape of the object exposed to icing and thereby the flow behavior and thus ice accretion was modelled in a dynamic manner. The mesh displacement algorithm was developed in the dynamic mesh environment using the DEFINE_GRID_MOTION macro.

Determination of inlet boundary conditions for the CFD-based icing model:
The work demonstrated that it is possible to establish boundary conditions for modelling icing using a CFD icing model using on-site measurements. It is concluded, that using on-site measurements is highly relevant because of the sampling time, which fits a CFD-based icing model very well. Furthermore, it was shown, that the ice specific parameters, such as cloud liquid water content and the median volume droplet diameter, can be found using the dataset. However, it should be emphasised, that since the parameters play a dominating role when modelling ice accretion, standards are currently needed in the industry to control the uncertainties related to these. Finally, this work demonstrated, that measurements can be used as constant inlet boundary conditions to simulate icing over one hour, as seen in Paper B, or by letting the boundary conditions be updated over time using the UDF developed.

Simulation of icing over time by a CFD-based icing model:
The main contribution of this work is a methodology to simulate and validate icing over time using general on-site met-mast data. As part of using on-site measurements the validation data was also found on-site, measured concurrently with the atmospheric conditions. Validation data obtained from image analysis was used to validate the modelled maximum ice thickness. The simulated maximum ice thickness after one hour corresponded very well to the results from image analysis and a small difference of 4% was found. However, validation data to evaluate the ice shape was not available and because of that, results using non-stationary boundary conditions have not been shown, even though the CFD Icing Model can handle non-stationary boundary conditions satisfactorily. Nevertheless, this work has demonstrated, that image analysis is a powerful tool for wind power applications to evaluate ice growth by thickness, shape and mass.

The dissertation has presented a multidisciplinary study, where a method to simulate icing over time has been developed in ANSYS Fluent using UDFs. A dataset consisting of weather data and images from sites was used to ensure realistic inlet boundary conditions for the model as well as validation data. Throughout the study, there has been a special focus on the final practical application.

5.2 Outlook

The perspectives of CFD Icing Model developed covers a wide field, from stall predictions to improved strength calculation (FEM calculations) and de-icing calculations for wind power applications. However, the author would like to suggest two topics for future work. The first is related to site assessment in cold climate regions and the potential impact of adding new ice predictors to the production loss assessment framework currently used as illustrated by Figure 1.11. The second topic is related to the physics of the CFD Icing Model.

As presented in Section 1.4, is it very relevant to enhance the possibilities of improving the modelling framework currently used for the production loss and production assessment for wind farms in a cold climate, by adding predictors established from a CFD Icing Model. To ensure a strong statistical foundation a database consisting of CFD simulations of ice accretion should be created for the wind turbine blade. Thus, it is suggested, that the blade is divided into n elements, exposed to several different angles of attack and freestream velocities. Furthermore, the ice specific parameters should be varied, which, all in all, leads to a multidimensional matrix. From such a matrix, a *database* can be created and the power degradation can be found from the different combinations by using for example the Blade Element Method. Figure 5.1 presents a suggestion to the practical *application* of the CFD Icing Model. The use of inlet boundary conditions obtained from NWP models, running with low time scales, should be considered for this application.

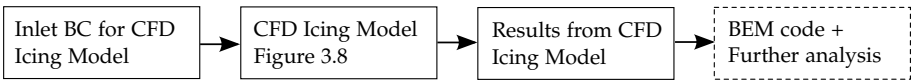

Figure 5.1: Illustration of the perspectives of the methodology of simulating icing over time (Figure 4.1 in Chapter 4) by using the results from the CFD Icing Model as inputs to a BEM code and for various future analysis.

Even though the CFD Icing Model developed in this work was able to produce a maximum ice thickness very similar to that obtained from image analysis, there are still some topics, which could be improved to ensure reliable simulated results. Since the atmospheric conditions resulting in an icing event varies from location to location and over time, the type of ice growth also varies, as seen in Figure 1.9 where *dry-growth* and *wet-growth* of ice are illustrated. The simulations of ice accretion presented were made assuming dry-growth of ice during in-cloud icing conditions. This is a simplification, since wet-growth of ice can also happen during in-cloud icing. Thus, in the future there might be a need to include a thermodynamic film model in the

flow diagram of the CFD Icing Model (Figure 3.8) as illustrated in Figure 5.2. Incorporating a thermodynamic film mode expands the icing conditions that can be modelled and will improve the overall accuracy of the model and its capabilities.

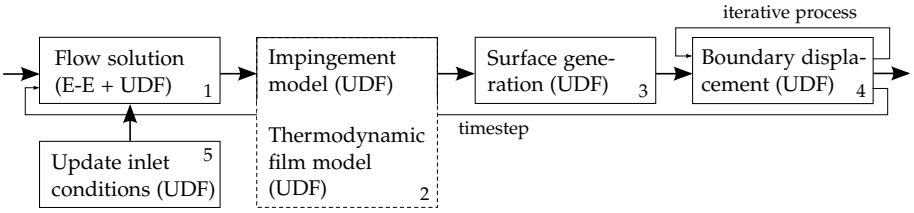

Figure 5.2: Flow diagram of the developed CFD icing model, showing the five steps seen in Figure 3.8, with an extension of step 2 to include a thermodynamic film model, which could be developed using available macros and UDFs.

References

[1] V. Lehtomäki, "Emerging from the cold." Wind Power Monthly, August 2016. http://www.windpowermonthly.com/article/1403504/emerging−cold.

[2] G. Ronsted, T. Wallenius, H. M., I. Baring-Gould, R. Cattin, M. Durstewitz, A. Krenn, T. Lakkso, A. Lacroix, L. Tallhaug, Ø. Kjedal, and E. Peltola, "State-of-the-Art of Wind Energy Cold Climate," tech. rep., IEA Wind Task 19, 2012.

[3] P. Frohboese and A. Anders, "Effects of icing on wind turbine fatigue loads," in *Journal of Physics: Conference Series*, vol. 75, p. 012061, IOP Publishing, 2007.

[4] R. Cattin, S. Kunz, A. Heimo, G. Russi, M. Russi, and M. Tiefgraber, "Wind turbine ice throw studies in the Swiss Alps," in *European Wind Energy Conference Milan*, 2007.

[5] S. Biswas, P. Taylor, and J. Salmon, "A model of ice throw trajectories from wind turbines," *Wind Energy*, vol. 15, no. 7, pp. 889–901, 2012.

[6] R. E. Bredesen and R. H. Ausland, "Methods for evaluating risk caused by ice throw and ice fall from wind turbines and other tall structures," in *16th International Workshop on Atmospheric Icing on Structures (IWAIS, Uppsala, Sweden, July 2015)*, 2015. http://iwais.org/proceedings/.

[7] Vattenfall, "Turbine icing program," September 2017. Internal material, https://corporate.vattenfall.com/.

[8] T. Lakkso, H. Holttinen, L. Ronsted, G. Tallhaug, R. Horbaty, I. Baring-Gould, A. Lacroix, E. Peltola, and B. Tammelin, "State-of-the-art of wind energy cold climates," tech. rep., IEA Wind Task 19, 2003.

[9] Navigant Research, "World market update 2012," tech. rep., Navigant Research, Copenhagen, Denmark, 2013. ISBN: 978-87-994438-4-0 .

[10] A. Krenn, J. J. Pieter, M. Wadham-Gagnon, N. Davis, N.-E. Clausen, V. Lehtomäki, T. Jokela, S. Kaila, G. Ronsten, H. Wickmann, R. Klintström, and R. Cattin, "Available technologies of wind energy in cold climates," tech. rep., IEA Wind Task 19, 2016.

[11] R. Bredesen, R. Cattin, N.-E. Clausen, J. P. Davis, Neil Jordaens, Z. Khadiri-Yazami, R. Klintström, A. Krenn, V. Lehtomäki, G. Ronsten, M. Wadham-Gagnon, and H. Wickmann, "13 wind energy projects in cold climate, 2. edition," tech. rep., IEA Wind, 2017.

[12] I. Baring-Gould, R. Cattin, M. Durstewitz, M. Hulkkonen, A. Krenn, T. Laakso, A. Lacroix, E. Peltola, G. Ronsten, L. Tallhaug, and T. Wallenius, "13 wind energy projects in cold climate, 1. edition," tech. rep., IEA Wind, 2011.

[13] Winterwind, "International wind energy conference," 2017.

[14] WindPower Monthly, "Optimizing wind power in cold climate," 2017. https://www.windpowermonthly.com/event/optimising-wind-farms-in-cold-climates.

[15] S. M. Fikke, G. Ronsten, A. Heimo, S. Kunz, M. Ostrozlik, P. Persson, J. Sabata, B. Wareing, B. Wichura, J. Chum, *et al.*, *COST 727: atmospheric icing on structures: measurements and data collection on icing: state of the art*. Meteo, Schweiz, 2006.

[16] Statnett, "Nordic power flow." Online, September 2017. http://www.statnett.no/.

[17] Nord Pool Group, "Historical market data." Online, September 2017. https://www.nordpoolgroup.com/historical-market-data/.

[18] D. Gustafsson, (project manager Vattenfall), "Vattenfall," September 2017. Internal correspondence, https://corporate.vattenfall.se/om-oss/var-verksamhet/var-elproduktion/vindkraft/pagaende-vindkraftprojekt/vindkraftprojekt-pa-land/blakliden-och-fabodberget/.

[19] R. Cattin, "Evaluation of ice detection systems for wind turbines, final report," Tech. Rep. VGB Research Project No. 392, METEOTEST, Andermatt, Switzerland, 2016.

[20] T. Laakso, I. Baring-Gould, M. Durstewitz, R. Horbaty, A. Lacroix, E. Peltola, G. Ronsten, L. Tallhaug, and L. T. . T. W. Walenius T. Göran Ronsten, "State-of-the-art of wind energy in cold climates," tech. rep., VTT Technical Research Centre of Finland, 2010. http://www.vtt.fi/inf/pdf/workingpapers/2010/W152.pdf.

[21] iso, "Atmospheric icing on structures, iso 12494:2001(e)," tech. rep., ISO, Geneva, Switzerland, 2001.

[22] M. Bragg, A. Broeren, H. Addy, M. Potapczuk, D. Guffond, and E. Montreuil, "Airfoil ice-accretion aerodynamic simulation," in *45th AIAA Aerospace Sciences Meeting and Exhibit*, p. 85, 2007. http://icing.ae.illinois.edu/papers/07/AIAA-2007-0085.pdf.

[23] D. Switchenko, W. G. Habashi, G. Baruzzi, and I. Ozcer, "Fensap-ice simulation of complex wind turbine icing events, and comparison to observed performance data," in *32nd ASME Wind Energy Symposium*, p. 1399, 2014.

[24] H. Wickman, "Evaluation of field tests of different ice measurement methods for wind power," Master's thesis, 2013. http://www.diva-portal.org/smash/record.jsf?pid=diva2

[25] Campbell Scientific (Canada) Corp., "0872f1 ice detector," tech. rep., 2018. https://www.campbellsci.eu/0872f1.

[26] COMBITECH AB, "The ice load surveillance sensor icemonitor^{TM}," tech. rep., 2018. http://www.rwis.net/res/pdffiles/icemonitor_web1.pdf.

[27] Labkotec, "Lid-3300ip ice detector, installation and operating instructions," tech. rep., 2018. https://www.labkotec.fi/sites/default/files/tiedostot/d80186je-3-4372_0.pdf.

[28] HoloOptics, "User guide, t40 series of icing rate sensors^{TM}, user guide edition 2.0," tech. rep., 2018. http://holooptics.utrymmet.com/Dokument/651.Userguide%20T40.004.En.pdf.

[29] M. Wadham-Gagnon, N. Swytink-Binnema, D. Bolduc, K. Tété, and C. Arbez, "Ice detection methods and measurement of atmospheric icing," in *16th International Workshop on Atmospheric Icing on Structures (IWAIS, Uppsala, Sweden, July 2015)*, IWAIS, 2015. http://iwais.org/proceedings/.

[30] UCAR - National Center for Atmospheric Research, "Weather research and forecasting model." Online, February 2018. https://www.mmm.ucar.edu/weather-research-and-forecasting-model.

[31] Naval Research Laboratory, Monterey Marine Meteorology Division (Code 7500), "Coupled ocean/atmosphere mesoscale prediction system." Online, February 2018. https://www.nrlmry.navy.mil/coamps-web/web/home.

[32] J. Nissen Nielsen, *On the application of a numerical model to simulate the coastal boundary layer*. PhD thesis, Faculty of Science, Univerity of Copenhagen, Denmark, 2008. Risø-PhD-39(EN), ISBN: 978-87-550-3682-6.

[33] G. Thompson, B. E. Nygaard, L. Makkonen, and S. Dierer, "Using the weather research and forecasting (wrf) model to predict ground/structural icing," in *13th International Workshop on Atmospheric Icing on Structures*, IWAIS, 2009. http://iwais.compusult.net/html/IWAIS_2013_Proceedings.pdf.

[34] L. Makkonen, "Models for the growth of rime, glaze, icicles and wet snow on structures," *Philosophical Transactions of the Royal Society of London A: Mathematical, Physical and Engineering Sciences*, vol. 358, no. 1776, pp. 2913–2939, 2000.

[35] Ø. Byrkjedal, J. Hansson, and H. van der Velde, "Development of Operational Forecasting for Icing and Wind Power at Cold Climate Sites," in *16th International Workshop on Atmospheric Icing on Structures (IWAIS, Uppsala, Sweden, July 2015)*, 2015. http://www.vindteknikk.no/_extension/media/336/orig/IWAIS2015_Paper_Byrkjedal.pdf.

[36] N. Davis, *Icing Impacts on Wind Energy Production*. PhD thesis, The Technical University of Denmark, , DTU Wind Energy, 2014. ISBN: 978-87-92896-61-2.

[37] N. Davis, A. N. Hahmann, N.-E. Clausen, and M. Žagar, "Forecast of icing events at a wind farm in sweden," *Journal of Applied Meteorology and Climatology*, vol. 53, no. 2, pp. 262–281, 2014.

[38] J. I. Madsen, (Wind R&D portfolio manager Vattenfall), "TIP - Turbine Icing Program (R&D)," October 2014. Internal presentation.

[39] Y. Bourgault, Z. Boutanios, and W. G. Habashi, "Three-Dimensional Eulerian Approach to Droplet Impingement Simulation Using FENSAP-ICE, Part 1: Model, Algorithm, and Validation," *Journal of Aircraft*, vol. 37, no. 1, pp. 95–103, 2000.

[40] Y. Bourgault, H. Beaugendre, and W. G. Habashi, "Development of a shallow-water icing model in fensap-ice," *Journal of Aircraft*, vol. 37, no. 4, pp. 640–646, 2000.

[41] NTI, *User Manual FENSAP-ICE, Version 2012 release 1.1*, 2012. Manual.

[42] I. P. Mazin, "Cloud water content in continental clouds of middle latitudes," *Atmospheric research*, vol. 35, no. 2, pp. 283–297, 1995.

[43] Y. Gjessing, A. Skartveit, and K. Utaaker, "Vurdering av sikt -og vindforhold på hurumåsen," tech. rep., Meteorological report series, Universitetet i Bergen, Norway, 1990.

[44] Flight Safety Foundation (Aviation Safety Network), "McDonnell Douglas DC-9-81 (MD-81)." Online, February 2018. https://aviation-safety.net/database/record.php?id=19911227-0.

[45] B. L. Messinger, "Equilibrium Temperature of an Unheated Icing Surface as a Function of Air Speed," *Journal of the Aeronautical Sciences (Institute of the Aeronautical Sciences)*, vol. 20, no. 1, pp. 29–42, 1953.

[46] L. Makkonen, "Notes: Estimating intensity of atmospheric ice accretion on stationary structures," *Journal of applied meteorology*, vol. 20, pp. 595–600, 1981.

[47] L. Makkonen, "Modelling of ice accretion on wires," *Journal of Climate and Applied Meteorology*, vol. 23, pp. 929–939, 1984.

[48] L. Makkonen, "Heat transfer and icing of a rough cylinder," *Cold Regions Science and Technology*, vol. 10, pp. 105–116, 1985.

[49] L. Makkonen and J. Stallabrass, "Experiments on the cloud droplet collision efficiency of cylinders," *Journal of climate and applied meteorology*, vol. 26, no. 10, pp. 1406–1411, 1987.

[50] L. Makkonen, "Estimation of wet snow accretion on structures," *Cold Regions Science and Technology*, vol. 17, pp. 83–88, 19895.

[51] L. Makkonen, "Analysis of rotating multicylinder data in measuring cloud-droplet size and liquid water content," *Journal of Atmospheric and Oceanic Technology*, vol. 9, no. 3, pp. 258–263, 1992.

[52] G. A. Ruff and B. M. Berkowitz, "Users manual for the NASA Lewis ice accretion prediction code (LEWICE)," 1990. https://ntrs.nasa.gov/archive/nasa/casi.ntrs.nasa.gov/19900011627.pdf.

[53] W. B. Wright, *User's Manual for LEWICE Version 3.2*, 2008.

[54] J. L. Hess and A. O. Smith, "Calculation of potential flow about arbitrary bodies," *Progress in Aerospace Sciences*, vol. 8, pp. 1–138, 1967.

[55] W. B. Wright, R. W. Gent, and G. D., "DRA/NASA/ONERA collaboration on icing research part II - prediction of airfoil accretion," tech. rep., 1997. https://ntrs.nasa.gov/archive/nasa/casi.ntrs.nasa.gov/19970023937.pdf.

[56] W. B. Wright, "Validation Process for LEWICE by Use of a Naviér-Stokes Solver," in *8th AIAA Atmospheric and Space Environments Conference*, p. 4349, 2016.

[57] W. B. Wright, "A Revised Validation Process for Ice Accretion Codes," in *9th AIAA Atmospheric and Space Environments Conference*, p. 3415, 2017.

[58] NASA Glenn Research Center, "Software: LEWICE and LEWICE3D." Online, February 2018. https://www1.grc.nasa.gov/aeronautics/icing/software/.

[59] T. Hedde and D. Guffond, "ONERA three-dimensional icing model," *AIAA journal*, vol. 33, no. 6, pp. 1038–1045, 1995.

[60] P. Villedieu, P. Trontin, D. Guffond, and D. Bobo, "SLD Lagrangian modeling and capability assessment in the frame of ONERA 3D icing suite," in *4th AIAA Atmospheric and Space Environments Conference*, p. 3132, 2012.

[61] L. Makkonen, T. Laakso, M. Marjaniemi, and K. Finstad, "Modelling and prevention of ice accretion on wind turbines," *Wind Engineering*, vol. 25, no. 1, pp. 3–21, 2001.

[62] K. Beard and H. Pruppacher, "A determination of the terminal velocity and drag of small water drops by means of a wind tunnel," *Journal of the Atmospheric Sciences*, vol. 26, no. 5, pp. 1066–1072, 1969.

[63] I. Langmuir, K. Blodgett, *et al.*, "Mathematical investigation of water droplet trajectories," 1946.

[64] H. Beaugendre, F. Morency, and W. G. Habashi, "Development of a second generation in-flight icing simulation code," *Journal of fluids engineering*, vol. 128, no. 2, pp. 378–387, 2006.

[65] H. Beaugendre, F. Morency, and W. G. Habashi, "Fensap-ice's three-dimensional in-flight ice accretion module: Ice3d," *Journal of Aircraft*, vol. 40, no. 2, pp. 239–247, 2003. http://arc.aiaa.org/doi/abs/10.2514/2.3113.

[66] W. G. Habashi, J. Dompierre, Y. Bourgault, M. Fortin, and M.-G. Vallet, "Certifiable computational fluid dynamics through mesh optimization," *AIAA journal*, vol. 36, no. 5, pp. 703–711, 1998.

[67] C. N. Aliaga, M. S. Aubé, G. S. Baruzzi, and W. G. Habashi, "Fensap-ice-unsteady: Unified in-flight icing simulation methodology for aircraft, rotorcraft, and jet engines," *Journal of Aircraft*, vol. 48, no. 1, pp. 119–126, 2011.

[68] ANSYS, Inc., *ANSYS Fluent User's Guide*, 2017.

[69] T. Reid, G. Baruzzi, I. Ozcer, D. Switchenko, and W. Habashi, "Fensap-ice simulation of icing on wind turbine blades, part 1: Performance degradation," in *51st AIAA aerospace sciences meeting including the new horizons forum and aerospace exposition, Grapevine, Texas*, pp. 7–10, 2013.

[70] T. Reid, G. Baruzzi, I. Ozcer, D. Switchenko, and W. G. Habashi, "Fensap-ice simulation of icing on wind turbine blades, part 2:ice protection system design," in *51st AIAA aerospace sciences meeting including the new horizons forum and aerospace exposition, Grapevine*, 2013.

[71] R. Gent, N. Dart, and J. Cansdale, "Aircraft icing," *Philosophical Transactions of the Royal Society of London A: Mathematical, Physical and Engineering Sciences*, vol. 358, no. 1776, pp. 2873–2911, 2000.

[72] M. Etemaddar, M. O. L. Hansen, and T. Moan, "Wind turbine aerodynamic response under atmospheric icing conditions," *Wind Energy*, vol. 17, no. 2, pp. 241–265, 2014.

[73] J. Jonkman, S. Butterfield, W. Musial, and G. Scott, "Definition of a 5 - MW Reference Wind Turbine for Offshore System Development," tech. rep., 2009. https://www.nrel.gov/docs/fy09osti/38060.pdf.

[74] T. J Larsen and A. M. Hansen, "How 2 HAWC2, the user's manual," tech. rep., 2007. http://orbit.dtu.dk/en/publications/how-2-hawc2-the-users-manual

[75] L. Hu, X. Zhu, C. Hu, J. Chen, and Z. Du, "Wind turbines ice distribution and load response under icing conditions," *Renewable Energy*, vol. 113, pp. 608–619, 2017.

[76] S. Wirogo and S. Srirambhatla, "An Eulerian Method to Calculate the Collection Efficiency on Two and Three Dimensional Bodies," in *41st Aerospace Sciences Meeting and Exhibit, Reno, Nevada*, vol. 1073, 2003.

[77] L. Hu, X. Zhu, C. Hu, J. Chen, and Z. Du, "Calculation of the water droplets local collection efficiency on the wind turbines blade," *Journal of Energy Resources Technology*, vol. 139, no. 5, p. 051211, 2017.

[78] Y. Cao, Q. Zhang, and J. Sheridan, "Numerical simulation of rime ice accretions on an aerofoil using an eulerian method," *The Aeronautical Journal*, vol. 112, no. 1131, pp. 243–249, 2008.

[79] Y. Cao, G. Zhong, and C. Ma, "Numerical simulation of ice accretion prediction on multiple element airfoil," *Science China Technological Sciences*, vol. 54, no. 9, pp. 2296–2304, 2011.

[80] Y. Cao, C. Ma, Q. Zhang, and J. Sheridan, "Numerical simulation of ice accretions on an aircraft wing," *Aerospace Science and Technology*, vol. 23, no. 1, pp. 296–304, 2012.

[81] Y. Cao, J. Huang, and J. Yin, "Numerical simulation of three-dimensional ice accretion on an aircraft wing," *International Journal of Heat and Mass Transfer*, vol. 92, pp. 34–54, 2016.

[82] F. Villalpando, M. Reggio, and A. Ilinca, "Prediction of ice accretion and anti-icing heating power on wind turbine blades using standard commercial software," *Energy*, vol. 114, pp. 1041–1052, 2016.

[83] T. G. Myers, "Extension to the messinger model for aircraft icing," *AIAA journal*, vol. 39, no. 2, pp. 211–218, 2001.

[84] C. T. Crowe, *Multiphase Flow Handbook*. CRC Press, Taylor & Francis Group, 6000 Broken Sound Parkway NW, Suite 300, Boca Raton, FL 33487-2742, USA: Taylor & Francis, 1 ed., 2006.

[85] ANSYS, Inc., *ANSYS Fluent Theory Guide*, 2017.

[86] Z. Boutanios, "An Eulerian 3D analysis of water droplets impingement on a Convair-580 nose and cockpit geometry," Master's thesis, Concordia University, 1999.

[87] Ansys, Inc., *ANSYS Fluent Costumization Manual*, 2017.

[88] M. C. Pedersen, H. Sørensen, N. Swytink-Binnema, and T. Condra, "Computational fluid dynamics analysis and field measurements on ice accretion on a cup anemometer support arm," *Applied Thermal Engineering*, vol. 135, pp. 530–536, 2018.

[89] M. C. Pedersen, H. Sørensen, N. Swytink-Binnema, B. Martinez, and T. Condra, "Measurements from a cold climate site in canada: Boundary conditions and verification methods for cfd icing models for wind turbines," *Cold Regions Science and Technology*, vol. 147, pp. 11–21, 2017.

[90] B. E. K. Nygaard, J. E. Kristjánsson, and L. Makkonen, "Prediction of In-cloud Icing Conditions at Ground Level Using the WRF Model," *Journal of Applied Meteorology and Climatology*, vol. 50, no. 12, pp. 2445–2459, 2011.

[91] F. Lamraoui, G. Fortin, R. Benoit, J. Perron, and C. Masson, "Atmospheric icing impact on wind turbine production," *Cold Regions Science and Technology*, vol. 100, pp. 36–49, 2014.

[92] P. M. Blasco, J. Palacios, and S. Schmitz, "Investigation of wind turbine power generation during atmospheric icing by multi-disciplinary experimentation," in *33rd Wind Energy Symposium*, p. 0496, 2015.

[93] A. Hudecz, *Icing Problems of Wind Turbine Blades in Cold Climates*. PhD thesis, Department of Wind Energy, Technical University of Denmark, 2014. ISBN: 978-87-92896-80-3.

[94] National Instruments, "NI Vision, National Instruments," 2016.

[95] EasyCalculation.com, "How to calculate dewpoint and wet bulb temperature - tutorial, formula, example." Online, January 2016. https://www.easycalculation.com/weather/learn-dewpoint-wetbulb.php.

[96] K. J. Finstad, E. P. Lozowski, and L. Makkonen, "On the Median Volume Diameter Approximation for Droplet Collision Efficiency," *Journal of the atmospheric sciences*, vol. 45, no. 24, pp. 4008–4012, 1988.

[97] C. Son, S. Oh, and K. Yee, "Quantitative analysis of a two-dimensional ice accretion on airfoils," *Journal of mechanical science and technology*, vol. 26, no. 4, pp. 1059–1071, 2012.

Part II

Appendices

Appendix 1

Proposed Method for Image Analysis

In Paper B the CFD results were validated using data from image analysis, which were collected by TechnoCentre éolien (TCE). Due to right causes the data treatment and the image analysis tool cannot be described with full details in this dissertation. Thus, this appendix presents a method developed, to extract the ice thickness L_{ice} from images, which is an alternative method to the one presented in Paper A, Section A.2.6. The method was developed using the software LabVIEW by National Instruments [94] and can conduct image analysis of similar pictures with an accuracy like the one used in Paper B. The method is explained by the flow diagram in Figure 1.1, where ice accretion on a circular cylinder is used as an example.

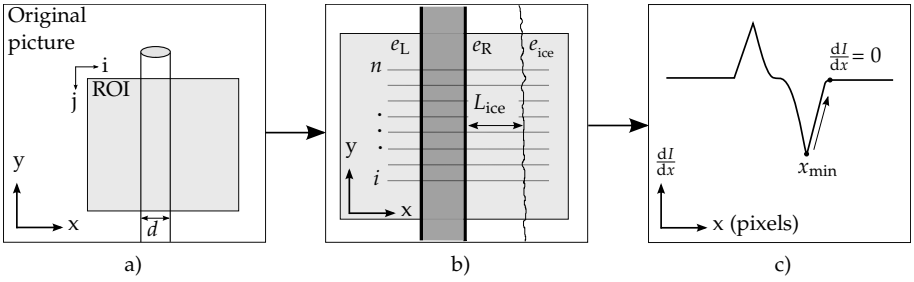

Figure 1.1: Flow diagram of image analysis, a) original picture and definition of region of interest (ROI), b) n numbers of line profiles are added. The line profiles span from the left side in the ROI, over the left edge, e_L, of the object to the right edge, e_R, and further over the accreted ice mass thickness marked with L_{ice}. And c) grey scale intensity along the n number of line profiles were analysed by two approached, depending on the picture background, to obtain the pixel location of the edge of the accreted ice e_{ice}.

The approach is based on the following assumptions:

- The camera should be fixed and has a constant distance to the object exposed to icing
- The object exposed to icing does not move in the picture
- The object exposed to icing has a known diameter before ice accretion
- A calibration number, *cn* between the picture-plane and object-plane can be found in mm/pixels
- Ice only grows in one direction (x-direction in this example), equivalent to the definitions by ISO Standard 12494 [21]

As seen from Figure 1.1 the first step a) is to define Region Of Interest (ROI) on the original image and prepare the pictures, so that the background can be separated from the ice rear edge e_{ice}. From experience, it was found that a good solution for in-cloud icing was to apply a mean filter in the y-direction, while the ice thickness was detected in the x-direction. Any noise could then be smoothened out by the mean filter, so that e_{ice} could be identified. Since the ice thickness is likely to vary in the vertical direction on a cylinder, several line profiles should be added to the frame to find the vertical distribution or a good measure of the average thickness, see Figure 1.1 b). In this way the ice thickness L_{ice} was defined in every ROI as follows:

$$L_{\text{ice}} = \frac{1}{n} \sum_{i=n}^{n} L_{\text{ice,i}} \tag{1.1}$$

where is n is the number of line profiles within the ROI. The gradients of a grey-scale intensity plot along the pixels of the line profiles can be used to detect the edge of the object exposed to icing and the ice rear edge, see Figure 1.1 c). The ice thickness at every line profile, $L_{\text{ice,i}}$ is obtained at the distance from the right edge of the object to the rear edge of the ice times the scaling factor, as follows:

$$L_{\text{ice,i}} = cn(e_{\text{ice}} - e_{\text{R}}) \tag{1.2}$$

When performing image analysis for icing applications and during icing events, every picture is most likely different. In this work, it was found, that the appearance of the object exposed to icing in comparison to the background would determine the treatment of each picture in the algorithm. To solve this, the pictures were divided into two categories, which *will* determine the approach of identifying the ice rear edge as follows:

- Category 1: the ice rear edge is found by looping (left to right) over the pixels from the minimum gradient value until the pixel where $\mathrm{d}I/\mathrm{d}x = 0$, see example Figure 1.1 c).

- Category 2: the ice rear edge is found by looping (right to left) and identifying the maximum pixel gradient, followed by identifying the pixel where $\mathrm{d}I/\mathrm{d}x = 0$. See example Figure 1.1 c).

Appendix 1. Proposed Method for Image Analysis

Appendix 2

Calculation of the Adiabatic Cloud Water Gradient

In Paper A the cloud liquid water content, W_c, was found by a method proposed by Gjessing et al. (1990) [43] based on the difference between the location of measurement equipment and the cloud base, the wet bulb temperature, θ_w and the adiabatic cloud water gradient, δ. The wet bulb temperature was calculated based on the measurements of T, RH and P by an iterative process, by solving the equations described below [95].

The dew point temperature T_{dew} was calculated as follows:

$$T_{dew} = \frac{243.5 \ln\left(\frac{P_v}{6.112}\right)}{17.67 - \ln\left(\frac{P_{vs}}{6.112}\right)} \tag{2.1}$$

where

$$P_v = P_{vs}\left(\frac{RH}{100}\right)$$

$$P_{vs} = 6.112 e^{\left(\frac{17.67T}{T+243.5}\right)}$$

where P_v is the vapour pressure, P_{vs} is the saturated vapour pressure and P the measured pressure in kPa. The wet bulb temperature θ_w was found when the absolute vapour pressure difference $\Delta P_v \leq 0.05$ as follows:

$$
\begin{aligned}
P_{\mathrm{vs,w}} &= 6.112e^{\left(\frac{17.67\theta_{\mathrm{w}}}{\theta_{\mathrm{w}}+243.5}\right)} \\
P_{\mathrm{v,w}} &= P_{\mathrm{vs,w}} - P(T-\theta_{\mathrm{w}})0.00066(1+0.00115\theta_{\mathrm{w}}) \\
\Delta P_{\mathrm{v}} &= P_{\mathrm{v}} - P_{\mathrm{v,w}}
\end{aligned}
\tag{2.2}
$$

Using the measurements of T, RH and P presented in Paper A, Figure A.7, the wet bulb temperature and corresponding adiabatic cloud water gradient used in Paper A are seen in Figure 2.1 and Figure 2.2, respectively.

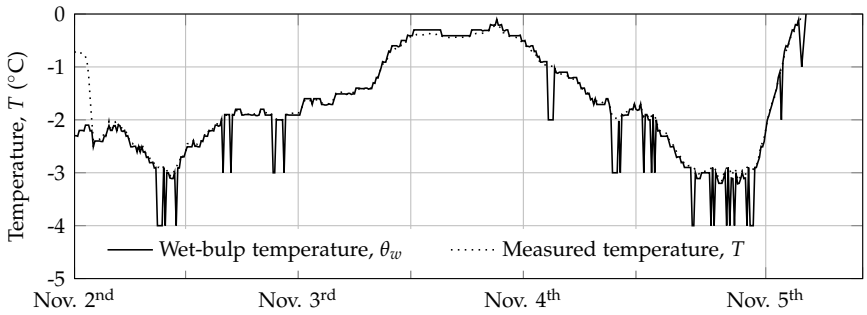

Figure 2.1: Calculated wet bulb temperature θ_{w} and the measured temperature T from icing event November 2nd to November 5th.

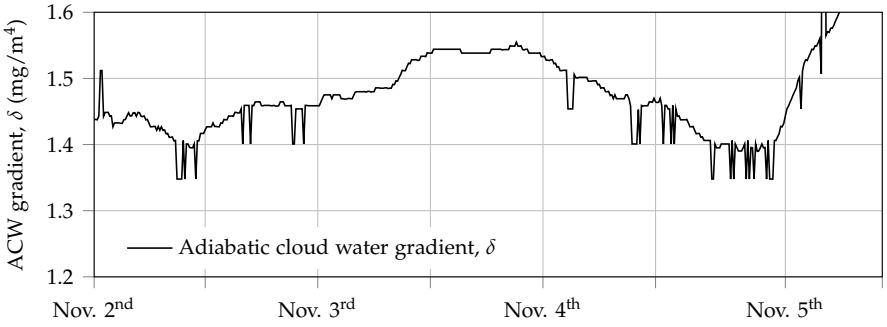

Figure 2.2: Calculated adiabatic cloud water (ACW) gradient δ from icing event November 2nd to November 5th.

Part III

Papers

Paper A

Measurements from a Cold Climate Site in Canada: Boundary Conditions and Verification Methods for CFD Icing Models for Wind Turbines

Marie Cecilie Pedersen, Henrik Sørensen,
Nigel Swytink-Binnema, Benjamin Martinez
and Thomas Condra

The paper has been published in *Cold Regions Science and Technology* Vol. 147, pp. 11–21, March 2018, https://doi.org/10.1016/j.coldregions.2017.12.007

The layout has been revised.

Measurements from a Cold Climate Site in Canada: Boundary Conditions and Verification Methods for CFD Icing Models for Wind Turbines

M. C. Pedersen [a,b], H. Sørensen[b], N. Swytink-Binnema[c], B. Martinez[b] and T.J. Condra[b]

[a] *Vattenfall Vindkraft A/S, Jupitervej 6, DK-6000 Kolding, Denmark*
[b] *Aalborg University, Department of Energy Technology, Pontoppidanstræde 111, DK-9220 Aalborg, Denmark*
[c] *TechnoCentre éolien, 70 rue Bolduc, Gaspé (Québec) G4X 1G2, Canada*

Abstract

This study presents an analysis of icing measurements from a cold climate site in Canada. The collected dataset provides a set of inlet boundary conditions suitable for the modelling of icing events. The study attempts to quantify the uncertainties associated with the established boundary conditions. To construct the dataset, effort was put in determining the icing specific atmospheric variables. In particular, two methods for retrieving the cloud liquid water content and the associated droplet size were used. Furthermore, ice growth was measured on a cup anemometer support arm to provide an experimental comparison. From image analysis the ice growth was observed. The resulting dataset can provide inlet boundary conditions for simulating an icing event and additionally a set of data used for verification purposes.

Keywords: ice detection; cloud liquid water content; boundary conditions; production losses; wind turbines

A.1 Introduction

Northern regions with cold climate or high altitudes are attractive for wind energy harvesting because of favourable wind conditions, low temperatures and so high air density [31]. Additionally, cold climate areas are most often remote and have a low population density, unlike many continental onshore sites. However, wind power in cold climates faces challenges due to the often harsh weather conditions, which lead to icing of the wind turbine and a number of icing induced risks. These risks are all caused by the complex phenomena of *atmospheric icing* and include, amongst others, reduced

power production, reduced wind turbine life time, noise emissions and the risk of ice shedding. The magnitude of the icing induced risks is a major concern for wind turbine owners and challenges the future development of wind power in cold climates. In 2002, IEA WIND Task 19 was established to gather information and provide recommendations for developing wind energy in cold climate. This led to the first state-of-the-art report being published in 2003 [22]. Since then, the installed capacity has expanded [29] and with the new energy targets, the industry is aiming to establish more knowledge and optimum solutions for the future wind energy projects in cold climates .

Atmospheric icing is a complex phenomenon; it is difficult to measure and to model. The phenomenon covers all processes where any phase of water freezes or sticks to a surface, *e.g.* an aircraft wing, sea-going vessels or wind turbine blades. In general terms the phenomenon can be divided into two main processes; precipitation icing and in-cloud icing. Precipitation icing covers ice accretion from freezing rain, drizzle and wet snow; whereas in-cloud icing happens when a cloud of heavy fog, consisting of super-cooled water droplets, meets an object and freezes upon contact [19]. When modelling ice accretion or ice loads for wind power applications, it is common practice to assume in-cloud icing [34], even though an icing event might consist of a combination of in-cloud icing and different types of precipitation [35].

The flow diagram in Figure A.1 presents the typical modelling framework for evaluating production losses or the expected production for wind farms in cold climate. The modelling framework is at present the most used and widely accepted approach within the community. Currently, the modelling framework consists of three steps: 1) atmospheric data is obtained from mesoscale Numerical Weather Prediction (NWP) models. The data includes amongst others; wind speeds (v), temperature (T), relative humidity (RH) and the cloud liquid water content (W). From the W and a droplet concentration (N_c), the droplet size, *e.g.* the median volumetric diameter (MVD), is derived, typically following Thompson et al. (2009) [33]. 2) The atmospheric conditions (*i.e.* ice model boundary conditions) are fed into an empirical icing model, typically based on Makkonen's ice model [27] to retrieve an ice load. The ice load is typically validated according to standard icing, defined in the ISO standard 12494 (2001) [19]. Standard icing is defined as the ice accretion occurring on a rod with diameter of 0.03 m and a length of 0.5 m which can freely rotate and a constant diameter is assumed during the ice accretion. 3) The ice load is used as a predictor to a statistical model. The statistical model is trained by the predictors to obtain the target. The target could be to predict the aggregated production losses of a wind farm or the expected aggregated production. If SCADA data is available, the training data of the production losses due to icing could be obtained by following the standardised power

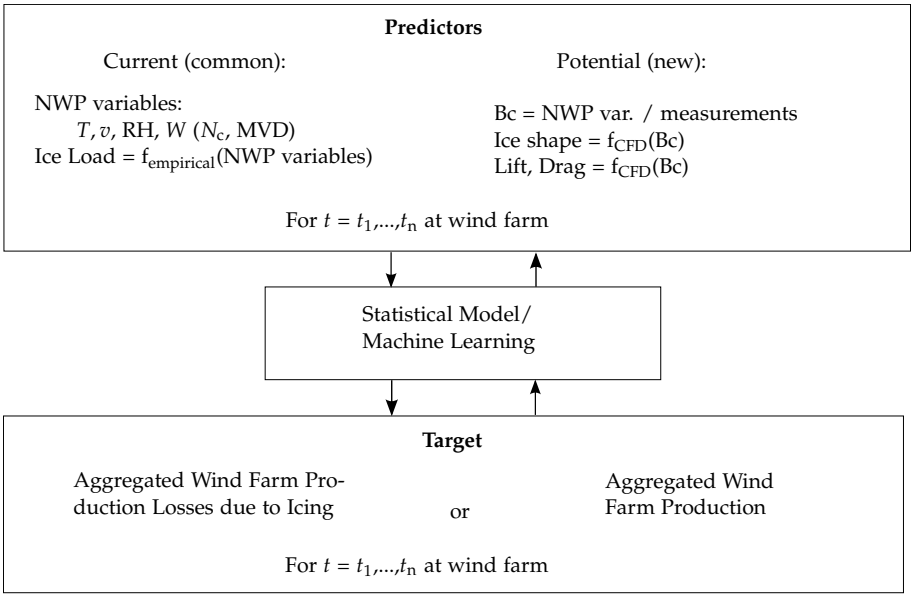

Figure A.1: Typically used modelling framework for evaluating wind farm production and wind farm production losses due to icing over time (t). The currently used predictors are seen to the left in the topmost box and the proposed new predictors are seen to the right in the topmost box (Bc = Boundary conditions).

curve method by the IEA Wind Task 19 [21]. Byrkjedal et al. (2015) [9] used the ice load to fit a three-dimensional power curve to estimate power production, when the wind turbine was iced, and Davis et al. (2014) [11] proposed a power loss approach using different power forecast models, which were refined in Davis (2014) [10]. Other models based on neural networks, using ice load and NWP model results were presented at the Winterwind conference [3]. Besides forecasting, the framework (Figure A.1) has also been used to produce icing maps of, for instance, Finland, Sweden and Norway ([14] and [8]) or furthermore for more detailed icing maps as seen in Figure A.2, for the Gaspé Peninsula in the south-eastern part of Québec, Canada [25]. The icing map colouring varies from ice class 2, corresponding to intermediate icing frequency along the coast, to class 5 more inland, which corresponds to moderate to a high icing frequency.

Following the modelling framework (Figure A.1) it is possible to obtain production losses over large time scales ($t = t_1,...,t_n$) with a relatively low processing time. However, small scale details of ice accretion and the aerodynamic changes of the lift and drag forces are not captured, as a result of the empirical ice model approach [27]. Davis et al. (2014) [11] showed improved results

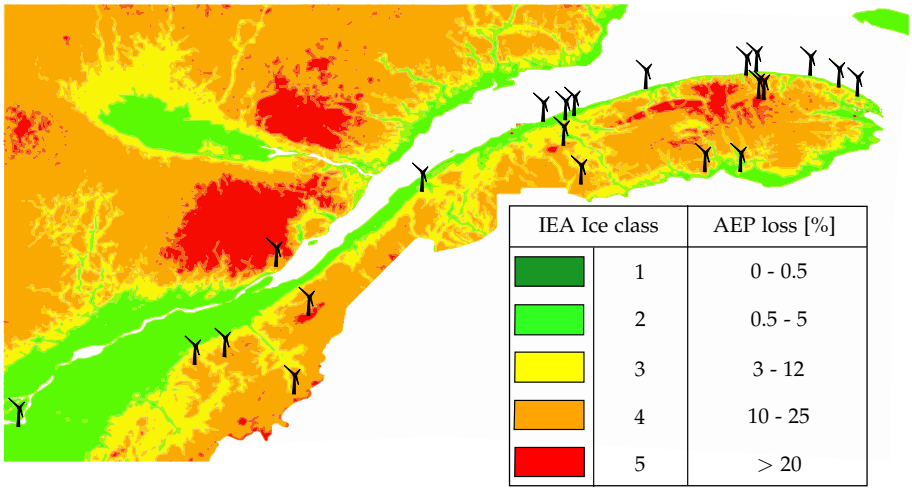

Figure A.2: Icing map of the Gaspé Peninsula in the south easterly part of Québec, Cananda [25]. The icing map is coloured according to the IEA ice class definition and the corresponding percentage loss of the annual energy production (AEP) [4].

by representing the wind turbine as a 1 m long cylinder with a diameter based on a reference turbine, instead of the a rotating cylinder. However, the model did not update the diameter of the object exposed to icing and adding such an ice shape-parameter as a predictor is expected to improve the modelling framework. At this time, it is unknown, whether including the small-scale effects, such as the ice shape, and the lift and drag forces as predictors will improve the modelling framework. Studies by Davis (2014) [10] point in this direction and suggest, for future research, the use of a more advanced ice model to obtain the ice load, for example based on computational fluid dynamics (CFD). Implementing predictors from a dynamic CFD-based ice model into Figure A.1 is a new approach, and to ensure dynamic transient modelling of ice accretion, rethinking of the inlet boundary conditions is required. This is due to a big time scale difference between a standard ice model using NWP variables and a CFD-based ice model, which is in the order of 10^6 as illustrated:

$$\begin{aligned} \Delta t_{\text{CFD}} &\approx \mathcal{O}(10^{-3}\text{s}) \\ \Delta t_{\text{NWP}} &\approx \mathcal{O}(1\text{h}) \\ \frac{\Delta t_{\text{NWP}}}{\Delta t_{\text{CFD}}} &= \frac{\mathcal{O}(1\text{h})}{\mathcal{O}(10^{-3}\text{s})} \approx 10^6 \end{aligned} \tag{A.1}$$

This study aims to construct a dataset consisting of boundary conditions and validation data for CFD-based predictors, which can be added to modelling framework (Figure A.1). Validation data are needed, since a CFD-based

icing model would update the shape of the object exposed to icing over time. Therefore, besides using the ice load, it is interesting to validate the thickness of the accreted ice and the ice shape. On-site observation of the ice shape can be obtained by ice detection using web cameras [21]. In this study using image analysis. Because of the time scale issue (Equation A.1) the use of on-site measurements from a cold climate site in Canada was found ideal for establishing the dataset. The dataset is gathered with the following objectives:

- Establish inlet boundary conditions based on measurements
- Estimate W from temperature measurements and cloud base height
- Construct validation data through image analysis

The approach of how to retrieve specific icing parameters is presented in the following section. This is followed by a presentation of the measurements and the methods used to obtain the ice specific parameters and the validation data.

A.2 Method

A.2.1 Icing Event Parameters

Atmospheric icing is difficult to model, particularly because of the ice specific parameters; such as the cloud liquid water content and the corresponding droplet concentration and droplet size. Currently, no standard way of measuring the cloud liquid water and droplet size is available for low-level clouds [21]. As illustrated by Figure A.1, obtaining the parameters from NWP models is an option, but studies have shown, that the modelled cloud liquid water content strongly depends on the choice of parametrisation scheme. Nygaard et al. [30] used three different parametrisation schemes in the NWP model WRF (Weather Research and Forecasting model) and three different model resolutions. The model would predict the cloud liquid water quite accurate at the lowest model resolution but decreasing the model resolution would decrease the prediction quality of the liquid water content. By using a gamma distribution for the cloud water particles [32], the median volume droplet size (MVD) were calculated and the modelled values were compared to measurements based on a regression approach by Makkonen (1992) [26]. Nygaard et al. (2011) [30] showed an over-prediction of MVD, because of a high sensitivity to the prescribed droplet concentration N_c. Davis et al. (2014) [11] performed nine sensitivity studies with WRF to evaluate the liquid water content distribution variability. The study showed, that the choice of microphysical and planetary boundary layer (PBL) schemes in WRF has a

large impact on the amount of estimated ice mass. [11] also stressed the uncertainties related to the prescribed N_c and the calculated MVD. Since MVD is directly connected to the collision of droplets and thereby ice accretion, it directly affects the ice mass forecast. This study uses measurements, as an alternative method from the NWP models, for obtaining the cloud liquid content water (W).

The cloud liquid water content has a long history in the aircraft industry and especially in the fifties and sixties a large bulk of data was collected through airborne measurements [7]. Later, the accuracy and techniques were improved (the hot-wire techniques gained ground) because of the requirement of data for, amongst others; NWP models, aircraft icing and cloud parametrisation. In Mazin (1995) [28], a large collection of data on the total cloud water content (water plus ice) were measured over eight years and the cumulative curves of the total cloud water content frequencies of occurrences ($F(W)$) were mapped. It was found that the cloud water content, W, could be described as a log-normal distribution and the median distribution parameter W_m could be described as a linear function of the temperature for the temperature interval [0; -40 °C]. Thorsson et al. (2015) [34] used the expression derived by [28] to model icing based on on-site measurements of temperature, relative humidity and wind speed from 4 sites in northern Sweden. The modelled icing was compared to results using two NWP models (WRF and COAMPS) and to measurements of standard icing. Thorsson et al. (2015) [34] showed, that the approach sometimes underestimated the numbers of active icing hours, though for some sites the approach proved to be fairly accurate when compared to the observations.

Since wind turbines operate in the lower level of the atmosphere, it can be argued, that the conditions during in-cloud icing may not agree to those in higher levels in the atmosphere, which come from airborne observations. Thus, an approach by Gjessing et al. (1990) [13] based on the vertical visibility gradient in low hanging cloud, was also used in the present work to estimate the cloud liquid water content. In general, clouds can be detected using the cloud base height and/or horizontal visibility, and from the visibility distance the cloud liquid water content can be estimated [20]. Harstveit (2009) [15] used the approach by Gjessing et al. (1990) [13] to model atmospheric icing based on measurements from freely exposed hills in coastal cold climate regions in Norway and the UK. The calculated ice mass showed good agreement with measured standard icing, following the [19].

In this study the cloud liquid water content is estimated from the available measurements of temperature (T) and cloud base height (CBH) using:

- The approach derived from airborne observations (Mazin (1995) [28]), where cloud liquid water is based on measurements of the temperature only. The approach showed reasonable results near the ground in [34].
- The approach derived based on the vertical gradient in cloud visibility (Gjessing et al. (1990) [13]). The approach showed reasonable results for modelling in-cloud icing in Harstveit (2009) [15].

A.2.2 On-site Measurements and Observations

The measurements used in this study are provided by TechnoCentre éolien (TCE) from a measurement campaign using sensors installed at the Site Nordique Expérimental en Éolien Corus (SNEEC), Riviére-au-Renard, Quebec, Canada [35]. The site (SNEEC) is indicated by the most easterly wind turbine in Figure A.2. The Gaspé Peninsula is known for its favourable wind potential [16], but unfortunately the area suffers from atmospheric icing and high icing severity, especially in the coastal regions [23]. The site is located near the coast, 340 m above sea level and has a complex topography with high turbulence corresponding to IEC wind class 2 [17]). The measurements were collected from a 126 m high meteorological mast (met mast), which has a total number of 37 instruments installed at 16 different heights including ground level. The highest location of 126 m corresponds to the blade tip of the farm's 2.05 MW Senvion MM92 CCV wind turbines. According to Bolduc et al. (2015) [6], SNEEC can be classified as an IEA ice class 2 - 3 site, as seen in Figure A.2.

Table A.1: Experimental set-up, [2].* The SAAB Combitech ice detector is a freely rotating cylinder with a load sensor, comparable to the ISO Standard 12494:2001 [19].

Atmospheric condition	Instrument	Location (met mast)	Acronym
Wind speed	Heated ultrasonic anemometer Windmaster pro 3D Ultrasonic	78 m	v_{h}
Wind speed	Unheated cup anemometer, THIES first Class	80 m	v_{uh}
Wind direction	Gill WindMaster Pro	78 m	v_{dir}
Ice load	SAAB Combitech ice detector*	82 m	IL
Temperature	Risoe P1867	80 m	T
Relative humidity	Rotronic HC2S3XT	80 m	RH
Atmospheric pressure	Setra 278	10 m	p
Cloud base height	Vaisala CL31	ground level	CBH
Ice measurement	Image analysis of anemometer support arm, (d = 26.7 cm)	103 m, (z = ref. height)	L_{im}

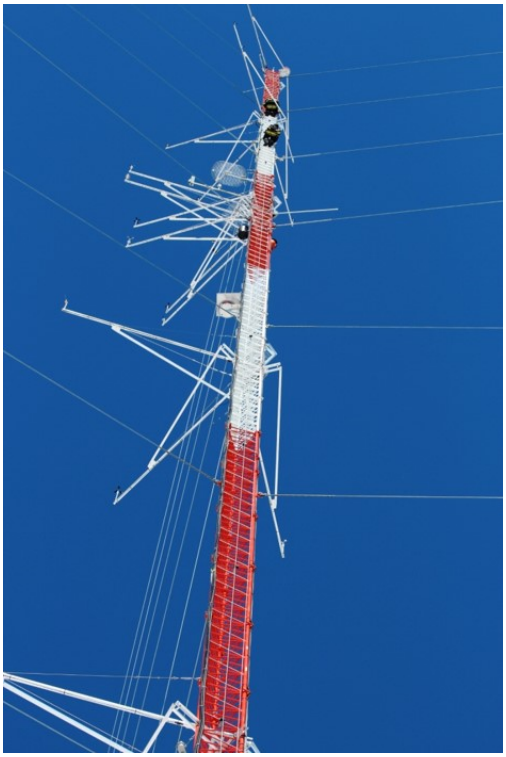

Figure A.3: Met mast located in Site Nordique Expérimental en Éolien Corus (SNEEC), Riviére-au-Renard, Quebec, Canada [2]. The experimental set-up is designed for operation during icing conditions.

A picture of the met mast is seen in Figure A.3 and Table A.1 presents the measurements used under the headings; atmospheric conditions, equipment type and location on met mast. A camera was installed to observe ice accretion on a cup anemometer support arm at the location of 103 m (Figure A.4). The pictures are JPG images with a resolution of 800 x 450 pixels and 24 bit RGB colour.

A.2.3 Estimating the Cloud Water Content from Measured Temperature

From the measured temperature, the median cloud water content can be found using the log-expression presented by Mazin (1995) [28] as follows:

$$\log_{10} W_{\mathrm{m}} = \begin{cases} -1.03739 + 0.03130T, & \text{if} \quad 1)\ T < 0\ ^{\circ}\mathrm{C} \\ & \qquad\ \ 2)\ \mathrm{RH} > 75\ \% \\ 0, & \text{otherwise} \end{cases} \tag{A.2}$$

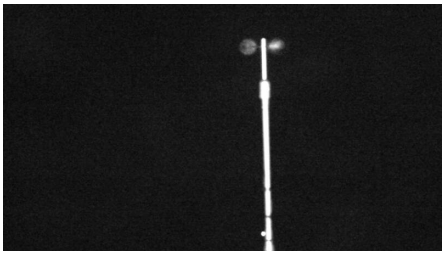

(a) Non iced, night background.

(b) Lightly iced, forested background.

(c) Medium iced, misty background.

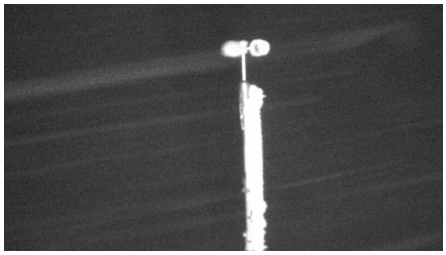

(d) Heavily iced, night background.

Figure A.4: Selection of pictures of the cup anemometer support during the icing event at reference height (z = 103 m). Different combinations of weather conditions and ice coverage exist during the event, which are seen by picture a) - d) (provided by TechnoCentre éolien).

where W_{m} is the median cloud water content ($\mathrm{g/m^3}$) and T the temperature (°C). To adapt the expression to in-cloud icing near the ground, the expression is constrained by; 1) temperature, which must by below 0 °C and 2) relative humidity must be above 75 % following Thorsson et al. (2015) [34].

A.2.4 Estimating the Cloud Water Content from Cloud Base Height and Visibility

From the measured cloud base height, the cloud water content can be found based on the vertical visibility gradient in low hanging clouds [13]. The model assumes, that from the cloud base and above, the air will be very well mixed in the vertical direction, see illustration Figure A.5. This means, that the potential wet-bulb temperature and the mixture of water and water vapour is almost independent of the height. Only close to the top of the cloud, dry air will influence the mixture. It is assumed, for the homogeneous part of the cloud, that the cloud water content is proportional to the adiabatic cloud water gradient and height above cloud base:

$$W_c = \begin{cases} \alpha\delta(z - \text{CBH}), & \text{if} \quad 1)\ T < 0\ ^\circ\text{C} \\ & \quad\ 2)\ \text{CBH} < z\ \text{m} \\ 0, & \text{otherwise} \end{cases} \tag{A.3}$$

where W_c is the cloud water content (g/m^3), at the distance ($z - \text{CBH}$) above the cloud base, z is the reference height and δ is the adiabatic cloud water gradient (mg/m^4). The cloud water content will increase with height according to the adiabatic cloud water gradient, if the humid air is lifted adiabatically and all condensed water stay in the mass as liquid water [15]. It is assumed in this study, that all the water in the cloud is in the liquid phase and α = 1. An $\alpha \leq 1$ means a deviation from the adiabatic cloud water gradient [15]. Equation D.2 is constrained by; 1) the temperature, which must by below 0 °C and 2) the cloud base height, which must be below the reference height z. An average value of the adiabatic cloud water gradient can be derived using an Amble-diagram for the lowest 500 me of the atmosphere:

$$\delta = 1.56(1 + 0.034\theta_w) \tag{A.4}$$

where θ_w is the wet-bulb temperature (°C) [13]. In this study, the wet-bulb temperature was found by an iterative approach based on the measurements of T, RH and p and the dew point temperature.

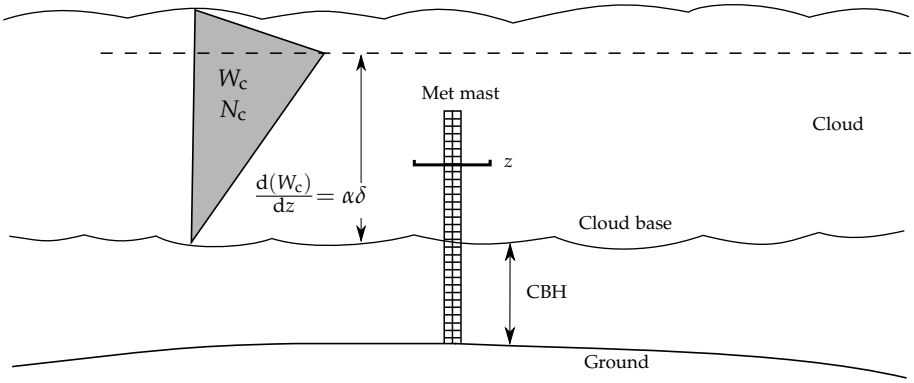

Figure A.5: Met mast surrounded by a low hanging cloud, with cloud base height (CBH). A boom marks the equipment location at reference height z. A linear increase in W_c is shown from the cloud base height towards the top of cloud, where a decrease happens because of dry air influence on the mixing ratio. Inspired by [13].

A.2.5 Estimating a Droplet Spectrum

In the cloud, the droplet's size can be estimated by a droplet spectrum. The most commonly used droplet spectrum estimation is by the median volumet-

ric diameter (MVD) [12]. Thompson et al. (2009) [33] derived an expression of the MVD by letting the cloud water follow a gamma distribution and diagnosing the shape parameter (μ) from a pre-specified N_c as follows.

$$\text{MVD} = \frac{3.672 + \mu}{\lambda} \tag{A.5}$$

where λ is the slope of the distribution obtained by integration over a distribution of spherical droplets. The shape parameter and the distribution slope is found as follows:

$$\mu = \min\left(\frac{1000}{N_c} + 2,\ 15\right)$$
$$\lambda = \left(\frac{\pi\rho_w}{6}\frac{\Gamma(4+\mu)}{\Gamma(1+\mu)}\left(\frac{N_c}{W}\right)\right)^{1/3}$$

where W is the cloud liquid water content (kg/m^3) and ρ_w is the density of water (kg/m^3). MVD will be compared to an estimated mean volumetric droplet diameter (D_{mv}), using the W_c found from Equation D.2 and the W_m found from Equation A.2. If the droplet volume is defined by the average liquid water per droplet and the radius of a spherical droplet is $r = (3V/4\pi)^{1/3}$, the D_{mv} can be expressed as:

$$D_{mv} = \left(\frac{6W_c}{\pi N_c \rho_w}\right)^{1/3} \tag{A.6}$$

where W_c/N_c is the average cloud water content per droplet and N_c is constant with height [13].

A.2.6 Estimation of the Ice Thickness by Image Analysis

Rime ice accreting horizontally on a vertical tube may be modelled using Equations A.7 - A.9 of ISO standard 12494 (2001) [19]. If the wind comes from a single direction, then the rime ice accretion may be approximated by a section of an ellipse as described in Figure A.6. Glaze ice accretion follows a different model which is not discussed here.

A previous measurement campaign of ice accretion on tubes was presented in Bolduc et al. (2013) [5]. In that study, a camera was placed upwind of the tube, and the distance t was measured. That meant, however, that no measurement of ice thickness could be made until ice had accreted beyond d_{max}. As well, the method was very sensitive to small changes in ice thickness: once d_{max} has accreted, 8 mm of ice is accreted in front of the tube for every millimetre of ice on the side (t). Therefore, in subsequent studies, the camera was oriented perpendicular to the wind direction to be able to measure the

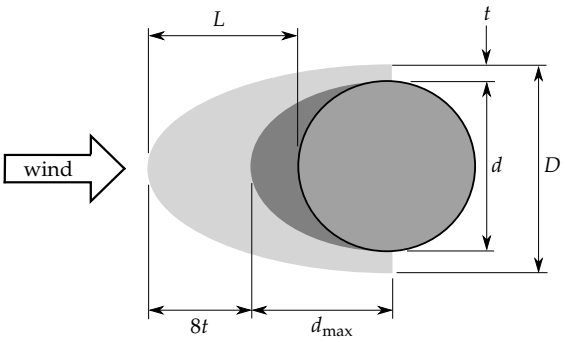

Figure A.6: Cross-section of an ice accretion profile on a vertical tube with diameter d (Inspired by the [19]).

ice profile length L directly by image analysis.

The reference tube in this set-up was the anemometer support arm (Table A.1), which had a diameter d of 26.7 mm. With a camera oriented perpendicular to the distance L, the number of pixels per millimetre may be calibrated using a tube free of ice. On subsequent images with ice, the distance L may be calculated by counting pixels between the upwind side of the ice and the downwind side of the tube and subtracting the known diameter of the tube. For more details on image analysis techniques, see Arbez et al. (2016) [1].

The two main limitations of this set-up are the camera's resolution and its orientation. The camera was installed for monitoring the met mast equipment, *i.e.* not for image analysis, and its resolution was therefore limited. In addition, the measurement was made in the image plane (the plane perpendicular to the camera lens optical axis) which is not necessarily the direction of the wind (nor therefore ice accretion). However, a variation in the wind direction of $\pm$ 10° to the optical axis, would give an insignificant error of 1.5 %. The measurements therefore likely underestimate the ice accretion, if the wind would come from multiple directions. The orientation of the camera on the met mast is 315°, *i.e.* North-West (N-W).

From the ice thickness L, the ice load m_{ice} was found following the rime ice model by the ISO standard 12494 (2001) [19], see Figure A.6. For $L \leq \frac{d}{2}$:

$$L = \frac{4m_{ice}}{\pi\rho d} \cdot 10^6 \tag{A.7}$$

where L is the length of the ice vane (mm), m_{ice} is the mass of accreted ice

per unit length (kg/m) and ρ the density (kg/m^3). For $L > \frac{d}{2}$:

$$L = \frac{d}{2} + 8t \tag{A.8}$$

where t is the ice thickness on the side of the cylinder in (mm), described as:

$$t = \frac{1}{32}\left(-10d + \left(68d^2 + \frac{m_{\text{ice}}}{\rho}8.149 \cdot 10^7\right)^{1/2}\right) \tag{A.9}$$

For this study, an image analysis methodology was used to measure the ice thickness L. Rime ice with a density of 600 kg/m^3 was assumed.

A.3 Results

The data were collected throughout the winter of 2014 - 2015 at the SNEEC. Three significant icing events were identified, with the one beginning on November 2$^{\text{nd}}$, 2014 being the most interesting in terms of quantity of ice and quality of data. The data presented below refer to this event.

A.3.1 Dataset of Atmospheric Conditions

Measurements of the atmospheric conditions during the icing event from November 2$^{\text{nd}}$ to November 5$^{\text{th}}$ are presented in Figure A.7.

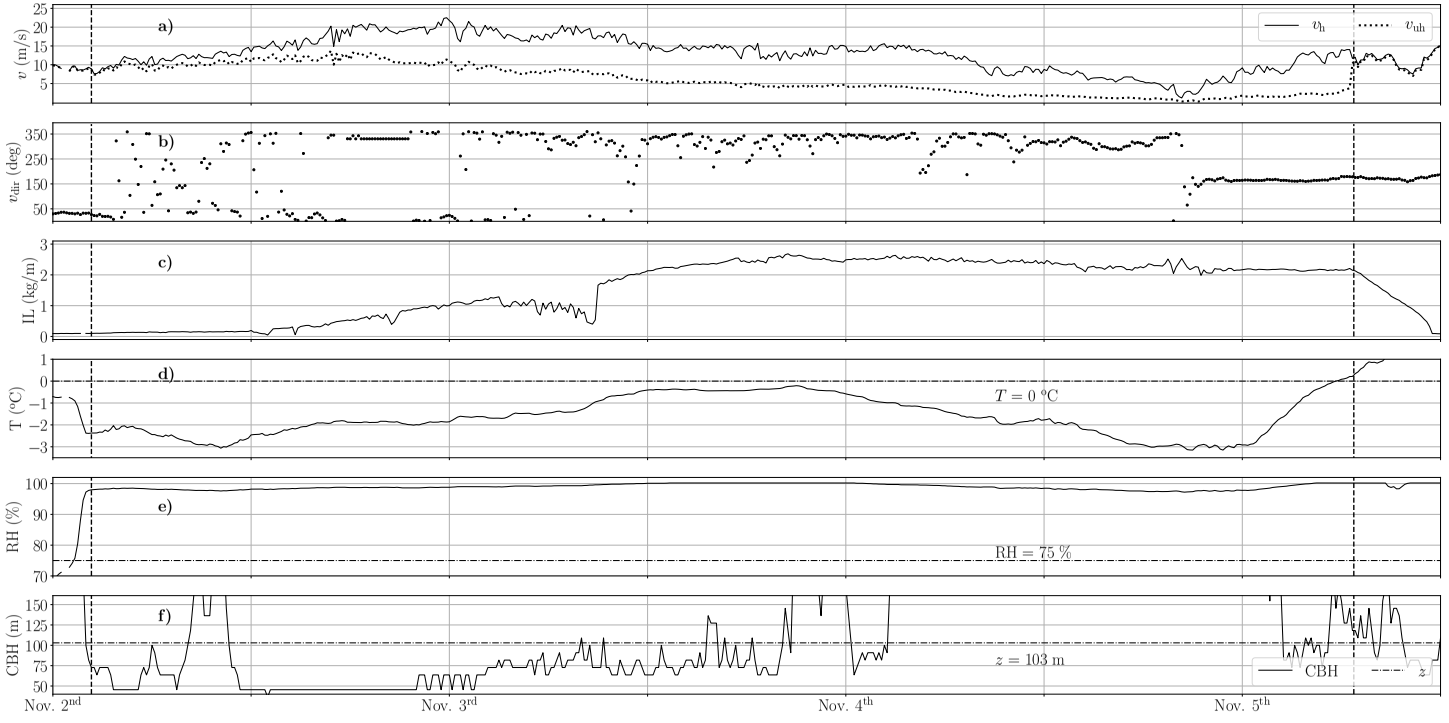

Figure A.7: Atmospheric conditions from icing event November 2nd to 5th. a) wind speed by heated and unheated anemometer (v_{h}, v_{uh}), b) wind direction (v_{dir}), c) measured ice load by ice detector (IL), d) temperature (T), e) relative humidity (RH) and f) cloud base height (CBH) and defined reference height z (location of the anemometer used for image analysis).

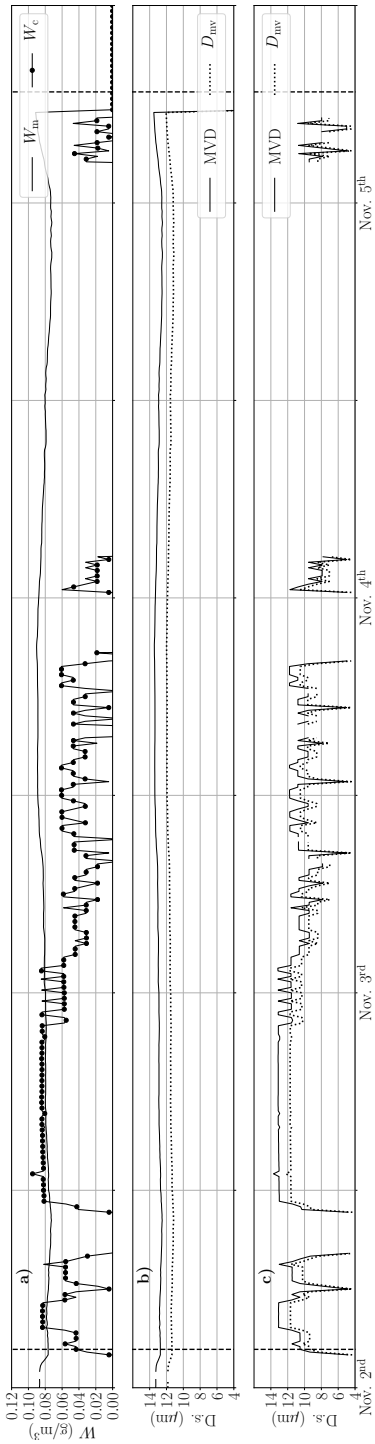

Figure A.8: Estimated values of W_m and W_c during the icing event November 2nd to 5th and the calculated values of MVD and D_{mv}. a) Estimated values of W_m and W_c, b) MVD and D_{mv} calculated using W_m and c) MVD and D_{mv} calculated using W_c (D.s. = Droplet size).

One way to identify the start of the icing event is by the technique of double anemometry, where the start is obtained by the difference in wind speeds of the heated anemometer v_{h} and the unheated anemometer v_{uh}, Figure A.7 a). Exceeding a certain threshold, for example ± 5 % at wind speed > 2 m/s [18], defines the start of the icing event. When the two curves meet again, defines the end of the icing event, which happens after T gets above 0°C and the anemometer unfreezes (Figure A.7 d)). Based on double anemometry, the start and end of the icing event for the period Nov. 2^{nd} - Nov. 5^{th} is illustrated by the vertical black dotted lines (Figure A.7 a) - A.7 f)). Double anemometry gives a good indication of the duration of the icing event, but provides no information about the icing phases during the event. In general, an icing event is dominated by two phases: 1) meteorological icing, periods favourable for active icing (ice accretion) and 2) instrumental icing, periods where ice is present on the structure and disturbs the instruments [4]. Meteorological icing and instrumental icing are clearly seen by the measured IL (Figure A.7 c)). As RH increases (Figure A.7 e)) and the wind speed increases (Figure A.7 a)), the ice detector gets iced up and ice accretion begins (IL > 0 kg/m), *i.e.* meteorological icing. Periods where the ice detector is not constantly covered by clouds, reduce the ice accretion contribution from in-cloud icing. Figure A.7 f) shows measurements of the CBH and the reference height z, which is marked by the horizontal dotted line. The reference height of 103 m was chosen, since this is the location of the ice measurement by image analysis and since this is the highest location of the measurement equipment (see Table A.1). As CBH moves above the reference height z around Nov. 4^{th} (Figure A.7 f)) and the wind speed decreases (Figure A.7 a)), the ice accretion stops and the IL stays rather constant until the end of the icing event. This period can be defined as instrumental icing. The effect of v_{dir} (Figure A.7 b)), on the icing event is difficult to determine, but the variation contributes to the 3-dimensional effects of ice accretion on any structure. Such effects cannot be seen by common measurements, but are seen by images or videos. However, Figure A.7 b) shows that the southerly wind directions towards the end of the icing event, result in warm and wet conditions, since T increases while RH stays at approx. 100 %. In the following section the cloud liquid water content will be estimated by Equation A.2 and D.2 using the measurements presented in Figure A.7. And in Section A.3.2, pictures from the icing event are used to estimate the ice thickness, ice load and ice mass rate to form a complete dataset.

The Cloud Liquid Water Content

The cloud liquid water content has been derived based on Equation A.2 and D.2 using the measurements available in Figure A.7. Because of the geographical location of SNEEC close to the ocean an N_{c} of 100 cm^{-3} was used

when calculating MVD and D_{mv}. Figure A.8 a) shows the estimated cloud liquid water W_m and W_c for the icing event Nov. 2nd to Nov. 5th. Figure A.8 b) shows the calculated MVD and D_{mv} using W_m and Figure A.8 c) shows the calculated MVD and D_{mv} using W_c. W_m is based on the measured temperature and follows the small variations in T. W_c was estimated using the measurements of T, p, RH and the CBH. The value of W_m follows the measured CBH and drops to zero as the CBH moves above z (Figure A.7 f)). The magnitude of the W_m and W_c are quite consistent with local maximums around 0.1 g/m^3 for $T < 0$ °C. However, the values of W_m and W_c might seem a bit low compared to commonly seen modelled NWP values, but they are in the similar range of results presented by Lamraoui et al. (2013) [23] for the Gaspé Peninsula. Lamraoui et al. (2013) [23] used reanalysis data from the North American Regional Reanalysis (NARR) to detect in-cloud icing events, ice accumulation and icing severity (only at ground level) by mapping the climatology of the Quebec region and Gaspé Peninsula. Like the current study, Lamraoui et al. (2013) [23] only includes strati-form clouds at low altitudes or supercooled fog, which is interesting for wind turbine icing. Typical values of the cloud liquid water contents were associated to ice severity classes where values of 0.04-0.07 g/m^3 corresponded to light to moderate icing and 0.2-0.36 g/m^3 corresponded to severe to extreme icing (Lamraoui et al. (2014) [24]). Thus, the estimated values of W_m and W_c compare well to other studies at Gaspé Peninsula. By definition, W_c is found at one specific location inside the cloud and is sensitive to the distance (z - CBH) (Equation D.2) and thereby sensitive to the uncertainties of measurements connected to the CBH. The estimated W_m provides an estimation of median cloud water content at the given temperature but cannot provide information about the location inside the cloud or about the local visibility. From this observation, the estimated cloud liquid water content (W_c) is preferred when assembling the complete data-set of boundary conditions for modelling in-cloud icing.

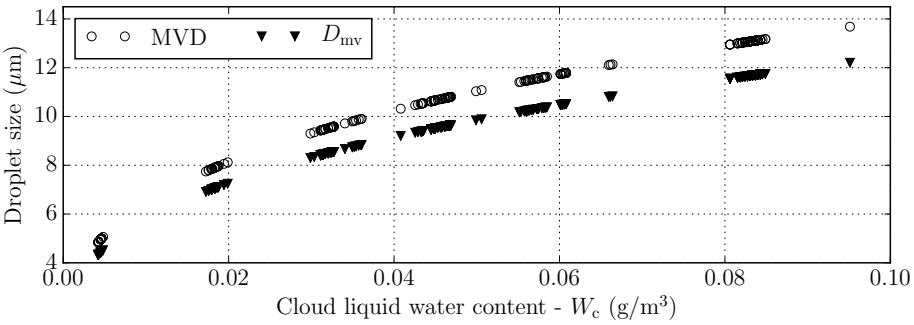

Figure A.9: Relation between estimated W_c and droplet sizes at reference location z for N_c = 100 cm^{-3}.

Figure A.9 shows the calculated MVD and D_{mv} for the estimated values of W_c using an N_c = 100 cm^{-3}. Comparing the two droplet size distributions, MVD was found more reasonable, since the MVD was 10.82 % larger than the D_{mv}, which seems as a more likely size for in-cloud icing. Furthermore [12] showed that the best approximation for the collision efficiency was by the MVD. MVD has been shown to be very sensitive to the setting of N_c ([11] and [30]). The SNEEC wind farm is located near the ocean ($\approx$ 5 km) and so a low droplet concentration of 75-100 cm^{-3} can be assumed compared to continental air, which typically has a higher droplet concentration of 100-200 cm^{-3} [32]. However, N_c might be higher than 100 cm^{-3}, due to air mixing and wood burning in the house nearby during the winter. Figure A.10 shows theoretical lines of MVD for a cloud liquid water content from 0.0-0.3 g/m^{3}and a N_c of 50-1000 cm^{-3}. The calculated MVD for the estimated W_c is shown by black circles. The shaded grey area illustrates, that N_c must be considered as a number between 75-200 cm^{-3} and that the size of the MVD will vary with this number. Thus, the setting of N_c must be evaluated when using the data-set in an icing model.

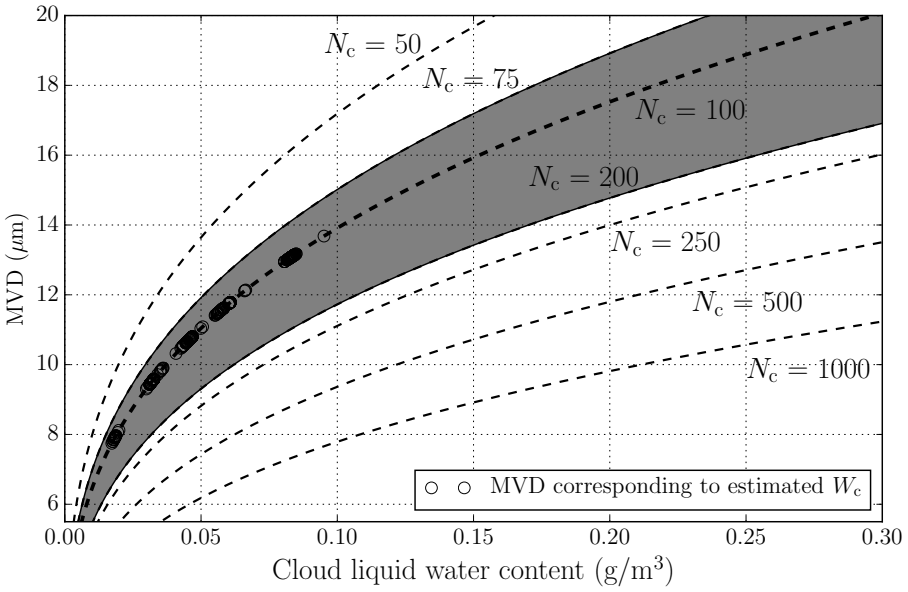

Figure A.10: The dashed lines show the theoretical droplet distribution of MVD [33] for droplet concentrations of N_c ranging from 50-1000 cm^{-3} and a cloud liquid water content ranging from 0.0 to 0.3 g/m^3 . The black circles shows the MVD calculated using W_c and N_c = 100 cm^{-3} . The shaded grey are between N_c = 75 - 200 cm^{-3} illustrates the expected variation of the MVD at the location.

A.3.2 Image Analysis

The ice thickness L obtained by image analysis is seen for the entire event in Figure A.11, during the icing event Nov. 2^{nd} - Nov. 5^{th}.

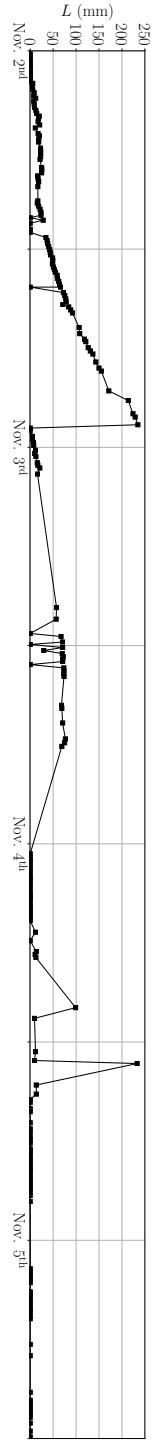

Figure A.11: Ice thickness L by image analysis during icing event Nov. 2nd to Nov. 5th.

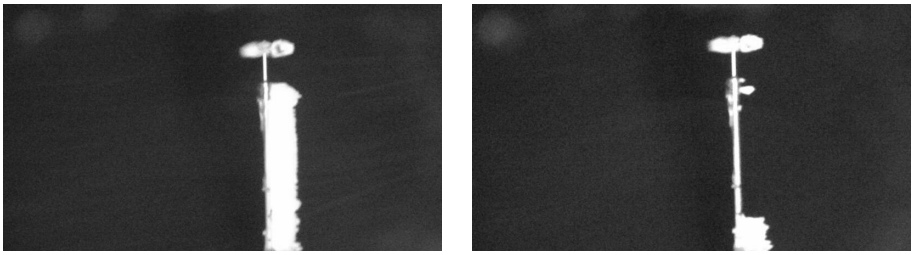

(a) Nov. 2nd, 10:38 pm. (b) Nov. 2nd, 10:50 pm.

Figure A.12: Anemometer support after approximately 24 hours of active icing, a) anemometer support heavily iced up and b) ice falls of anemometer support (credit TechnoCentre éolien).

From an analysis of the images, it was found that a big piece of ice fell off the anemometer support approximately 24 h after the start of the icing event, as seen in Figure A.12. The reason for the ice to fall off the anemometer support arm is due to the combination of; ice load, ice density, vibration of the anemometer support, wind speed, wind direction, and temperature. Ice shed, and the relationship between ice shed on the anemometer support arm and that on other instruments or wind turbines, may be made the object of other studies. Figure A.13 shows ice thickness L and the corresponding ice load m_{ice} until the ice falls off. A maximum ice thickness of 234.7 mm and maximum ice load of 6.75 kg/m was found at Nov. 2nd 10:40 pm, whereupon it falls off the anemometer support arm (Figure A.12).

In terms of modelling and validating ice accretion by a CFD icing model, the period until the ice falls off, shown in Figure A.13, is found ideal. During this period, ice accretion is clearly seen and good validation data are available. The period extends over Nov. 2nd from 02:00 am to 11:00 pm. The remaining part of the icing event is dominated by instrumental icing, which might not be interesting to model when using a transient CFD based icing model. During instrumental icing there will be no ice accretion and the input boundary conditions will be more or less constant, resulting in solving the same flow field repeatedly.

A.4 Discussion

A.4.1 Image Analysis

From the ice thickness L, the ice load m_{ice} was estimated. Another significant parameter within modelling of ice accretion is the rate of ice formation. The ice mass rate $\frac{\mathrm{d}m_{\text{ice}}}{\mathrm{d}t}$, was found by a curve-fit using a 4th order polynomial, see Figure A.14 a). A curve-fit was found necessary to avoid possible negative

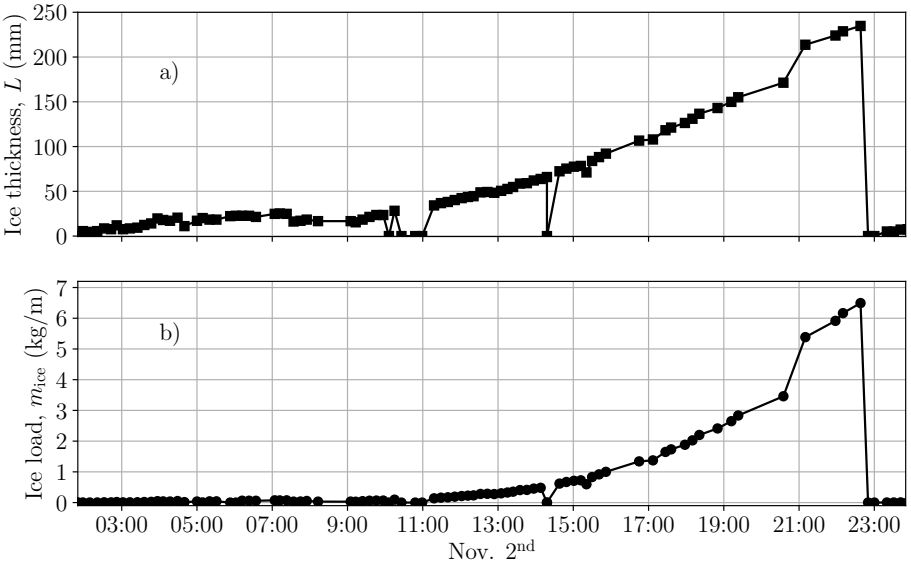

Figure A.13: Ice thickness L by image analysis and calculated accumulated mass of accreted ice per unit length m_{ice} over time during Nov. 2nd.

rates due to uncertainties in the image analysis. The ice mass rate is shown in Figure A.14 b) for Nov. 2nd until the ice falls off. Knowledge about the ice rate at different combinations of atmospheric parameters can be used in ice forecasting and for production loss assessment. Furthermore, it is a significant parameter when modelling icing over time.

Figure A.13 and Figure A.14 are obtained from the pictures from the dataset. Despite the relatively low quality of the pictures, image analysis showed promising results which can be improved by higher resolution pictures. Especially the light variation of the pictures is of great importance and a place to improve the dataset. There are several factors which affect the quality of the ice thickness measurements. The camera resolution has already been mentioned; higher resolutions provide a better mm/pixel scale. In addition, missing data may be due to contrast issues (dense cloud or daytime/night-time differences) or obstruction of the structure by ice accumulation on the camera lens (as this set-up was not originally intended for ice measurements). The overall uncertainty in L has been estimated at around 4.3 mm for the good quality images from this dataset. The image analysis approach assumes a wind direction perpendicular to the camera lens optical axis. Figure A.15 (a) shows the wind direction distribution over the 16 wind sectors during Nov. 2nd and Figure A.15 (b) shows the relation between wind direction and wind speed. Since the dominating wind direction is N-E to N-N-E the wind direc-

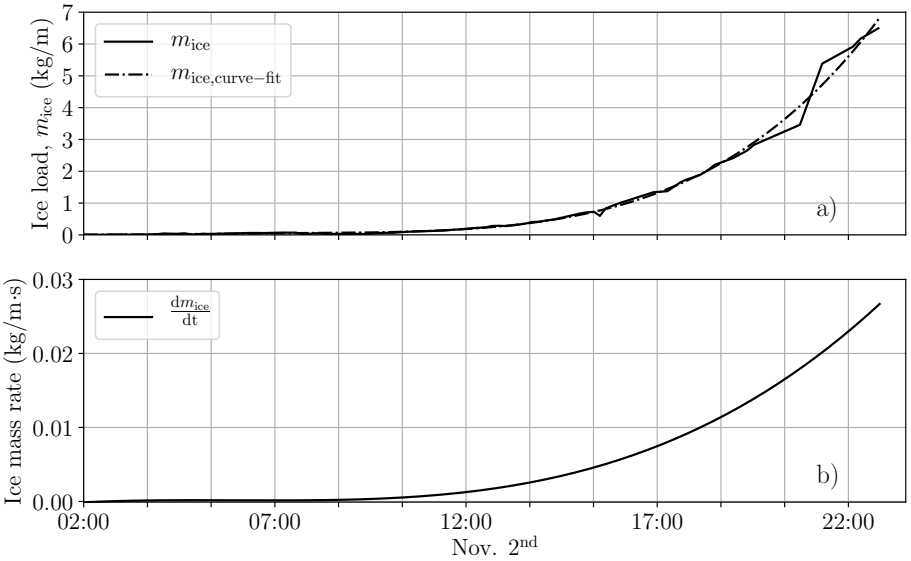

Figure A.14: Ice load and ice mass rate during Nov. 2nd. a) Curve-fit and ice load m_{ice} and b) ice mass rate ($\frac{dm_{ice}}{dt}$) based on curve-fit data.

tion was perpendicular to the camera orientation (315°) during the period, which minimise errors connected to the orientation of the camera.

A.4.2 Boundary Conditions for the Icing Model

Figure A.16 presents the complete dataset for simulating ice accretion and performing verification of the results for the period of interest during Nov. 2nd. The period fulfils the definitions of in-cloud icing and for this period it will be possible to model ice accretion over time by a complete set of boundary conditions. Furthermore, the modelled results can be validated by the ice thickness, ice load and ice mass rate obtained by image analysis (Figure A.14). Parameters such as pressure (P) and the relative humidity (RH) are not included in Figure A.16 since they do not vary significantly during the period. The dataset is unique, since it provides all atmospheric conditions, the ice load, ice thickness and ice mass rate over time at a low time-stamp suitable for a CFD-based icing model. From the dataset, new predictors for the modelling frame (Figure A.1) can be established, which is expected to improve the frame work. Similar datasets can be obtained from other cold climate sites, if the necessary measurements are available.

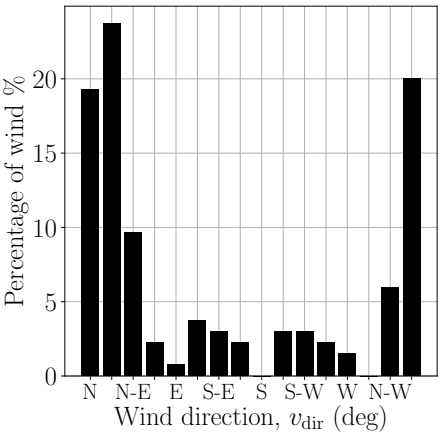

(a) Percentage of wind in each sector.

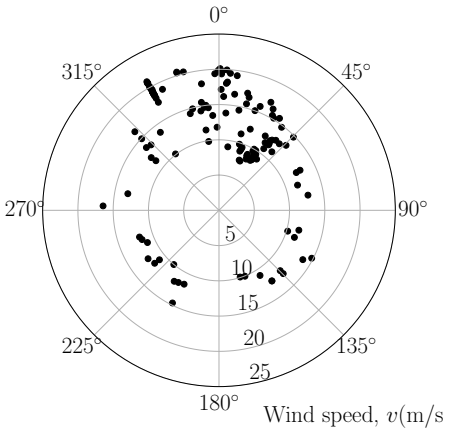

(b) Distribution of wind direction in each sector by the black circles, where 0° is North (N). The wind speed is marked in the radial direction.

Figure A.15: Distribution of wind direction over wind sectors during Nov. 2nd.

A.5 Summary and Conclusions

Measurements from the Site Nordique Expérimental en Éolien Corus (SNEEC) test site were combined with estimations of the cloud liquid water content to create a dataset of icing conditions. The cloud liquid water content was determined by two different approaches using the measurements. By the values of W_{c} and MVD and the original measurements a complete dataset of atmospheric boundary conditions for an icing model was constructed. The estimated values of W_{m} and W_{c} corresponded to light to moderate icing conditions and the MVD size distribution was 10.82 % larger than the D_{mv} size distribution for the estimated cloud liquid water content when using an N_{c} of 100 cm^{-3}. From the definitions of in-cloud icing, the dataset was analysed to identify periods of meteorological icing and ice accretion. Together with the results from image analysis of ice accumulation, a period of interest was defined, which is ideal for simulating icing by a CFD based icing model. The maximum ice thickness measured was 234.7 mm; this corresponds to an ice load of 6.49 kg/m. A complete dataset of boundary conditions has been created for a 22 h icing event at a maritime site in eastern Québec, Canada. The boundary conditions can be used for a dynamic simulation of in-cloud icing by a CFD-based icing model and for validation by the L, m_{ice} and $\frac{\mathrm{d}m_{\mathrm{ice}}}{\mathrm{d}t}$ over time.

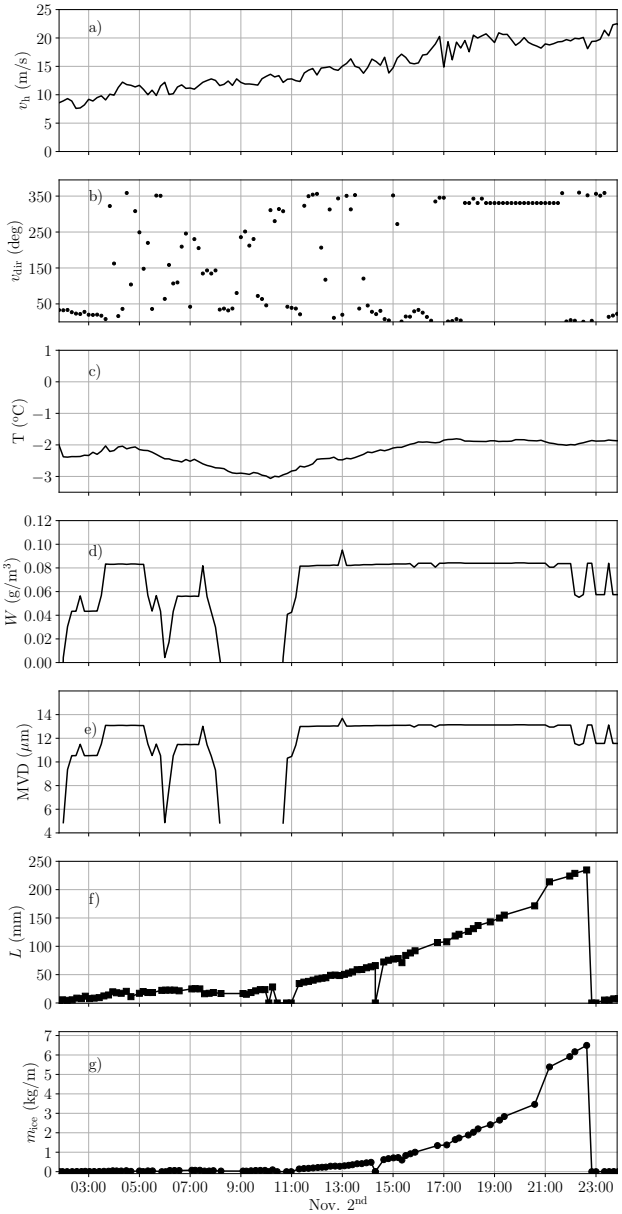

Figure A.16: Complete set of boundary conditions for icing model during Nov. 2nd. a) Wind speed by heated anemometer (v_h), b) wind direction (v_{dir}), c) temperature (T), d) liquid water content at reference location z (W_c), e) mean volume droplet diameter (D_{mv}) at reference location z, f) ice thickness on the anemometer support (L) extracted by image analysis and g) ice mass on the anemometer support (m_{ice}) extracted by image analysis.

A.6 Acknowledgement

This work as been partly founded by Innovation Fund Denmark as part of the Danish Industrial PhD program (No. 1355-00120B) and Vattenfall Vindkraft A/S, Kolding, Denmark. Furthermore the author would like to thank TechnoCentre éolien for providing the raw data and their generous hospitality during a research stay winter 2015 - 2016.

References

[1] Arbez, C., Clément, M., Godreau, C., Swytink-Binnema, N., Tete, K., Wadham-Gagnon, M., 2016. Development and Validation of an Ice Prediction Model for Wind Farms. Tech. rep., TechnoCentre éolien, Gaspé, Québec, Canada.

[2] Arbez, C., Tuoyomel, R., 2015. Projet Mise en place de mât de mesure visant à caractériser la couche limite atmosphérique et la performance des éoliennes, MMV1 (Mât de Mesure de Vent). Tech. rep., TechnoCentre éolien, Gaspé, Québec, Canada.

[3] Baltscheffsky, M., 2013. Modelling of Production Losses due to Icing for Individual Turbines in a Wind Farm-development of Techniques for Forecasting and Site Assessment. http://winterwind.se/.

[4] Baring-Gould, I., Cattin, R., Durstewitz, M., Hulkkonen, M., Krenn, A., Laakso, T., Lacroix, A., Peltola, E., Ronsten, G., Tallhaug, L., Wallenius, T., 2011. 13 Wind Energy Projects in Cold Climate. Tech. rep., IEA Wind, http://ieawind.org.

[5] Bolduc, D., Wadham-Gagnon, M., Boucher, B., Jolin, N., Petersen, J., Friedrich, H., 2013. Field Measurements of Wind Turbine Icing. In: 15th International Workshop on Atmospheric Icing on Structures (IWAIS, St. Johns, NL, Canada, September 2013). http://iwais.compusult.net/html/IWAIS_2013_Proceedings.pdf.

[6] Bolduc, D., Wadham-Gagnon, M., Petersen, J., Friedrich, H., Camion, A., 2015. Ice Monitoring for R&D projects. In: Winterwind - International Wind Energy Conference (Luleå, Sweden, 2015). WINDREN, http://winterwind.se/program/presentations-2016/.

[7] Borovikov, A., Gaivoronskii, I., Kostarev, V., Mazin, I., Minervin, V., Khrgian, A., Shmeter, S., 1963. Cloud Physics, Transl. from Russian. Israel Program for Scientific Translation, Jerusalem 392.

[8] Byrkjedal, Ø., 2012. Icing Map. Online, KJELLER Vindteknik, http://www.vindteknikk.com/services/analyses/wind-power/pre-construction/icing−map.

[9] Byrkjedal, Ø., Hansson, J., van der Velde, H., 2015. Development of Operational Forecasting for Icing and Wind Power at Cold Climate Sites. In: 16th International Workshop on Atmospheric Icing on Structures (IWAIS, Uppsala, Sweden, July 2015). http://www.vindteknikk.no/_extension/media/336/orig/IWAIS2015_Paper_Byrkjedal.pdf.

[10] Davis, N., 2014. Icing Impacts on Wind Energy Production. Ph.D. thesis, The Technical University of Denmark, DTU Wind Energy, ISBN: 9788792896612.

[11] Davis, N., Hahmann, A.N., Clausen, N.-E., Žagar, M., 2014. Forecast of icing events at a wind farm in Sweden. Journal of Applied Meteorology and Climatology 53 (2), 262-281. http://dx.doi.org/10.1175/JAMC-D-13-09.1

[12] Finstad, K.J., Lozowski, E.P., Makkonen, L., 1988. On the Median Volume Diameter Approximation for Droplet Collision Efficiency. Journal of the atmospheric sciences 45 (24), 4008-4012. http://dx.doi.org/10.1175/1520-0469(1988)045<4008:OTMVDA>2.0.CO;2

[13] Gjessing, Y., Skartveit, A., Utaaker, K., 1990. Vurdering av sikt -og vindforhold på hurumåsen. Tech. rep., Meteorological report series, Universitetet i Bergen, Norge.

[14] Hämäläinen, K., Niemelä, S., 2017. Production of a Numerical Icing Atlas for Finland. Wind Energy 20(1), 171-189. http://dx.doi.org/10.1002/we.1998

[15] Harstveit, K., 2009. Using Metar-data to Calculate In-cloud Icing on a Mountain Site Near by the airport. In: 13th International Workshop on Atmospheric Icing on Structures (IWAIS XIII, Andermatt, Switzerland, September 2009). IWAIS, http://iwais.compusult.net/html/IWAIS_Proceedings/IWAIS_2009/Session_6_poster/COST%20Action%20727%20WG1/poster_harstveit2.pdf.

[16] Hochart, C., Fortin, G., Perron, J., Ilinca, A., 2008. Wind turbine Performance Under Icing Conditions. Wind Energy 11 (4), 319-333. http://dx.doi.org/10.1002/we.258

[17] IEC, 2005. IEC 61400/AMD1–Wind turbines – Part 1 Design Requirements (3rd. ed.). Tech. rep., International Electrotechnical Commission, Geneva, Switzerland.

[18] Ilinca, A., 2011. Analysis and Mitigation of Icing Effects on Wind Turbines. InTech Europe, Croatia, http://biblio.uqar.ca/archives/30332211.pdf.

[19] ISO standard 12494, 2001. Atmospheric Icing on structures, ISO 12494:2001(E). Tech. rep., ISO, Geneva, Switzerland, https://www.iso.org/obp/ui/#iso:std:iso:12494:ed-1:v1:en.

[20] Kampe, H., 1950. Visibility and Liquid Water Content in Clouds in The Free Atmosphere. Journal of meteorology 7 (1), 54-57, http://journals.ametsoc.org/doi/pdf/10.1175/1520-0469(1950)007%3C0054%3AVALWCI%3E2.0.CO%3B2.

[21] Krenn, A., Pieter, J.J., Wadham-Gagnon, M., Davis, N., Clausen, N.-E., Lehtomäki, V., Jokela, T., Kaila, S., Ronsten, G., Wickmann, H., Klintström, R., Cattin, R., 2016. Available Technologies of Wind Energy in Cold Climates. Tech. rep., IEA Wind Task 19, http://www.ieawind.org.

[22] Lakkso, T., Holttinen, H., Ronsted, G. Tallhaug, L., Horbaty, R., Baring-Gould, I., Lacroix, A., Peltola, E., Tammelin, B., 2003. State-of-the-art of wind energy cold climates. Tech. rep., IEA Wind Task 19, http://www.ieawind.org.

[23] Lamraoui, F., Fortin, G., Benoit, R., Perron, J., Masson, C., 2013. Atmospheric icing severity: Quantification and mapping. Atmospheric research 128, 57-75.

[24] Lamraoui, F., Fortin, G., Benoit, R., Perron, J., Masson, C., 2014. Atmospheric icing impact on wind turbine production. Cold Regions Science and Technology 100, 36–49. http://dx.doi.org/10.1016/j.coldregions.2013.12.008

[25] Lehtomäki, V., Rissanen, S., Wadham-Gagnon, M., 2014. Low temperature & icing map for Québec. In: Québec wind conference, Gaspé, Canada, 2014.

[26] Makkonen, L., 1992. Analysis of Rotating Multicylinder Data in Measuring Cloud-droplet size and Liquid Water Content. Journal of Atmospheric and Oceanic Technology 9 (3), 258-263.

[27] Makkonen, L., 2000. Models for the Growth of Rime, Glaze, Icicles and Wet Snow on Structures. Philosophical Transactions of the Royal Society of London A: Mathematical, Physical and Engineering Sciences 358 (1776), 2913-2939. http://dx.doi.org/10.1098/rsta.2000.0690

[28] Mazin, I.P., 1995. Cloud Water Content in Continental Clouds of Middle Latitudes. Atmospheric research 35 (2), 283-297. http://dx.doi.org/10.1016/0169-8095(94)00024-8

[29] Navigant Research, 2013. World Market Update 2012. Tech. rep., Navigant Research, Copenhagen, Denmark, ISBN: 978-87-994438-4-0 .

[30] Nygaard, B. E. K., Kristjánsson, J. E., Makkonen, L., 2011. Prediction of In-cloud Icing Conditions at Ground Level Using the WRF Model. Journal of Applied Meteorology and Climatology 50 (12), 2445-2459. http://dx.doi.org/10.1175/JAMC-D-11-054.1

[31] Parent, O., Ilinca, A., 2011. Anti-icing and de-icing techniques for wind turbines: Critical review. Cold Regions Science and Technology 65 (1), 88-96. http://dx.doi.org/10.1016/j.coldregions.2010.01.005

[32] Thompson, G., Field, P. R., Rasmussen, R. M., Hall, W. D., 2008. Explicit forecasts of winter precipitation using an improved bulk microphysics scheme. part ii: Implementation of a new snow parameterization. Monthly Weather Review 136 (12), 5095-5115. http://dx.doi.org/10.1175/2008MWR2387.1

[33] Thompson, G., Nygaard, B. E., Makkonen, L., Dierer, S., 2009. Using the Weather Research and Forecasting (WRF) model to predict ground/structural icing. In: 13th International Workshop on Atmospheric Icing on Structures. IWAIS, http://iwais.compusult.net/html/IWAIS_2013_Proceedings.pdf.

[34] Thorsson, P., Söderberg, S., Bergström, H., 2015. Modelling Atmospheric Icing: A Comparison Between Icing Calculated with Measured Meteorological Data and NWP Data. Cold Regions Science and Technology 119, 124-131. http://dx.doi.org/10.1016/j.coldregions.2015.07.003

[35] Wadham-Gagnon, M., Swytink-Binnema, N., Bolduc, D., Tété, K., Arbez, C., 2015. Ice Detection Methods and Measurement of Atmospheric Icing. In: 16th International Workshop on Atmospheric Icing on Structures (IWAIS, Uppsala, Sweden, July 2015). IWAIS, http://windren.se/IWAIS_p/IWAIS2015/IWAIS2015_pa/40_06_02_Paper_WadhamGagnon_Ice_Detection_Methods_and_Measurement_of_Atmospheric_Icing.pdf.

Paper B

Computational Fluid Dynamics Analysis and Field Measurements on Ice Accretion on a Cup Anemometer Support Arm

Marie Cecilie Pedersen, Henrik Sørensen,
Nigel Swytink-Binnema and Thomas Condra

The paper has been published in *Applied Thermal Engineering* Vol. 135,
pp. 530–536, 2018-05, https://doi.org/10.1016/j.applthermaleng.2018.01.086

The layout has been revised.

Computational Fluid Dynamics Analysis and Field Measurements on Ice Accretion on a Cup Anemometer Support Arm

M. C. Pedersen [a,b], H. Sørensen[b], N. Swytink-Binnema[c], T.J. Condra[b]

[a] *Vattenfall Vindkraft A/S, Jupitervej 6, DK-6000 Kolding, Denmark*
[b] *Aalborg University, Department of Energy Technology, Pontoppidanstræde 111, DK-9220 Aalborg, Denmark*
[c] *TechnoCentre éolien, 70 rue Bolduc, Gaspé (Québec) G4X 1G2, Canada*

Abstract

Ice growth on structures is a problem in cold climate regions. A method to model ice accretion on the cross section of a cup-anemometer support arm is presented in this study. The model was developed in ANSYS Fluent by implementing existing icing theory and by developing the dynamic meshing package to match ice accretion through user defined functions (UDFs). The Euler-Euler multiphase model was used to model in-cloud icing conditions and an impingement model was implemented to extract the ice deposit per time step. A surface boundary displacement model was implemented to determine the new surface contour after ice deposit and the surface boundary is displaced by an iterative process between each time-step. Icing was simulated over time by using measurements of the atmospheric conditions from a cold climate site in Canada. The numerical results were validated using experimental data and compare well with the experiments, when simulating 1 hour of icing.

Keywords: ice model; computational fluid dynamics; ice accretion; dynamic meshing

B.1 Introduction

Structures located in cold climate regions with high air densities, low temperatures and a high relative humidity are exposed to icing during the winter time. Such structures can be overhead power lines and conductors [15, 20], meteorological masts (met masts), other tall structures and wind turbines [10, 16]. Iced power lines can lead to power failure and the power line and power pole can collapse due to the additional ice load. Ice shedding from structures and wind turbines is a danger to accidental passers-by, service personnel or nearby buildings. The performance of wind turbines located in

cold climates suffer from a loss of production and blade fatigue due to additional load on the blades. At some wind farms, the production losses due to icing are so high, that the total annual profit of the wind farm is threatened. The phenomenon leading to ice accretion is known as atmospheric icing. It covers the processes where water droplets- or drizzle, wet snow or rain will freeze and stick to an object and turn into ice. One normally makes a distinction between precipitation icing and in-cloud icing following the ISO standard 12494 [14]. Precipitation icing covers ice accretion caused by wet snow, drizzle and freezing rain, whereas in-cloud occurs when supercooled droplets in clouds or fog freeze upon contact with an object resulting in ice growth. With the expansion of wind power in cold climate[1] from around 500 MW in 2002 [16] to a cumulative capacity of 127 GW by the end of 2015 [9], knowledge and experience with operation and models have been requested by the related industry and academia to determine the potential icing risks of a site [5, 16]. Simulating icing in a climatic wind tunnel is an expensive affair and does not provide definitive conclusions for wind power applications. Whilst wind power sites, are most often equipped with measurements equipment it is evident, and more cost-effective, to combine on-site measurements with numerical models for simulation of icing. Since a wind turbine is difficult to access during icing conditions, wind turbines are typically observed by a combination of measurement equipment installed on met masts and on the ground. It is not trivial to measure atmospheric icing, since the instruments are also influenced by the harsh conditions and can be affected by ice themselves, as was shown by Wickman (2013) [33]. However, studies by Wadham-Gagnon et al. (2015) [32] and Krenn et al. (2016) [16] have shown that combining measurements of the atmospheric parameters such as wind speed, temperature, pressure and relative humidity with observations by web cameras can provide a good picture of the atmospheric icing at a site and thereby the potential icing risks. Observations from web cameras can be analysed using image analysis to provide additional icing information, such the ice thickness and the ice distribution, which are usually not available [1]. Thus, measurement equipment on met mast might just as useful for evaluating the ice risks at a site. And in the planning phase of the wind farm, met mast are often the only installations at the site.

A detailed icing model of the wind turbine blade provides information about the aerodynamic degradation of the blade during ice accretion. Detailed icing studies are seen in the aeronautics, which have primarily been developed for flight safety reasons [27]. Messinger (1953) [21] described the energy balance during ice accretion for an unheated surface, which has formed the

[1]Cold climate refers to sites, which experience severe periods of icing events and/or temperatures below the operation limits of a standard wind turbine [5]

basis of most icing models used today. An example is Makkonen's empirical model [19] and another example is the advanced icing models seen in the aircraft industry. Commercial ice models have been developed for aircraft icing [6,13,35], but those models are not likely to be accessible for wind power researchers and the model applications are tuned for in-flight conditions and not for icing near the ground. The aim of this study is to develop a framework for modelling icing using computational fluid dynamics (CFD), having icing on instruments as a starting point. The study is carried out based on the following objectives:

- The icing model will be developed in a commercial CFD software by; implementing existing icing theory and by modifying existing dynamic meshing package to match icing requirements, both by user defined functions (UDFs).
- The modelled ice thickness is compared to observed ice thicknesses obtained by image analysis

More specifically, the intention is to develop a model, which runs in software ANSYS Fluent using built-in packages and user defined functions (UDFs). In this way, the user can easily modify and control the model and no other software is needed, thereby decreasing the computational time required. Other studies showed promising initial results using ANSYS Fluent [30,34]. And recently, for predicting ice accretion in relation to anti-icing, ANSYS Fluent was used to simulated in-cloud conditions, where the ice contour and generation of the new mesh were performed using MATLAB [31]. In the study by Villalpando et al. (2016) [31], it is not the intention to compete with other highly specialised icing models from, for example, the aircraft industry. Rather it is to develop an easily accessible model for modelling ice accretion on structures near the ground, which runs as one unified model in ANSYS Fluent. In future studies the model framework can be extended for wind turbine blades, which will be interesting in terms of evaluating de-icing systems.

B.2 Materials and Methods

B.2.1 On-site Measurements of Ice Growth

Icing was simulated using measurements provided by TechnoCentre éolien from the Site Nordique Expérimental en Éolien Corus, Riviére-au-Renard, Quebec, Canada [32]. The measurements used were collected from a 126-meter-high met mast, which has equipment installed at 16 heights including ground level. Icing was recorded over time at 103 m on a cup anemometer support arm with a diameter (d) of 0.0267 m, see Figure B.1. Ice thickness L was extracted using image processing [25], as seen in Figure B.2 (left).

The camera was originally installed with the purpose of monitoring the mast equipment, but the pictures turned out to be of great value for observing ice accretion. The wind direction was shown to the perpendicular to the camera's axis, and the distance to the camera was fixed, which enabled image processing to derive the ice thickness [25].

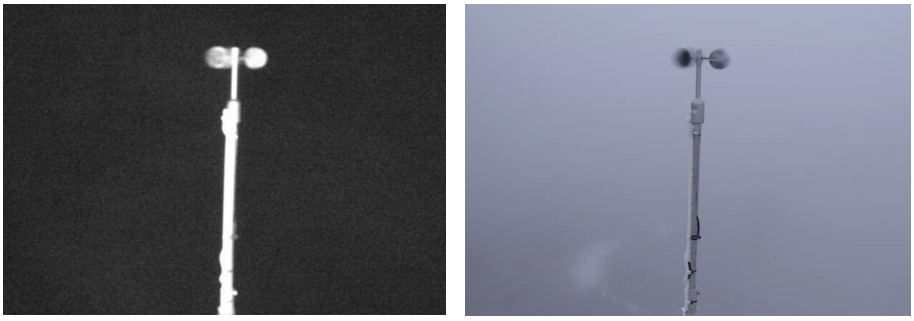

Figure B.1: The cup anemometer and support arm on the met mast in a Canadian wind farm. To the left at nighttime with no ice accretion and to the right at daytime during in-cloud conditions.

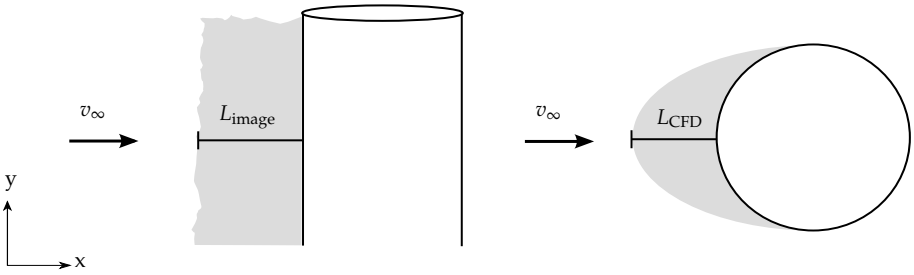

Figure B.2: Ice thickness L obtained from image analysis to the left and ice thickness L_{CFD} calculated from CFD icing model to the right. The wind free-stream velocity is given as v_∞.

B.2.2 Computational Domain

The computational domain consists of a C-grid, with a structured O-grid surrounding the cylinder representing the cup anemometer support arm, and an unstructured grid far downstream, see Figure B.3. A structured O-grid was chosen due to the dynamic mesh update approach. The cylinder was discretized by 160 cells having the highest density around the stagnation point, marked by the black square in Figure B.3. The flow Reynolds number of the simulations was $2.77 \cdot 10^4$. Since ice accretion happens at the leading edge of the cylinder, a relatively low cell density, downstream and far away from the cylinder surface, was allowed. The domain consists of a total of

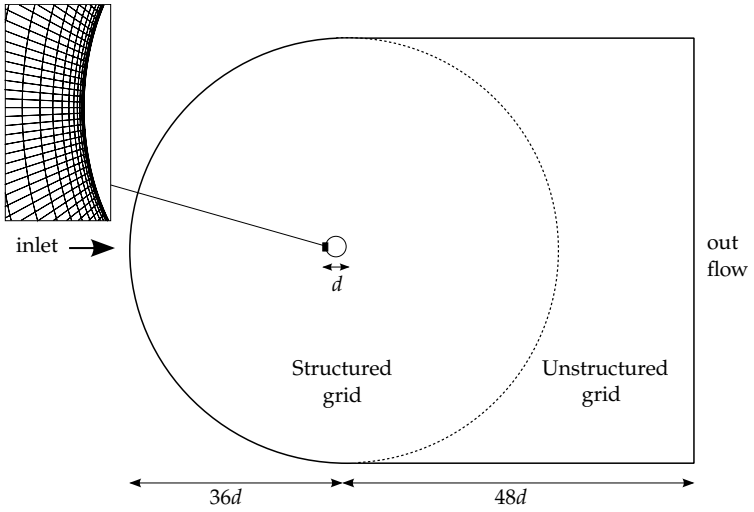

Figure B.3: Computational domain, as a C-grid with flow inlet and outlet from left to right. The black square on the front of cylinder illustrates the area of the zoom.

5454 mixed cells with dimensions of 36d upstream of the cylinder and 48d downstream of the cylinder. For the standard mesh design the first cell height was $1.33 \cdot 10^{-4}$ meters. Since the simulations covers one hour of icing and future simulations are intended to cover a full icing event of several hours, such simulations are not suited to be dissolved with a very small timestep nor a very fine spacious dissolution. The simulation set-up was defined based on a stability criterion, where a time-step size of 0.01 seconds was found reasonable. No change in ice shape, was found using a smaller time-step size.

B.2.3 CFD Icing Model

Ice accretion on the cup anemometer support arm was modelled based on the three overall steps: 1) model the multiphase flow of in-cloud icing, 2) calculate droplet impingement and ice deposit and 3) calculate the ice contour of the cylinder and generate the corresponding mesh. The steps are described in the section B.2.3 to section B.2.3.

Multiphase Flow Model

In this study, the Euler-Euler model in ANSYS Fluent [4] was used to model in-cloud icing conditions. The model treats the multiphase flow as interpenetrating continua, consisting of several volume fractions, which sum to 1 for

all phases q.

$$\sum_{q=1}^{n} \alpha_q = 1 \tag{B.1}$$

The flow is treated as a particle-laden one-way coupled flow, with a dilute dispersed secondary phase of super-cooled droplets. No mass or energy transfer is allowed between the phases. For each phase the conservation equations of continuity and momentum are solved as follows:

$$\frac{\partial(\alpha_q \rho_q)}{\partial t} + \nabla \cdot (\alpha_q \rho_q \boldsymbol{v}_q) = 0 \tag{B.2}$$

$$\frac{\partial(\alpha_q \rho_q \mathbf{v}_q)}{\partial t} + \nabla \cdot (\alpha_q \rho_q \boldsymbol{v}_q \boldsymbol{v}_q) = -\alpha_q \nabla \mathrm{p} + \nabla \cdot \overline{\overline{\tau}}_q + \alpha_q \rho_q \boldsymbol{g} + \mathrm{S} \tag{B.3}$$

where ρ_q is the density, $\boldsymbol{v}_q$ is the velocity vector, $\overline{\overline{\tau}}_q$ is the q^{th} phase stress-strain tensor and $\boldsymbol{g}$ is gravity. The pressure p, is shared by all phases, and the system is closed by a source term S:

$$\mathrm{S} = \sum_{p=1}^{n} \mathrm{K}_{pq}(\boldsymbol{v}_p - \boldsymbol{v}_q) \tag{B.4}$$

where K_{pq} is the interphase momentum exchange coefficient. The source term describes the interphase force between the phases q and dispersed phase p by the interphase momentum exchange coefficient as follows:

$$\mathrm{K}_{pq} = \frac{\rho_p f d_p \mathrm{A_i}}{6\tau_p} = \frac{3\mathrm{C}_D \mathrm{Re_r}(\alpha_p(1-\alpha_p))\mu_p}{4d_p^2} \tag{B.5}$$

where f is the drag function, d_p is the diameter of the dispersed phase, τ_p the particle response time, C_D the drag coefficient, $\mathrm{Re_r}$ is the relative particle Reynolds number and $\mathrm{A_i}$ is the interfacial area concentration. In the Euler-Euler model, $\mathrm{A_i}$ defines the interfacial area between two phases per unit mixture volume and is essential for predicting momentum and energy transfer between the phases. In this study the default symmetric model was used, where $\mathrm{A_i} = \frac{6\alpha_p(1-\alpha_p)}{d_p}$. To model drag, the Schiller-Neumann drag model was used as follows:

$$f = \frac{\mathrm{C_D Re_r}}{24} \tag{B.6}$$

where

$$\mathrm{C_D} = \begin{cases} 24\left(\frac{1+0.15\mathrm{Re_r^{0.687}}}{\mathrm{Re_r}}\right) & \text{for } \mathrm{Re_r} \leq 1000 \\ 0.44 & \text{for } \mathrm{Re_r} > 1000 \end{cases} \tag{B.7}$$

The conservation of energy is a separate enthalpy equation for each phase q [4]. For setting up the conditions of in-cloud icing the volume fraction of the super-cooled droplets is defined as [24]:

$$\alpha_{\mathrm{d}} = \frac{W}{\rho_{\mathrm{d}}} \tag{B.8}$$

where W is the cloud liquid water content ($\mathrm{g/m^3}$), assuming all liquid in the cloud is water and ρ_d is density of the droplets. The diameter of the droplets is described by the median volumetric diameter MVD, as recommended by Finstad et al. (1988) [96]. Turbulence was modelled using the two-equation shear-stress transport (SST) k-ω mixture turbulence model, based on a previous study [26].

Wall Conditions

In this study, the calculated mass of accreted ice will be added to the existing geometry by changing the surface contour of the geometry and by updating the mesh. To ensure mass conservation in the domain, the impinging droplets must disappear at the surface wall, which means that the wall exposed to icing must be able to act as a sink in the computational domain. This is not a standard boundary condition in the Eulerian frame, and thus source terms have been prescribed on the face of the cells adjacent to the surface wall. The source term formulation is inspired by Villalpando et al. (2016) [82] as follows:

$$\mathrm{S}_{\phi} = -(\boldsymbol{v}_{\mathrm{d}} \cdot \boldsymbol{A})\alpha_{\mathrm{d}}\rho_{\mathrm{d}}\phi \tag{B.9}$$

where ϕ is the dependent source variable, $\boldsymbol{A}$ is the face area vector and $\boldsymbol{v}_{\mathrm{d}}$ the droplets velocity vector. To ensure consistency in the system of equations the source term is added to the continuity equation, the x- momentum and y-momentum equations and energy equation.

During ice accretion, the surface roughness will change, which affects the flow transitions in the viscous boundary layer. For wind turbines and icing on airfoils, the roughness is especially important, since it will increase drag [28]. A constant high wall roughness was included through the NASA sand-grain correlation for icing in air flows [29].

Ice Model

The ice model consists of two steps: 1) calculation of droplet impingement, collection efficiency and mass flux of ice, and 2) calculation of the new surface contour and displacement of surface nodes by a developed surface boundary displacement model. The ice model is developed in the DEFINE_GRID_MOTION macro, available in ANSYS Fluent [3]. From fundamental studies by

Langmuir et al. (1946) [18], it can be assumed that it will be the behaviour of the droplets, which will influence the ice deposit the most in the CFD model. The behaviour of the droplets is controlled by the droplet size, the droplet momentum and the dimensions of the object exposed to icing. The collection of water droplets on the object's surface is expressed by the collection efficiency β. When expressing in-cloud conditions in the Eulerian frame, the collection efficiency is found as follows [7]:

$$\beta = \alpha_{\boldsymbol{n}}(\boldsymbol{v}_{\mathrm{n}} \cdot \boldsymbol{n}) \tag{B.10}$$

where α_{n} is the normalised droplet volume fraction, $\boldsymbol{v}_{\mathrm{n}}$ is the normalised droplet velocity and $\boldsymbol{n}$ is the unit surface normal vector. For validation, the collection efficiency is calculated for flow over a circular cylinder of 0.1016 m, with a free stream velocity of 80 m/s and a Langmuir-D distribution with an MVD of 16 µm equivalent to references cases [8, 34].

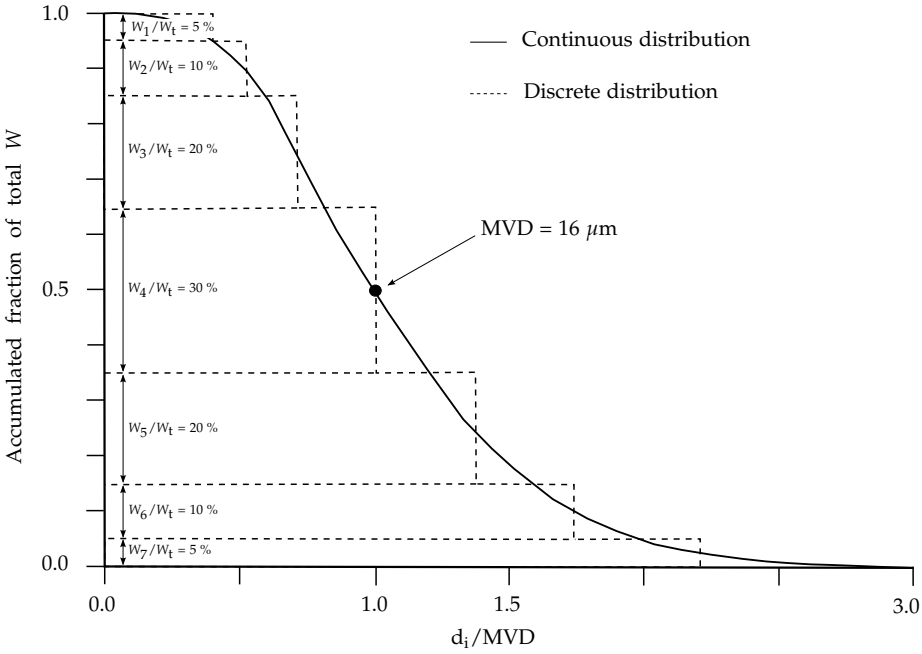

Figure B.4: Dimensionless Langmuir D distribution plotted as discrete cumulative distribution and a continuous cumulative distribution, with a total of 7 groups. The x-axis shows the relation of (d_i/MVD) and the y-axis the cumulative fraction of the total liquid water content. $W_{1\text{-}7}$ is the liquid water content at group i and W_t is the total liquid water content. As by definition, the MVD is found where a cumulative distribution is 0.5 and the relation of d_i/MVD = 1.0 [23].

The composition of droplet sizes in the cloud is generally described by a droplet distribution [11]. A distribution often used for aircraft icing applications are the Langmuir D distribution defined by Langmuir and Blodgett

(1946) [18]. Langmuir et al. (1946) [18] established several droplet distributions by correlating the rate of ice deposition on slowly rotating cylinders exposed to supercooled clouds on the Mount Washington, to theoretical calculations. Later, Papadakis et al. (1989) [23] showed how the MVD can be found from a continuous or discrete droplet distribution based on Langmuir D distribution of droplets. The Langmuir D distribution with and MVD=16 µm used in [8, 34] and in this work, is seen in Figure B.4. The droplet sizes ($d_{1\text{-}7}$) used in each bin are seen in Figure B.7.

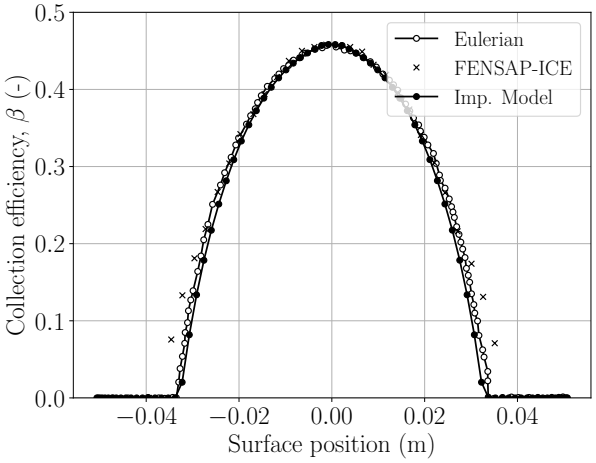

Figure B.5: Comparison of collection efficiency β, for an MVD = 16 µm with an Eulerian model developed in ANSYS Fluent [34] and FENSAP-ICE [8] and the proposed impingement model, Equation B.10.

Figure B.5 shows that the impingement model compares well with the reference cases. The percentage deviation to the Eulerian model presented by [34], is shown in Figure B.6. The figure shows an average deviation below 10 % until the surface position of 0.026m. Towards the impingement limits the deviation increases. However, the significant deviation above 20 % is seen for the last three data points. This deviation is due to a numerical error, when the flow attack angle approaches zero, *i.e.* becomes parallel to the surface. This can cause large relative deviations even for small absolute deviations.

The effect of the droplet inertia is shown by Figure B.7 and Figure B.8. Figure B.7 shows the complete Langmuir-D distribution for an MVD = 16µm, ranging from 5µm to 35.5µm. It is shown, that the impingement area increases with droplet size. In Figure B.8, the effect of the free-stream inlet velocity was shown. The figure illustrates, that an increase in droplet impingement velocity increases the collection efficiency and reverse. Also, the size of the

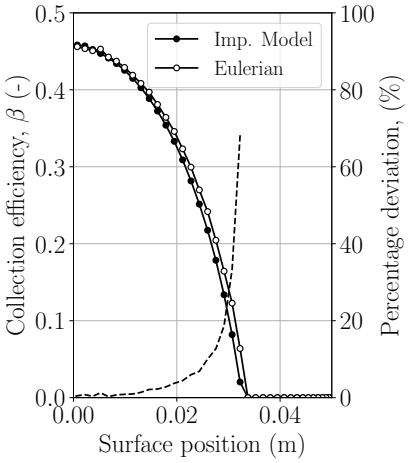

Figure B.6: The percentage deviation found by liner interpolation in collection efficiency presented by [34].

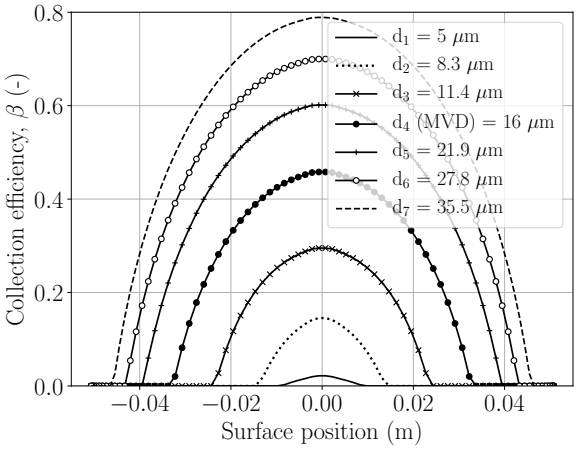

Figure B.7: The collection efficiency for droplet sizes, d_{1-7} for a Langmuir-D distribution with an MVD of 16 µm.

object exposed to icing affect the amount of ice accretion. In Figure B.9 the collection efficiency of the reference case is compared to the diameter of the cup-anemometer support arm (Figure B.1).

The ice model considers only rime ice accretion, which means that all impinging mass will stick to surface and turn into ice. The mass flux of water impingement is found at every cell adjacent to the surface boundary as:

$$\dot{m}_{\text{ice}} = \beta W v_\infty \tag{B.11}$$

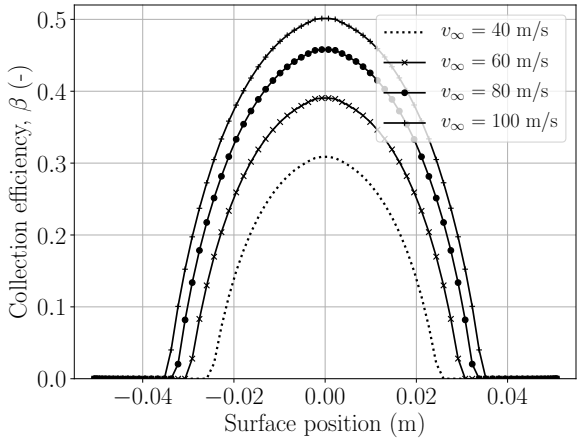

Figure B.8: The collection efficiency for a variation of inlet freestream velocities of 40, 60, 80 and 100 m/s.

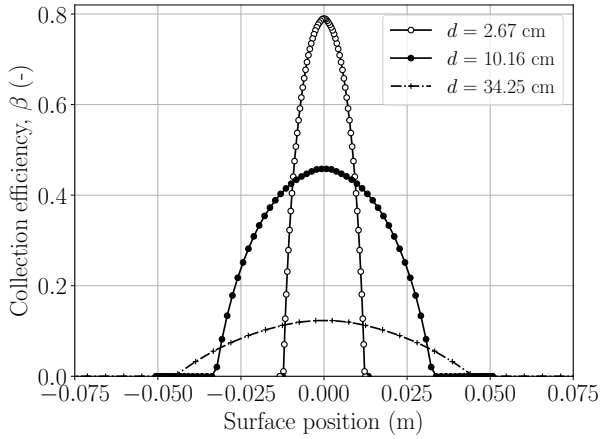

Figure B.9: Comparison of collection efficiency β, for an MVD = 16µm, where d = 2.67cm is the diameter of the cup anemometer support arm, d = 10.16cm corresponds to the reference cases ([34] and FENSAP-ICE [8]).

where v_∞ is the free-stream velocity and $\dot{m}_{\text{ice}}$ is the mass flux of ice (kg/sm^2). The collection efficiency and the mass flux of ice are solved by a face-loop, which goes through every face adjacent cell every time-step, see Figure B.10 (right). In this way, the model always uses the CFD solution of the flow field according to the current time-step and the collection efficiency will always be based on the shape of the cylinder at the current time-step.

Surface Boundary Displacement

The dynamic mesh model in ANSYS Fluent allows for cell zones relative to other boundaries to be moved or adjusted [4]. The ice mass flux is used to calculate a new surface contour of the geometry. Using the developed surface boundary displacement model, the surface nodes ($n_{i,j}$) and the mesh are updated to match the new surface. Mechanisms from the dynamic mesh packages are used to control the remaining of the domain mesh. The surface node displacement vectors are calculated from the ice accretion speed vectors as follows [2, 22]:

$$\mathbf{v}_{n,i} = \frac{\dot{m}_{ice}}{\rho_{ice}} \boldsymbol{n} \tag{B.12}$$

$$\mathbf{V}_{n,i} = \mathbf{v}_{n,i} \Delta t \tag{B.13}$$

where $\mathbf{v}_{n,i}$ is the ice accretion speed vector (m/s) always normal to the surface face, Δt is the time step and $\mathbf{V}_{n,i}$ is the node displacement vector (m) containing the distance from the current positions to the new position. The impingement model was solved on every face center and thus the ice accretion speed vectors were found as face vectors and converted to node vectors by linear interpolation. Figure B.10 (left) illustrates how the ice accretion speed vector was found at node (n_i) by interpolation from the node neighbouring faces (f_l and f_r). The surface nodes are displaced every time-step to

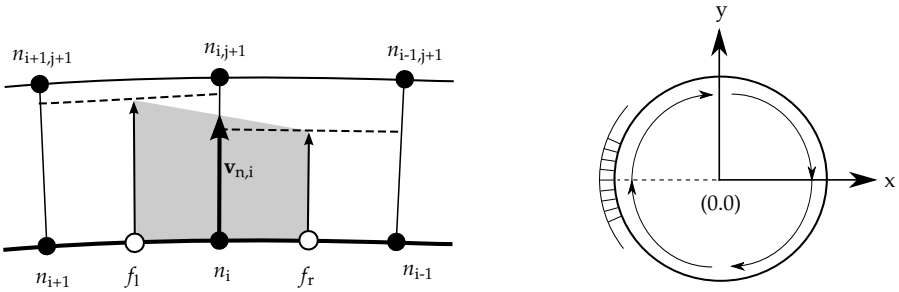

Figure B.10: Left, the ice accretion speed vector $\mathbf{v}_{n,i}$ is calculated based on interpolation from the vectors obtained at the neighbour face centers (f_l and f_r). The shaded grey area illustrates the area of the cells, which will covered by ice according to the calculated $\mathbf{v}_{n,i}$. The area will become a part of the default geometry after the surface boundary displacement (Equation B.14). Right, illustration of the face loop on the cylinder and the wall adjacent cell layer.

new positions by an iterative loop by adding the node displacement vectors to the positions of the nodes at time t as follows:

$$p_{n,i}^{t+\Delta t} = p_{n,i}^{t} + \mathbf{V}_{n,i}^{t} \tag{B.14}$$

where $p_{n,i}$ is the node position, t is the current time and Δt the time-step. Mechanisms used by the dynamic mesh package to control the remaining

domain are: 1) the implicit mesh update, 2) layering and 3) smoothing. Dynamic layering is used to remove or add cells adjacent to the moving surface boundary and is controlled based on the height of the first cell layer adjacent to the moving boundary. The UDF is compiled on the surface boundary of the cylinder and the inlet surface boundary was defined as a stationary surface in the dynamic mesh settings. A ratio-based option is used to control the com-

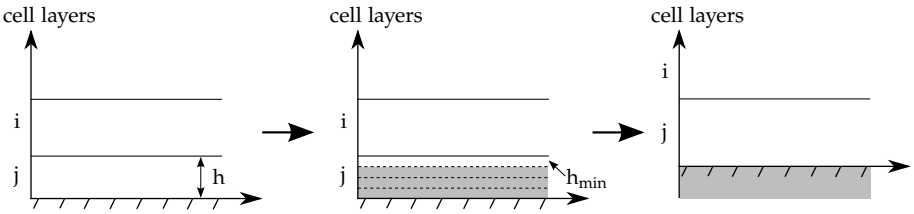

Figure B.11: Compression of cell layer j into cell later i, by allowing cell layer j to be compressed until the specified minimum cell height, h_{min}, is met. The ratio based option ensures that the mesh grading is retained, *i.e.* the first cell layer does not get larger than the second layer.

pression of the first layer of cells (j) before it is merged into the second layer of cells (i), as illustrated in Figure B.11. The cells can be compressed until the ratio $h_{min} < \alpha_{cf} h_{ideal}$ is met, where h_{min} is a specified minimum allowed cell height. In this study a collapse factor α_{cf} is used, which ensures that h_{ideal} is close to the first cell height of the smooth cylinder. The ratio-based option makes sure that the mesh grading is retained. Smoothing is applied at the interior nodes to absorb the mesh movement, without changing the number of nodes and their connectivity.

B.3 Results

Icing was simulated over 1h and compared to the ice thickness L obtained from the image analysis of the cup anemometer support arm. Measurements were used to set the inlet boundary conditions of the model, see Table B.1. The mean value of wind speed was used and a Langmuir-D distribution [18] with a MVD of 16µm was used to specify the dispersed phase conditions. Based on previous studies of the cloud liquid water content in the area [17], a W of $0.3 g/m^3$ was chosen as a reasonable value corresponding to moderate to severe icing. At the wall the NASA-correlation was used, which corresponds to a constant sand grain roughness of $6.19 \cdot 10^{-4}$m.

The development of ice accretion over time is seen by the change of shape of the cylinder. Figure B.12, shows the surface contours calculated based on the displacement vectors $\mathbf{V}_i$ (Equation B.13) after 30, 45 and 60 min of ice accretion. The ice shape changes from a smooth cone at 30 min towards a

Table B.1: Simulation conditions for the flow inlet and the ice specific conditions of the dispersed phase.

Simulation	Mixture inlet	Dispersed phase	Wall conditions
t_{total} = 60 min	v_∞ = 13 m/s	MVD = 16 µm	NASA correlation
Δt = 0.01 s	T_∞ = -3 °C	W = 0.3 g/m^3	source terms
		ρ_{ice} = 600 kg/m^3	

more pointed cone. This happens, because the collection efficiency β (equation B.10) changes over time, as seen in Figure B.13. Towards the 60 min of ice accretion, the deflection of droplets increases, resulting in an increase in the collection efficiency around the stagnation point, but a decrease at the remaining impingement area, see Figure B.13. Small oscillations are seen as the collection efficiency develop over time, but those does however not affect the ice shape. This is due to that the oscillation magnitudes are small, which in combination with low impingement velocities, which do not affect the ice shape significantly.

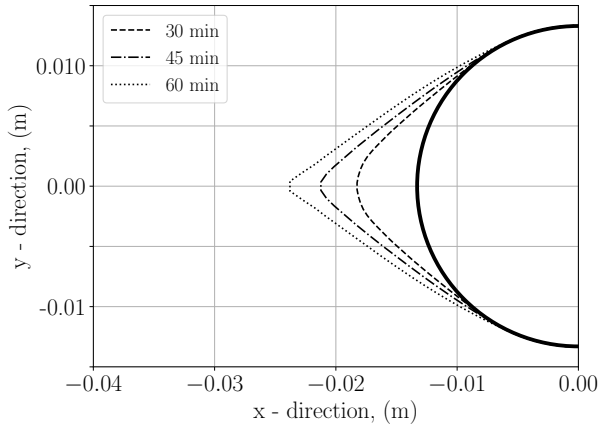

Figure B.12: The surface contour over time after 30, 45 and 60 min of ice accretion. The cylinder without ice corresponds to the black line.

The corresponding development of the mesh surrounding the cylinder is seen before ice accretion to the left in Figure B.14 and to the right at simulation time t = 30 min. The surface boundary displacement model updates the mesh by an iterative process in between each time step according to the calculated surface contour, as explained by Equation B.14. In this way, the ice deposit will always be based on a flow solution which corresponds to the current time step.
In Figure B.15, the ice thickness L obtained from the image analysis of the cup anemometer support arm is plotted against the calculated shapes of the

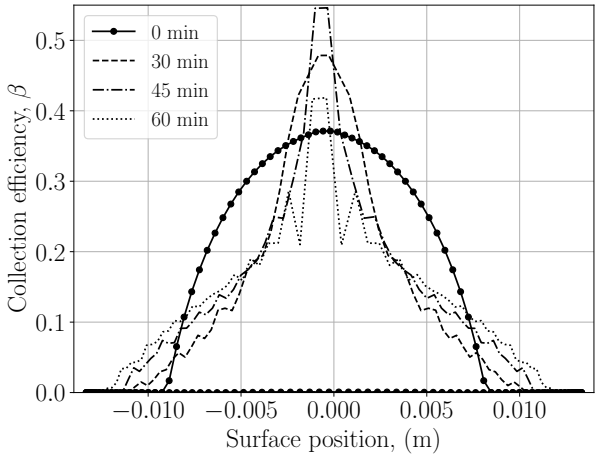

Figure B.13: The collection efficiency over time after 30, 45 and 60 min of ice accretion. The cylinder without ice corresponds to the black line.

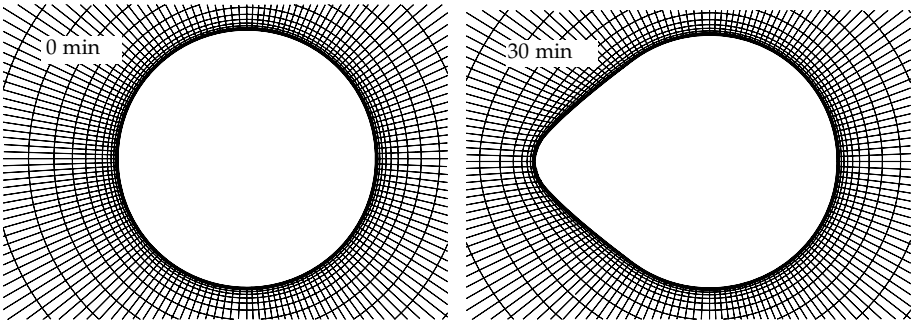

Figure B.14: Mesh surrounding the cylinder, with no surface boundary displacement to the left at time, t = 0 minutes and to the right after 30 minutes of simulation ice accretion, where the surface boundary and the connecting mesh has been displaced according to the amount of accreted ice.

cylinder from the CFD icing model.
Based on the ice shapes shown over time in Figure B.15, the maximum ice thickness L was extracted. Figure B.16, compares the ice thickness obtained from image analysis, L_{image}, to the ice thickness obtained from the CFD icing model, L_{CFD}. The results compare well. A difference in the maximum length of 11.9 % after 30 min, 1.8 % after 45 min and 4 % after 60 min of ice accretion are observed. The deviations in maximum length seen in Figure B.16, are most likely due to the small difference of inlet boundary conditions. The inlet boundary conditions used for the simulation (Table B.1) are representative for the case, but they are not resolved over time. However, the conditions on-site experience by the cup-anemometer arm vary over time and small variations

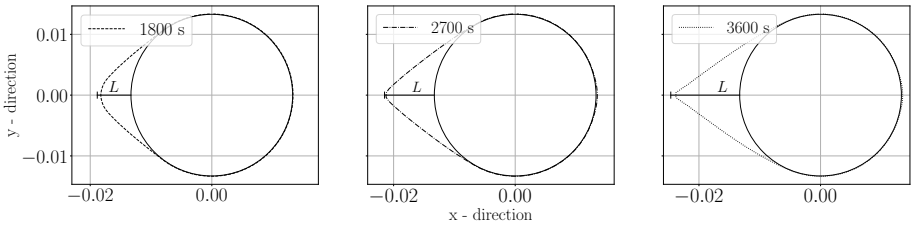

Figure B.15: Ice shapes over time obtained by CFD icing model. The vertical black line denoted by L, shows the ice thickness obtained by experiments using image analysis at the corresponding time.

of for example the droplet size, cloud liquid water content or velocity might have caused the seen deviation.

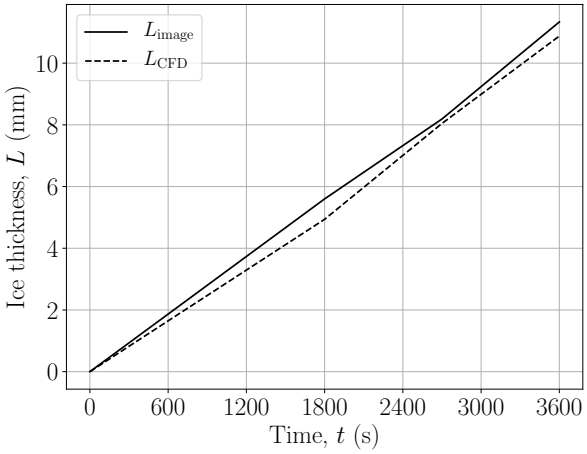

Figure B.16: Comparison of maximum ice thickness calculated by the CFD icing model, L_{CFD} and maximum ice thickness obtained from the experimental data, L_{image}.

B.4 Discussion and Conclusions

Several factors are in evidence of the development of the accreted ice shape, such as the free-stream velocity, the droplet size, the ice density and the size of the object exposed to icing. According to the ISO 12494 standard, rime ice accretion on profiles up to 30cm should be considered vane-shaped, *i.e.* elliptical [14]. The numerical results showed, that the ice shape would be elliptical but change to a more pointed shape towards 60 min of simulated ice accretion. This can be explained by changes in the flow around the cylinder over time and thereby an increased deflection of droplets. Over time,

the droplet impingement area on the cylinder increases, the collection efficiency increases around the stagnation point but decreases at the remaining part of the frontal impingement area of the cylinder (Figure B.13). Since the accreted mass of ice depends on the calculated collection efficiency, the ice shape must develop a pointed shape. In this study, turbulence was modelled using the RANS formulation and the SST k-ω mixture turbulence model, which provides a time-averaged flow field. However, the numerical results might improve by resolving turbulence by a different modelling approach. By Large Eddy Simulations (LES) or Direct Numerical Simulation (DNS), the flow eddies at the boundary layer of the cylinder can be resolved, which might increase the ice accretion along the sides of the ice shape and thereby impose a more elliptical ice shape. As shown, the simulated ice thickness L_{CFD} agreed well with L_{image} and thus it is evident that the ice shape, found from the numerical results, represents reality . Thus, it can be concluded, that the modelling framework in combination with inlet boundary conditions based on measurements, can model icing over 1 h, which compares very well with the experimental data.

For future studies, pictures from the top view of the cup anemometer support arm would be valuable for the validation of the accreted ice shape. Furthermore, if pictures from the top view are available, it is also interesting to update the inlet boundary conditions over time according to measurements. In the presented modelling frame, it can be done by loading profiles of, for example, the velocity components in a UDF.

B.5 Acknowledgement

The work was partly founded by the Innovation Fund Denmark (No. 1355-00120B) and Vattenfall Vindkraft A/S, Denmark. The author would like to thank TechnoCentre éolien for providing the raw data and their generous hospitality during a research stay winter 2015-2016. The author would like to thank Benjamin Martinez from Vattenfall Vindkraft A/S for co-supervising the project.

References

[1] Akhloufi, M., Benmesbah, N., 2014. Outdoor ice accretion estimation of wind turbine blades using computer vision. In: Computer and Robot Vision (CRV), 2014 Canadian Conference on. IEEE, pp. 246–253.

[2] Aliaga, C. N., Aubé, M. S., Baruzzi, G. S., Habashi, W. G., 2011. Fensap-ice-unsteady: Unified in-flight icing simulation methodology for air-

craft, rotorcraft, and jet engines. Journal of Aircraft 48 (1), 119–126. http://arc.aiaa.org/doi/abs/10.2514/1.C000327

[3] Ansys, Inc., 2017. ANSYS Fluent Costumization Manual. Tech. Rep. Release 18.0, ANSYS.

[4] ANSYS, Inc., 2017. ANSYS Fluent Theory Guide. Tech. Rep. Release 18.0, ANSYS.

[5] Baring-Gould, I., Cattin, R., Durstewitz, M., Hulkkonen, M., Krenn, A., Laakso, T., Lacroix, A., Peltola, E., Ronsten, G., Tallhaug, L., Wallenius, T., 2011.13 Wind Energy Projects in Cold Climate. Tech. rep., IEA Wind,http://ieawind.org.

[6] Bourgault, Y., Beaugendre, H., Habashi, W.G., 2000. Development of a shallow-water icing model in fensap-ice. Journal of Aircraft 37 (4), 640–646.http://dx.doi.org/10.2514/2.2646

[7] Bourgault, Y., Boutanios, Z., Habashi, W.G., 2000. Three-dimensional eulerian approach to droplet impingement simulation using fensap-ice, part 1: Model, algorithm, and validation. Journal of Aircraft 37 (1), 95–103.http://dx.doi.org/10.2514/2.2566

[8] Boutanios, Z., 1999. An eulerian 3d analysis of water droplets impingement on a convair-580 nose and cockpit geometry. Master's thesis, Concordia University.

[9] Bredesen, R., Cattin, R., Clausen, N.-E., Davis, NeilJordaens, J. P., Khadiri-Yazami, Z., Klintström, R., Krenn, A., Lehtomäki, V., Ronsten, G., Wadham-Gagnon, M., Wickmann, H., 2017. 13 wind energy projects in cold climate, 2. edition. Tech. rep., IEA Wind.http://ieawind.org

[10] Bredesen, R.E., Ausland, R. H., 2015. Methods for evaluating risk caused by ice throw and ice fall from wind turbines and other tall structures. In: 16th International Workshop on Atmospheric Icing on Structures (IWAIS, Uppsala, Sweden, July 2015). Http://iwais.org/proceedings/.

[11] Crowe, C. ., Multiphase Flow Handbook. CRC Press, Taylor & Francis Group, 6000 Broken Sound Parkway NW, Suite 300, Boca Raton, FL 33487-2742, USA: Taylor & Francis, 1 ed., 2006.

[12] Finstad, K. J., Lozowski, E. P., Makkonen, L., 1988. On the Median Volume Diameter Approximation for Droplet Collision Efficiency. Journal of the atmospheric sciences 45 (24), 4008–4012.http://dx.doi.org/10.1175/1520-0469(1988)045<4008:OTMVDA>2.0.CO;2

[13] Hedde, T., Guffond, D., 1995. Onera three-dimensional icing model. AIAA journal 33 (6), 1038–1045.

[14] ISO standard 12494, 2001. Atmospheric Icing on structures, ISO 12494:2001(E). Tech. rep., ISO, Geneva, Switzerland,https://www.iso.org/obp/ui/#iso:std:iso:12494:ed-1:v1:en.

[15] Jiang, X., Wang, Q., Zhang, Z., Hu, Y., Pan, Y., Zhu, C., 2015. Study on icing characteristics of bundle conductors based on xuefeng mountain natural icing station. In: 16th International Workshop on Atmospheric Icing on Structures (IWAIS, Uppsala, Sweden, July 2015). IWAIS, http://iwais.org/proceedings/.

[16] Krenn, A., Pieter, J. J., Wadham-Gagnon, M., Davis, N., Clausen, N.-E., Lehtomäki, V., Jokela, T., Kaila, S., Ronsten, G., Wickmann, H., Klintström, R., Cattin, R., 2016. Available Technologies of Wind Energy in Cold Climates. Tech. rep., IEA Wind Task 19, http://www.ieawind.org.

[17] Lamraoui, F., Fortin, G., Benoit, R., Perron, J., Masson, C., 2014. Atmospheric icing impact on wind turbine production. Cold Regions Science and Technology 100, 36–49. http://dx.doi.org/10.1016/j.coldregions.2013.12.008

[18] Langmuir, I., Blodgett, K., et al., 1946. Mathematical investigation of water droplet trajectories. Tech. rep.

[19] Makkonen, L., 2000. Models for the Growth of Rime, Glaze, Icicles and Wet Snow on Structures. Philosophical Transactions of the Royal Society of London A: Mathematical, Physical and Engineering Sciences 358 (1776), 2913–2939. http://dx.doi.org/10.1098/rsta.2000.0690

[20] Makkonen, L., Laakso, T., Marjaniemi, M., Finstad, K., 2001. Modelling and prevention of ice accretion on wind turbines. Wind Engineering 25 (1), 3–21. http://dx.doi.org/10.1260/0309524011495791

[21] Messinger, B. L., 1953. Equilibrium Temperature of an Unheated Icing Surface as a Function of Air Speed. Journal of the Aeronautical Sciences (Institute of the Aeronautical Sciences) 20 (1), 29–42.http://dx.doi.org/10.2514/8.2520

[22] NTI, 2012. User Manual FENSAP-ICE, Version 2012 release 1.1. Manual.

[23] Papadakis, M., Zumwalt, G., Elangonan, R., Freund Jr, G., Breer, M., and Whitmer, L., 1989. An Experimental Method for Measuring Water Droplet Impingement Ef-

ficiency on Two-and Three-Dimensional Bodies, tech. rep. https://ntrs.nasa.gov/archive/nasa/casi.ntrs.nasa.gov/19900067654.pdf.

[24] Pedersen, M. C., Martinez, B., Yin, C., 2015. Development of cfd-based icing model for wind turbines: A case study of ice sensor. In: Proceedings of the 33rd Wind Energy Symposium. American Institute of Aeronautics &Astronautics. http://dx.doi.org/10.2514/6.2015-1472

[25] Pedersen, M. C., Sørensen, H., Swytink-Binnema, N., Martinez, B., Condra, T., 2018. Measurements from a cold climate site in Canada: Boundary conditions and verification methods for CFD icing models for wind turbines. Cold Regions Science and Technology. https://doi.org/10.1016/j.coldregions.2017.12.007

[26] Pedersen, M. C., Yin, C., 2014. Preliminary modelling study of ice accretion on wind turbines. Energy Procedia. http://dx.doi.org/10.1016/j.egypro.2014.11.1102

[27] Pouryoussefi, S. G., Mirzaei, M., Alinejad, F., Pouryoussefi, S. M., 2016. Experimental Investigation of Separation Bubble Control on an Iced Airfoil using Plasma Actuator. Applied Thermal Engineering 100, 1334–1341. https://doi.org/10.1016/j.applthermaleng.2016.02.133

[28] Shin, J., Berkowitz, B., 1994. Prediction of ice shapes and their effect on airfoil drag. Journal of aircraft 31 (2), 263–270. http://dx.doi.org/10.2514/3.46483

[29] Shin, J., Bond, T. H., 1992. Experimental and computational ice shapes and resulting drag increase for a naca 0012 airfoil. Tech. rep., NASA Technical Memorandum 105743.https://ntrs.nasa.gov/archive/nasa/casi.ntrs.nasa.gov/19930018251.pdf

[30] Villalpando, F., Reggio, M., Ilinca, A., 2012. Numerical study of flow around iced wind turbine airfoil. Engineering Applications of Computational Fluid Mechanics 6 (1), 39–45. http://dx.doi.org/10.1080/19942060.2012.11015401

[31] Villalpando, F., Reggio, M., Ilinca, A., 2016. Prediction of ice accretion and anti-icing heating power on wind turbine blades using standard commercial software. Energy 114, 1041–1052. http://dx.doi.org/10.1016/j.energy.2016.08.047

[32] Wadham-Gagnon, M., Swytink-Binnema, N., Bolduc, D., Tété, K., Arbez, C., 2015. Ice Detection Methods and Measurement of Atmospheric Icing. In: 16th International Workshop on Atmospheric

Icing on Structures (IWAIS, Uppsala, Sweden, July 2015). IWAIS, http://windren.se/IWAIS_p/IWAIS2015/IWAIS2015_pa/40_06_02_Paper_WadhamGagnon_Ice_Detection_Methods_and_Measurement_of_Atmospheric_Icing.pdf.

[33] Wickman, H., 2013. Evaluation of field tests of different ice measurement methods for wind power. Master's thesis, Uppsala University, Sweden,http://www.diva-portal.org/smash/record.jsf?pid=diva2%3A661721&dswid=438.

[34] Wirogo, S., Srirambhatla, S., 2003. An eulerian method to calculate the collection efficiency on two and three dimensional bodies. In: 41st Aerospace Sciences Meeting and Exhibit, Reno, Nevada. Vol. 1073. http://dx.doi.org/10.2514/6.2003-1073

[35] Wright, W., 2008. User's Manual for LEWICE Version 3.2. http://ntrs.nasa.gov/search.jsp?R=20080048307

Paper C

Preliminary Modelling Study of Ice Accretion on Wind Turbines

Marie Cecilie Pedersen and Chungen Yin

The paper has been published in *Energy Procedia* Vol. 61, pp. 258–261, 2014,
https://doi.org/10.1016/j.egypro.2014.11.1102

The layout has been revised.

Preliminary Modelling Study of Ice Accretion on Wind Turbines

M. C. Pedersen [a,b], C. Yin[b]

[a] *Vattenfall Vindkraft A/S, Jupitervej 6, DK-6000 Kolding, Denmark*
[b] *Aalborg University, Department of Energy Technology, Pontoppidanstraede 111, DK-9220 Aalborg, Denmark*
[c] *TechnoCentre éolien, 70 rue Bolduc, Gaspé (Québec) G4X 1G2, Canada*

Abstract

One of the main challenges associated with cold-climate wind energy is icing on wind turbines and a series of icing-induced problems such as production loss, blade fatigue and safety issues. Because of the difficulties with on-site measurements, simulations are often used to understand and predict icing events. In this paper, a new methodology for prediction of icing-induced production loss is proposed, from which the fundamentals of ice accretion on wind turbines can be better understood and the operational production losses can be more reliably predicted. Computational fluid dynamics (CFD) modelling of ice accretion on wind turbines is also performed for different ice events, resulting in a reliable framework for CFD-based ice accretion modelling which is one of the key elements in the new methodology.

Keywords: Ice accretion; CFD; multiphase flow; wind turbines; cold climate; user defined function

C.1 Introduction

Since 2008, the estimated annual wind power capacity placed at cold locations has more than tripled and the number is expected to increase in the upcoming years. Wind farms in cold climate areas are exposed to harsh conditions resulting in high annual production losses. An example is Vattenfall's second largest onshore wind farm located in Sweden. This wind farm suffers from icing-induced annual production losses in the order of 10 % of the total annual production. Losses of this magnitude impact greatly on the profitability of the wind farm and can result in devastating commercial consequences. The periods with icing occurs regularly through the winter period and range from a couple of hours up to several days and even periods of up to 2 weeks

of complete standstills has occurred [1]. Due to the relatively short history of wind energy in cold climate areas, complete knowledge about the so-called icing issue is still missing.

In the current research of modelling of icing on wind turbines, two conceptually different types of models are applied [3,45,97]. One is the ice accretion model proposed by Makkonen [2], describing in-cloud icing on a vertically placed, freely rotating cylinder. However, icing characteristics on a vertical, freely rotating cylinder are most likely different from icing on a wind turbine blade in circular motion in a vertical plane. The other conceptual model is dedicated for simulation of ice accretion on airfoils and has been widely used and also validated for aircraft applications [4] [5]. However, it has rarely been used in wind energy applications. Moreover, none of the mentioned models has been coupled with numerical weather models to address variations in external meteorological conditions during an icing event and none of the models appropriately takes ice melting and shedding effect into account so far.

This project aims to develop a general wind turbine icing model and based on which to derive a useful engineering model for power loss prediction. In this paper, a new methodology for predicting icing-induced power loss is presented. As one of the key elements in the new methodology, CFD-based ice accretion modelling is performed for two different cases (i.e., rime icing and glaze icing), from which a reliable CFD modelling framework is established. Here, only the key results are briefly presented and discussed. Upon request, all the details will be given in an extended version of this paper.

C.2 New Methodology Proposed for Prediction of Icing-induced Production Loss

Figure C.1 shows the new methodology proposed in this project to predict icing-induced production loss. The general CFD-based ice accretion model, which is to be coupled with the numerical weather forecast model and is to integrate important ice accretion and shedding effects, is the key element in the methodology and is the base to derive a new engineering model for icing-induced power loss prediction.

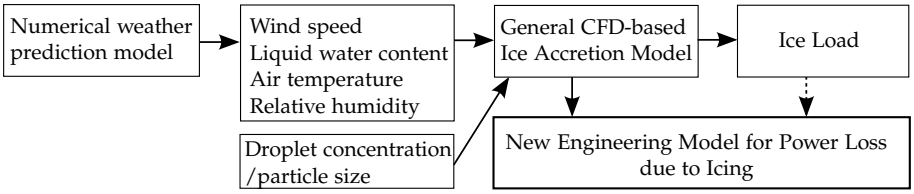

Figure C.1: New methodology proposed for prediction of icing-induced production loss.

C.3 CFD-based Ice Accretion Model

The general CFD-based ice accretion model mainly consists of the following tasks: (1) clear air flow modeling. Reliable modeling of air flow around wind turbine is very important, not only for subsequent ice accretion modeling but also for drag and lift prediction from which torque and power production are evaluated; (2) water droplet-air multiphase flow modeling and (3) ice accretion modeling.

Preliminary CFD modelling of different icing events are performed, using ANSYS FLUENT. The airfoil used is NACA63-3-418, which has a sharp trailing edge. As seen in Figure C.6 (top), the C-grid topology is used, since it allows the angle of attack to be varied. The direction to loop the ice accretion model over the airfoil surface is also indicated in Figure C.6 (bottom), i.e., counter-clockwise from the trailing edge to the trailing edge. In the glaze ice event to be presented in the paper, the LWC is assumed to be a constant of 0.7 g/kg, and the median volumetric diameters (MVD) of droplets are assumed to be 25 µm and 60 µm, respectively. In the CFD simulations, different turbulence models (i.e., the Spalart-Allmaras model, realizable k-ϵ and SST k-ω model) are compared for air flow modelling. The Eulerian multiphase model is used for droplet flow modelling, since it is applicable to 3D and eases the calculation of the collection efficiency [3]. A refined Messinger's model [4] is constructed for ice accretion modelling and implemented into FLUENT via user-defined function (UDF). The ice accretion model is based on an impingement model governed by the collection efficiency (β) and heat/mass balances over each control volume at the airfoil surface [5] [6].

In the general CFD-based ice accretion model, the transient buildup of ice on the airfoil surface will be modeled, in which the shape of the ice and its impact on local mesh and aerodynamics will be dynamically simulated. The force, torque and power production will be calculated during the icing event. At this stage, the shape of ice and dynamic mesh are not yet taken into account, since the preliminary CFD modelling is mainly to conclude on various sub-models or subroutines and to establish a reliable modeling

framework.

C.4 Results and Discussion

The predicted drag and lift are plotted in Figure C.2 and Figure C.3, together with experimental data.

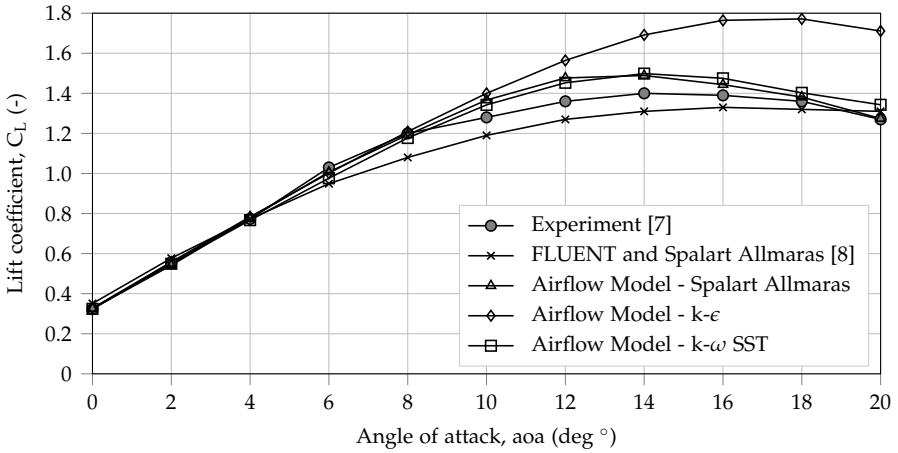

Figure C.2: Comparison of lift coefficient C_L as a function of angle of attack (AoA).

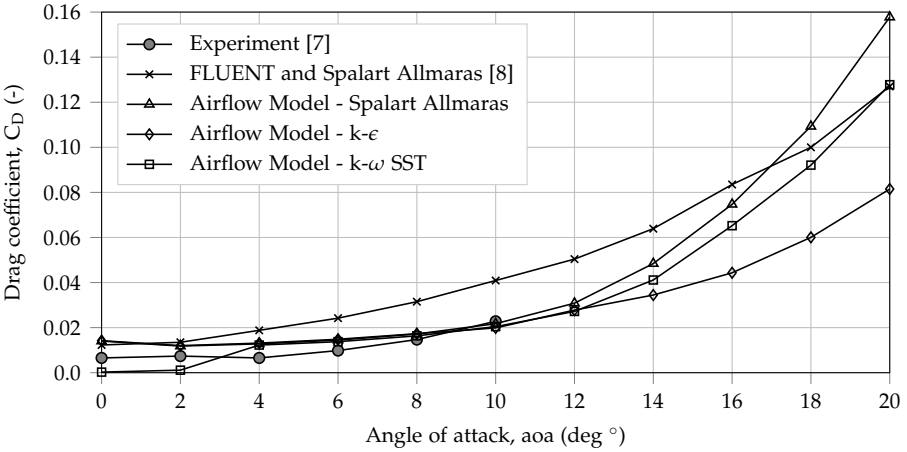

Figure C.3: Comparison of drag coefficient C_D as a function of angle of attack (AoA).

The SST k-ω model is found to outperform the realizable k-ϵ and Spalart-Allmaras model in the force prediction. Figure C.7 to the left shows the contours of droplet volume fraction and Figure C.7 to the right, shows the

droplet velocity for MVD of 25 µm. The droplet collection efficiency (β) is shown in Figure C.4 as a function of the cell number. Both curves have a sudden break around the peak value, which is supposed to be caused by a lower velocity at the stagnation point and the mesh density. The droplet volume fraction is plotted in Figure C.5 on the upper and lower side of the airfoil as a function of the chord length.

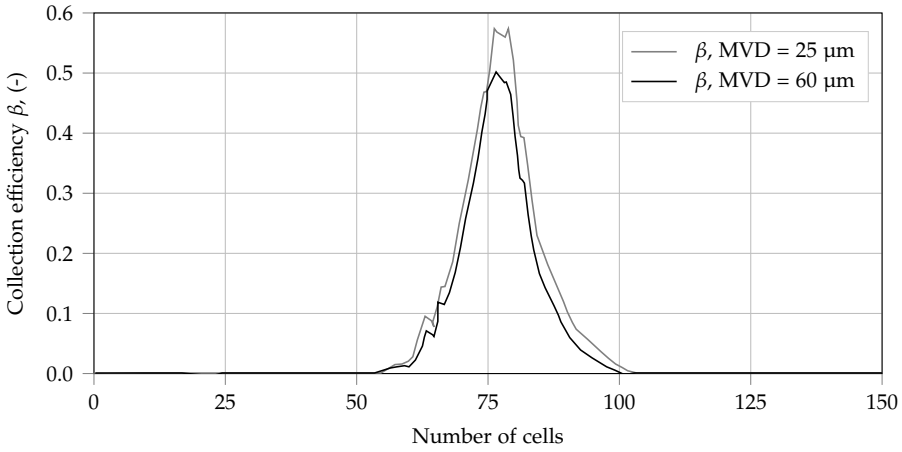

Figure C.4: Plot of droplet collection efficiency, (MVD = 25 µm).

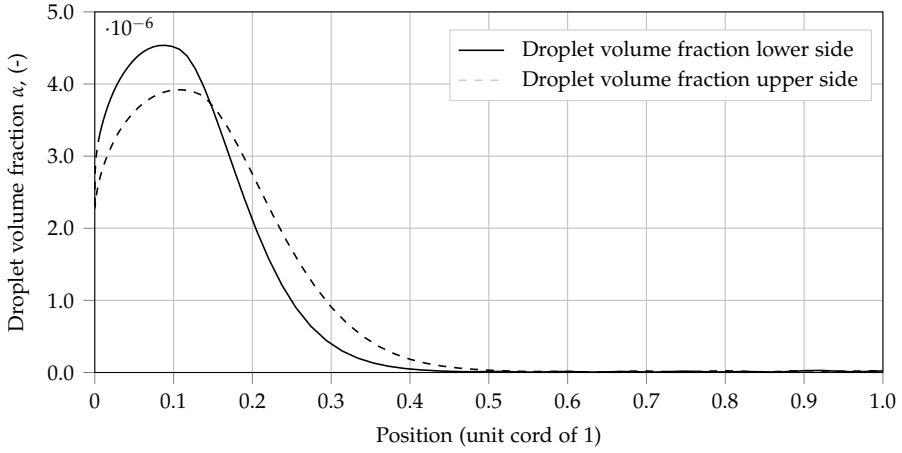

Figure C.5: Plot of droplet volume fraction on airfoil surface (MVD = 25 µm).

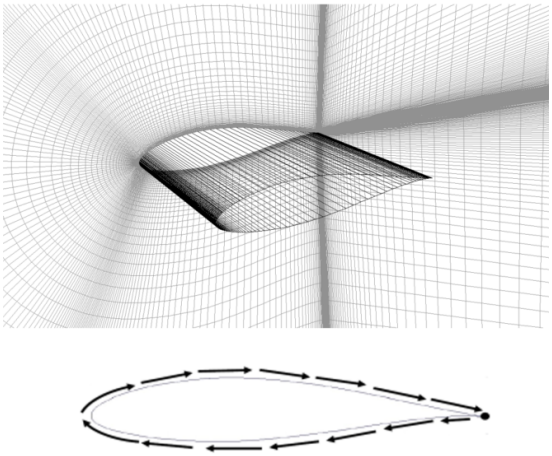

Figure C.6: The NACA63-3-418 airfoil.

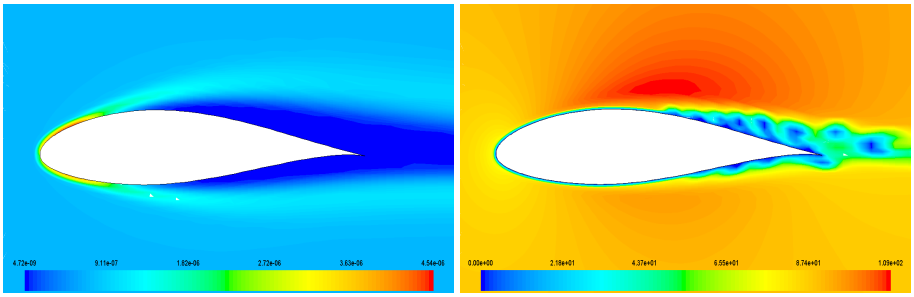

Figure C.7: Left, the droplet volume fraction and the droplet velocity to the right (MVD = 25 μm).

C.5 Conclusions

A new methodology for prediction of icing-induced production loss is proposed. The general CFD-based ice accretion model is the key element, which will be coupled with numerical weather prediction model and will appropriately address key ice accretion and shedding effects. Preliminary icing simulations have been performed. It is concluded that the SST k-ω turbulence model, Eulerian multiphase model and a refined Messinger's model are appropriate sub-models for air flow, droplet flow and ice accretion, respectively. They will be integrated in the newly proposed methodology for icing prediction.

C.6 Acknowledgement

This work was financially supported by the Industrial PhD Programme Grant, "WINDICE: Reliable prediction of icing on wind turbines and icing-induced power loss".

References

[1] Madsen J., Wind R&D Portfolio- Status Report, Wind R&D Portfolio, Vattenfall AB, Sweden, 2013.

[2] Makkonen, L., 2000. Models for the Growth of Rime, Glaze, Icicles and Wet Snow on Structures. Philosophical Transactions of the Royal Society of London A: Mathematical, Physical and Engineering Sciences 358 (1776), 2913–2939. http://dx.doi.org/10.1098/rsta.2000.0690

[3] Bourgault, Y., Boutanios, Z., Habashi, W.G., 2000. Three-dimensional eulerian approach to droplet impingement simulation using fensap-ice, part 1: Model, algorithm, and validation. Journal of Aircraft 37 (1), 95–103.http://dx.doi.org/10.2514/2.2566

[4] Messinger, B. L., 1953. Equilibrium Temperature of an Unheated Icing Surface as a Function of Air Speed. Journal of the Aeronautical Sciences (Institute of the Aeronautical Sciences) 20 (1), 29–42.http://dx.doi.org/10.2514/8.2520

[5] Son C., Oh S., and Yee K., 2012. Quantitative analysis of a two-dimensional ice accretion on airfoils, Journal of mechanical science and technology 26 (4), 1059–1071, 2012. http://dx.doi.org/10.1007/s12206-012-0223-z

[6] Martini F., and Ramdenee D., and Ibrahim H., and Ilinca A., 2012. A multiphase CFX based approach into ice accretion modeling on a cylinder. Electrical Power and Energy Conference (EPEC), 2011 IEEE, 450–455. http://dx.doi.org/10.1109/EPEC.2011.6070243

[7] D. A. Abbott, I.H, *Theory of wing sections*. New York, USA: Dover, 1 ed., 1959.

[8] K. Mortensen, CFD Simulations of an Airfoil With Leading Edge Ice Accretion, Master's thesis, 2008.

Paper D

Development of CFD-based Icing Model for Wind Turbines: A Case Study of Ice Sensor

Marie Cecilie Pedersen, Benjamin Martinez and Chungen Yin

The paper has been published in the *33rd Wind Energy Symposium, AIAA SciTech Forum* Kissemmee, Florida, USA, January 5-9, 2015,
https://doi.org/10.2514/6.2015-1472

The layout has been revised.

Development of CFD-based Icing Model for Wind Turbines: A Case Study of Ice Sensor

M. C. Pedersen [a,b], Benjamin Martinez[a], Chungen Yin[b]

[a] *Vattenfall Vindkraft A/S, Jupitervej 6, DK-6000 Kolding, Denmark*
[b] *Aalborg University, Department of Energy Technology, Pontoppidanstræde 111, DK-9220 Aalborg, Denmark*

Abstract

Operation of wind turbines in cold climate areas is challenged by icing-induced problems, such as loss of production, safety issues and blade fatigue. Production losses are especially a big issue in Sweden, and due to difficulties with on-site measurements, simulations are often used to get an understanding and to predict icing events. In this paper a case study of modeling icing using Computational Fluid Dynamics (CFD) is proposed. The case study aims to form the basic of a general CFD model for icing on wind turbine blade sections.

Nomenclature

LWC	Liquid Water Content, g/m^3
MVD	Median Volumetric Diameter, m
α	volume fraction, $-$
ρ	density, kgm^3
$\mathbf{u}$	droplet velocity, m/s
β	collection efficiency,$-$
$\dot{m}$	mass flux, kg/m^2s
U	velocity, m/s
$\vec{V}$	ice accretion speed, m/s
$\vec{\mathbf{n}}$	surface normal vector
$\Delta\vec{r}$	surface displacement vector

Subscript

d	dispersed phase
n	normalized
q	phases
abs	absolute
∞	infinity
imp	impingement

D.1 Introduction

Producers of wind energy are challenged in terms of finding lucrative available sites for wind energy and are forced to look at sites with higher risks. One example is cold climate areas, which are most often remote and sparsely populated and offers a vast of wind energy extraction, but also offers a great deal of icing induced problems such as production losses, blade fatigue and safety issue.

Cold climate areas are defined by experiencing temperatures below the operation limits of standard wind turbines and by the presence of icing events. During icing conditions, ice can be accreted on a structure by the impact of moisture at temperatures below 0 °C, also known as *atmospheric icing* [1]. Periods where the conditions are in favor of ice accretion is called *meteorological icing*, whereas the periods where the ice remains on the structure and most likely disturbs the performance of the wind turbine is called *instrumental icing*. For the reference wind farm of this work, periods of instrumental icing varies from a few hours up to weeks during the winter season and the annual production losses due to icing is in the range of 3-15% of the total production. Losses of this magnitude has tremendous impact of the profitability of the wind farm and enhances the need for knowledge within the field. Such areas be categorized as experiencing what is defined as *moderate to heavy icing* resulting in economic and safety risks. Today, the installed capacity experiencing such conditions is approximately 11 GW and is expected to double by 2017 [2].

Atmospheric icing can be divided into three main categories: 1) in-cloud icing, where super-cooled droplets are present in a cloud or in fog at cold temperatures resulting in the creation of hard rime, soft rime or glaze ice depending on the exact conditions; 2) freezing rain or 3) wet snow icing, which means snow accumulating on the structure when the ambient temperature is close to 0 °C [3]. The focus of this work is in-cloud icing, even though it is known that wet snow icing also happens at the reference site.

Atmospheric icing has been studied quite extensively for power lines and within the field aeronautics especially with the airfoil as the point of origin [4]. In general, modeling of atmospheric icing on wind turbines can be divided into two conceptually different approaches. One approach is based on Makkonen's [5] empirical model for a freely rotating cylinder. The model has been extensively applied for different cases and extended for different applications and recently seen in combination with meso-scale models [3]. However, icing on a freely rotating cylinder is most likely different from icing

on a turbine blade and yet not representative for a wind turbine blade. The other approach is based on modeling icing on an airfoil or wind section. This has been widely studied in aeronautics either by using panel based methods and solving potential flow equations on the boundaries or more recently by employing CFD, as seen in [6], [7], [8]. The advantage of developing an icing model in CFD is that the ice-induced changes in the aerodynamic properties can be easily inspected and determined. This is definitely an advantage over the panel based methods and it is furthermore of interest for establishing the relationship between the simulated icing events simulated and loss of power production, which the final goal of this project.

A common dilemma for all approaches is validation, since it is difficult to reproduce the exact conditions for icing in e.g. an climatic wind tunnel and since on-site measurements are often not available or of poor quality.

D.1.1 Objectives and Approach

This paper presents a case study of CFD modeling of icing on an ice sensor in a Swedish wind farm. The ice sensor is chosen for the case study, since it experiences conditions similar to the wind turbines on the site and since on-site measured data was available. The case study serves to form the basis of a general CFD icing model for wind turbines, as illustrated in Figure D.1. The figure shows the new methodology proposed to predict icing induced production losses. The general model is to be coupled with numerical weather forecast models and will be the key element in the methodology for finally deriving a new engineering model for icing induced power loss prediction.

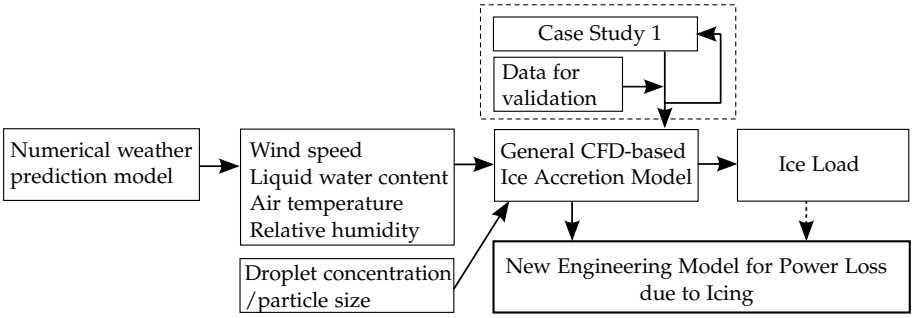

Figure D.1: Methodology for prediction of icing induced power losses for wind turbines.

D.2 Ice Load Measurements on Wind turbines

The harsh conditions, which the wind turbines are exposed to at the wind farm in Sweden are shown in Figure D.2. The first row presents four extreme cases of icing, whereas the second row illustrates changes in the conditions during 24 hours respectively. By inspecting the pictures the extreme conditions at the wind farm can clearly be identified, but it is difficult to get an exact measure of the actual ice load on the blade. As far as the author is aware no such system exist yet. Thus getting a measure of the ice load on the wind turbine is often done by a combination of pictures, ice sensor measurements and ice models. This fact is the prime reason for performing a case study of an ice sensor facing equivalent conditions as the wind turbine to form the basis for the general CFD model.

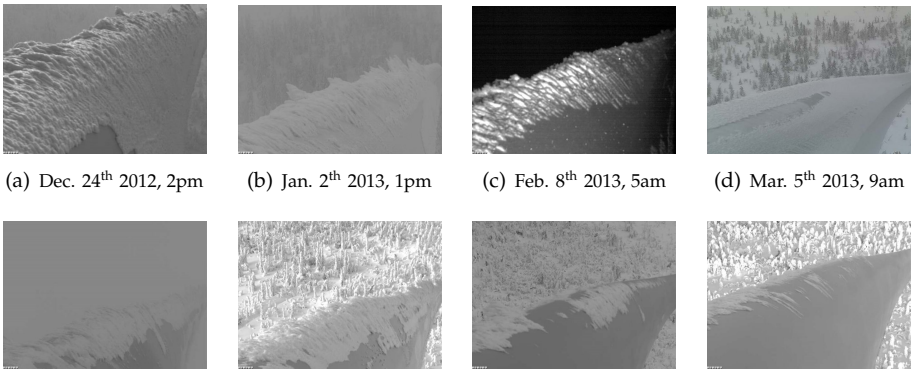

(a) Dec. 24th 2012, 2pm (b) Jan. 2th 2013, 1pm (c) Feb. 8th 2013, 5am (d) Mar. 5th 2013, 9am

(e) Feb. 16th 2013, 10am (f) Feb. 16th 2013, 1pm (g) Feb. 17th 2013, 8am (h) Feb. 17th 2013, 3pm

Figure D.2: Pictures taken from the hub looking towards the tip of the blade on one of the wind turbines in the Swedish wind farm.

D.3 Methods

The model is set up in the software ANSYS-FLUENT and the modeling routine follows a preliminary study, which expresses in-cloud icing in CFD [9]. Thus, in general the icing model is based on following the 5 steps [9], [10]:

1. Airflow of clean target object
2. Multiphase flow with airflow with super-cooled droplets
3. Collection of droplets on the target object (collection efficiency) and initiate the ice modeling

4. Ice modeling by solving thermodynamic equations on the object surface to obtain ice load

5. Generation of ice geometry and grid displacement by dynamic meshing

In-cloud icing conditions are expressed by a two-phase droplet laden flow with super-cooled droplets. Based on the preliminary study, the Euler-Euler framework will express the two-phase flow, in which the k-ω turbulence model and the Eulerian multiphase model will be employed for air flow and droplet flow respectively. In the Eulerian approach, the phases are treated as interpenetrating continua, which introduces the concept of phasic volume fractions. The total sum of the phases q are equal to one, as seen in Equation D.1 and the dispersed phase representing the droplets is given based on the Liquid Water Content (LWC) as seen in Equation D.2:

$$\sum_{q=1}^{n} \alpha_q = 1 \tag{D.1}$$

$$\alpha_d = \frac{LWC}{\rho_d} \tag{D.2}$$

The liquid water content is one of the key parameters, when modeling in-cloud icing. LWC in the cloud is extremely difficult to measure and is thus represented by using 1-hour meso-scale data. The value of LWC varies during the winter as illustrated in Figure D.3.

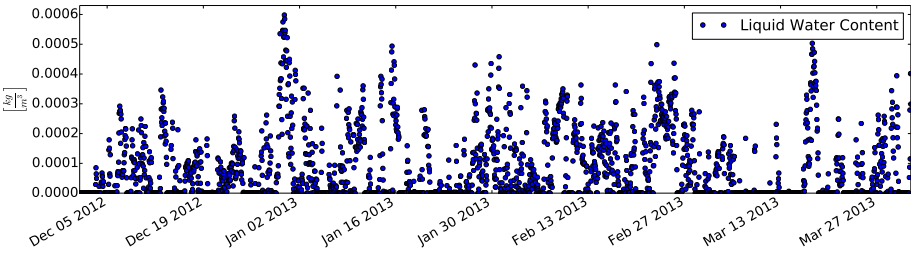

Figure D.3: Variation in LWC from the winter of 2012/2013 given in kg/m^3.

The inlet conditions will be tuned to represent the actual conditions at the site in Sweden. More icing events will be mimicked to foster a close relation to the measured data. The collection of droplets on the structure forms the basic of the icing model, which is inspired by Messenger's model [4] and will be implemented in the CFD framework by employing User Defined Functions.

D.3.1 Impingement Model

The impingement of droplet on the object surface initiates the icing model and is expressed by the collection efficiency β [8]. Since the flow solution

in the Eulerian frame yields the droplets volume fraction and the droplet velocity everywhere in the domain, β can be expressed as follows,

$$\beta = -\alpha_n \mathbf{u}_n \cdot \mathbf{n} \tag{D.3}$$

where α_n is the normalized droplet volume fraction on the surface, $\alpha_n = \left(\frac{\alpha_{abs}}{\alpha_\infty}\right)$, $\mathbf{u}_n$ the nondimenzionalised droplet velocity, $\mathbf{u}_n = \left(\frac{\mathbf{u}}{U_\infty}\right)$, and $\mathbf{n}$ the surface normal.
From the collection efficiency the mass flux of water impingement, $\dot{m}_{\text{imp}}$, can be determined everywhere on the object surface, see Equation D.4,

$$\dot{m}_{imp} = (LWC) U_\infty \beta \tag{D.4}$$

where U_∞ is the freestream velocity of the flow. By employing a control volume approach everywhere on the boundary of the object energy and mass conservation can be derived to find the mass flux of ice, $\dot{m}_{ice}$ and thereby the local accumulated ice load [10], [4]. For this case study it is assumed, that all droplets which impinge with the target object will stick to the object, freeze and turn into ice, which yields that:

$$\dot{m}_{imp} = \dot{m}_{ice} \tag{D.5}$$

The assumption in Equation D.5 would hold for cold icing days, with temperatures $\leq$ -5 °C, resulting in rime ice accretion [1], [11] . From the CFD solutions the needed values for Equation D.3 and EquationD.4 can be retrieved.

D.3.2 Mesh Displacement

The mesh displacement approach is inspired by [7], [10], [11] and has been implemented into ANSYS-FLUENT by applying user defined functions and Dynamic Meshing. Based on the mass flux of ice retrieved every where on the boundary by a faceloop, the thickness of the ice can be found, which is represented by an ice accretion speed $\vec{V}_{ice}$ as,

$$\vec{V}_{ice} = \frac{\dot{m}_{ice}}{\rho_{ice}} \vec{\mathbf{n}} \tag{D.6}$$

where $\vec{V}_{ice}$ is the ice accretion speed vector and $\vec{\mathbf{n}}$ is the surface normal vector. A surface displacement vector $\Delta\vec{r}$ is computed from the ice accretion speed vector to complete the displacement of mesh as follows,

$$\Delta\vec{r}^{\,t+\Delta t} = \Delta\vec{r}^{\,t} + \vec{V}_{ice}^{\,t} \Delta t \tag{D.7}$$

where $\Delta\vec{r}$ is the surface displacement vector and Δt is the time step. As seen from Equation D.7 the displacement vector directly reflects the growth of ice and the ice height during the displacement. A value of the surface displacement vector is retrieved on every node on the boundary and can be updated every time step if needed or at a given specific time.

D.4 Case Study 1

The CFD methodology, as outlined previously in the 5 steps, is expected to be applicable to different geometries. The main purpose of the case study is to establish a complete CFD method by applying the 5 steps to an ice sensor and evaluate the approach by on-site measurements. With this done, the same CFD method will be applied to a wind turbine model represented by blade sections.

The ice sensor or the IceMonitor, as it is called, is placed in the wind farm on a met mast 100 meters above the ground and seen in Figure D.4.

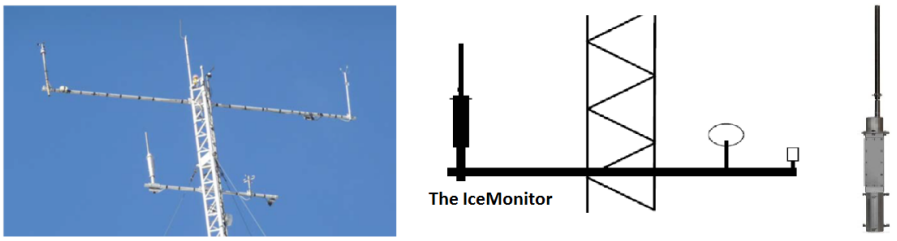

Figure D.4: The IceMonitor and the installation at the met mast in the Swedish wind farm.

The IceMonitor measures the ice load on a freely rotating 0.5 m long vertical cylinder with a diameter of 0.03 m. The bearings are heated to keep the cylinder turning in the extreme conditions. The rotations of the cylinder makes it able to detect ice from all wind directions. The measuring range of the IceMonitor is 0-10 kg with an accuracy of $\pm$50 g, which is quite rough. On-site measurements from the winter of 2012/2013 is seen in Figure D.5, notice that the load of almost 7 kg in the beginning of January 2013. The data from the IceMonitor will be used for validation in combination with meso-scale data, pictures of the IceMonitor and Vattenfall's existing in-house model.

D.4.1 Case Setup

The IceMonitor is modeled by using the C-grid topology and placing a cylinder of 0.5 m and a diameter(d) of 0.03 m in a domain with 70·d upstream and

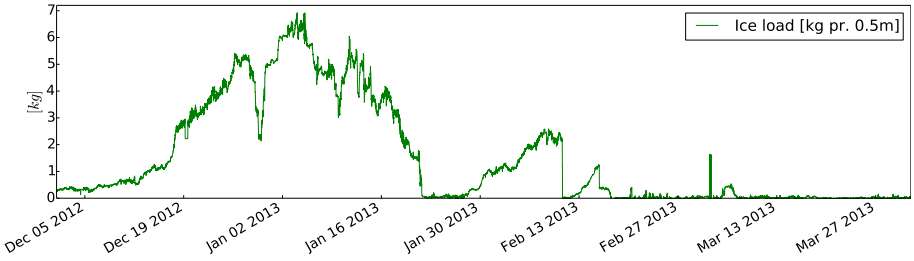

Figure D.5: Data from the IceMonitor from the winter of 2012/2013 given in kg per 0.5m, which correspond to the length of the monitor.

horizontal and 90·d downstream, see Figure D.6. The height of the domain is 1.5 times the height of the cylinder. The structure below the heated bearings is not taken into account, since no ice is measured here.

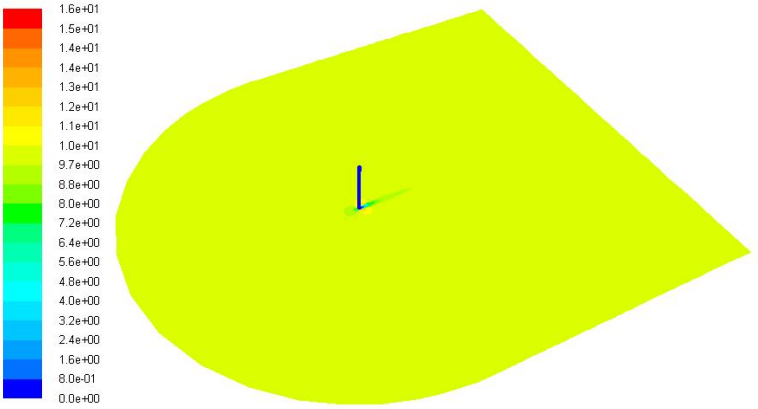

Figure D.6: The cylinder representing the IceMonitor in the domain. Only the bottom part of the domain is shown and the contour is colored by airflow velocity in $\frac{m}{s}$.

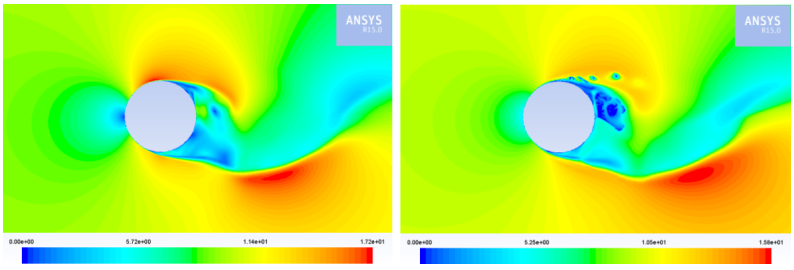

Figure D.7: Contour plots of airflow velocity and droplet velocity, $\frac{m}{s}$, to visualize the Eulerian frame.

As a starting point the IceMonitor is simulated in two-dimensions using the topology described above. The model is set up in ANSYS-FLUENT by combining an airflow model using the k-ω SST turbulence model with the Euler-Euler multiphase model, as described in Section D.3. By employing the Euler-Euler model it is possible to represent the conditions for in-cloud icing quite well and to extent the frame to also include e.g the distribution of the droplet's Median Volumetric Diameter (MVD), UDFs can be employed. The MVD is also a quantity, which cannot be measured but could be expressed by a gamma distribution [12] as presented in [13] .

To illustrate the Eulerian frame in CFD contour plots are seen in Figure D.7, from a case with: α_d = 7e-7, U_∞ = 10 m/s, MVD = 25 µm, LWC = 0.3 g/m^3 and a temperature of -5 °C. The calculated values of mass flux ($\dot{m}_{ice}$) of ice is seen in Figure D.8 (a), corresponding to 0.5 minutes of ice accretion with mesh update every iteration and the corresponding values of droplet volume fraction (α_d) is seen in Figure D.8 (b). According to the presentation of Equation D.3 and D.4 in this paper the volume fraction of droplets on both the upwind side of the cylinder and the "shadow side", the downwind side of the cylinder also yields ice accretion on both sides of the cylinder.

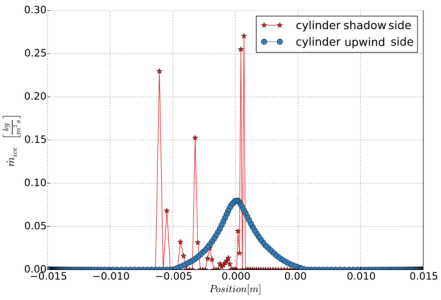

(a) Mass flux of ice kg/m^{3}s.

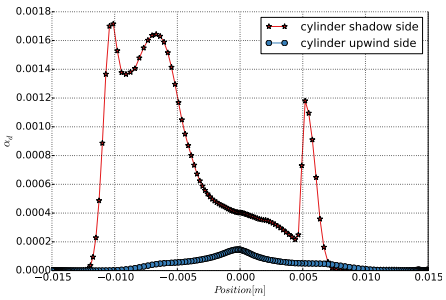

(b) Droplet volume fraction.

Figure D.8: Mass flux of ice (a) and droplet volume fraction on the upwind side of cylinder and on the shadow side of the cylinder.

The high concentrations of droplet volume fraction in small areas on the shadow side of the cylinder can result in sharp peaks of ice accretion, whereas the ice accretion is more even on the upwind side. The sharp peaks of ice accretion challenges the mesh update approach on the shadow side of the cylinder, as illustrated in Figure D.9 (c) and (d), from the case setup mentioned above.

The ice accretion speed V_{ice} , seen in Euqation D.6 is plottet in Figure D.10 (a), (b) and (c) for the situation seen by the contour plots in Figure D.9. The

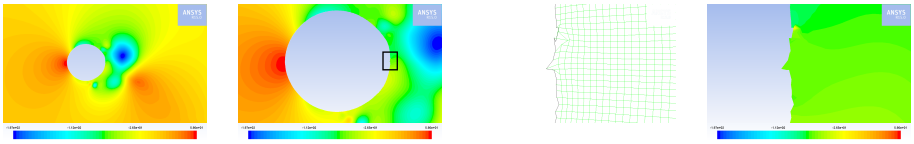

(a) The ice monitor in the domain.

(b) Indication of location of mesh problems.

(c) Zoom on the mesh at the critical area on the shadow side.

(d) Zoom on the mesh at the critical area on the shadow side.

Figure D.9: Contour plots colored by total pressure, colorbar: -197 to 58.6 Pa .

entire cylinder is seen in (a) and an almost uniform vector distribution is seen for the upwind side of the cylinder in (b), whereas the sharp peaks of ice accretion are clearly seen by vectors in (c).

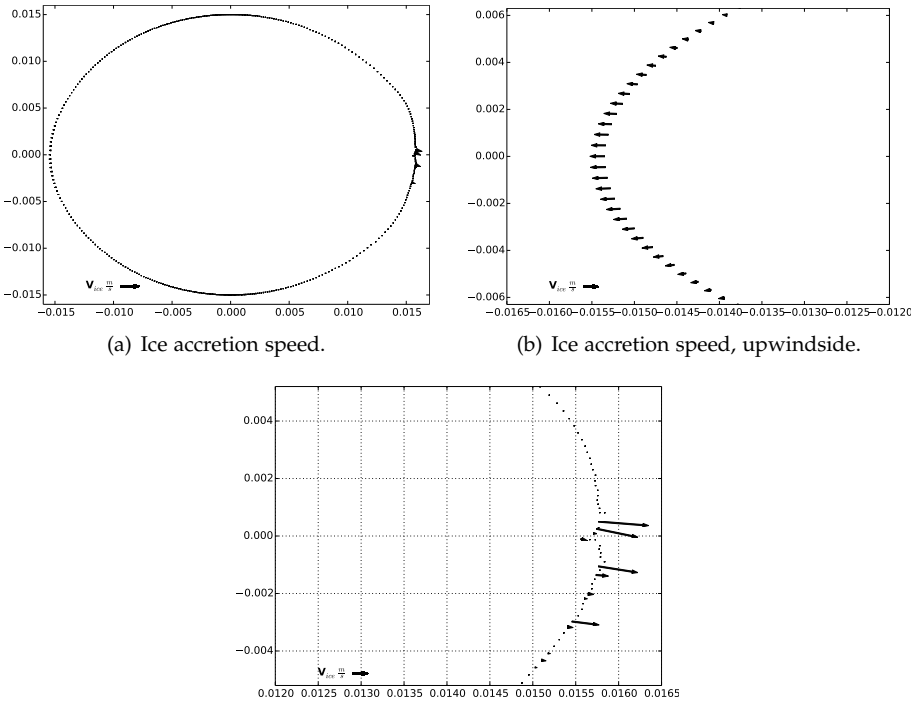

(a) Ice accretion speed.

(b) Ice accretion speed, upwindside.

(c) Ice accretion speed, shadowside.

Figure D.10: The accretion speed vector on the IceMonitor (a), upwind side (b) and shadow side (c) respectively.

D.5 Conclusion

It can be stated that the model frame for performing the case study for rime ice accretion has been defined and a useful database is available for validation of the model. Attention on the mesh-update approach is essential for establishing a reliable frame for the model and still more refinement is needed. Nevertheless a foundation of an icing model using ANSYS-FUENT has been established. Implementation of meso-scale data is important for comparison with the existing in-house model and the measured values of ice load from the IceMonitor. The expected final results are a reliable representation of the IceMonitor at the Swedish wind farm and thereby a solid foundation for developing the general CFD model for icing on wind turbines.

D.6 Acknowledgement

Marie Cecilie Pedersen would like to thank Vattenfall R&D and the Danish Agency for Science Technology and Innovation for their financial support of the PhD project.

References

[1] Svensk Standards Institute. SS-ISO 12494, Atmospheric icing of structures, 2001.

[2] BTM World Market Update 2012. Special Theme: Cold Climate Turbines, *A BTM Wind Report*, Chp. 7, March 2013.

[3] Davis N, Hahmann NA, Clausen N-E, Žagar M. Forecast of Icing Events at a Wind Farm in Sweden, *Journal of Applied Meteorology and Climatology*, Vol. 53, p. 262-281, February 2014.

[4] Messinger BL. Equilibrium Temperature of an Unheated Icing Surface as a Function of Air Speed, *Lockheed Aircraft Corporation*, I.A.S., Los Angeles, USA, 1953.

[5] Makkonen L. Models of Growth of Rime, Glaze, Icicles and Wet Snow on Structures, *Philosophical Transactions: Mathematical, Physical and Engineering Sciences* Vol. 358, No. 1776, Ice and Snow Accretion on Structures, p. 2913-2939, November 2000.

[6] Ping F, Farzaneh M. A CFD approach for modeling the rime-ice accretion process on a horizontal-axis wind turbine, *Journal of Wind Engineering and Industrial Aerodynamics*, Vol. 98, p. 181-188, 2010.

[7] Cao Y, Ma C, Zhang Q, Sheridan J. Numerical simulation of ice accretions on an aircraft wing, *Aerospace Science and Technology*, Vol. 23, p. 296-304, 2012.

[8] Bourgault Y, Boutanios Z, Habashi WG. Three-Dimensional Eulerian Approach to Droplet Impingement Simulation Using FENSAP-ICE, Part 1: Model, Algorithm, and Validation, *Journal of Aircraft*, Vol. 37, No. 1, January-February 2000.

[9] Pedersen MC, Yin C. Preliminary modelling study of ice accretion on wind turbines, Energy Procedia (2014), http://dx.doi.org/10.1016/j.egypro.2014.11.1102.

[10] Son C, Sejong O, Kwanjung Y. Quantitative analysis of a two-dimensional ice accretion on airfoils, *Journal of Mechanical Science and Technology*, Vol. 26, p. 1059-1071, 2012.

[11] User Manual FENSAP-ICE. Newmerical Technologies International, Version 2012 release 1.1, Newmerical Technologies International, Montreal, Quebec, Canada, 2012.

[12] Thompson G, Field PR, Rasmussen RM, Hall WD, Explicit Forecasts of Winter Precipitation Using an Improved Bulk Microphysics Scheme. Part II: Implementation of a New Snow Parameterization, *American Meteorological Society*, Vol. 132, p.519-542, February 2004.

[13] Thompson G, Nygaard BE, Makkonen L, Dierer S. Using the Weather Research and Forecasting (WRF) Model to Predict Ground/Structural Icing *American Meteorological Society*, Vol. 132, p.519-542, February 2004.

Paper E

Case Study of an Ice Sensor using Computational Fluid Dynamics, Measurements and Pictures - Boundary displacement

Marie Cecilie Pedersen, Henrik Sørensen, Benjamin Martinez and Thomas Condra

The paper has been published in the *International Workshop on Atmospheric Icing on Structures (IWAIS)* Uppsala, Sweden, June 28-July 31, 2015.

The layout has been revised.

Case Study of an Ice Sensor using Computational Fluid Dynamics, Measurements and Pictures - Boundary displacement

M. C. Pedersen [a,b], H. Sørensen[b], Benjamin Martinez[a] and T.J. Condra[b]

[a] *Vattenfall Vindkraft A/S, Jupitervej 6, DK-6000 Kolding, Denmark*
, [b] *Aalborg University, Department of Energy Technology, Pontoppidanstræde 111, DK-9220 Aalborg, Denmark*

Abstract

This paper presents an icing model developed using Computational Fluid Dynamics (CFD). One key part part of the model development is the surface boundary displacement due to the accumulated mass of ice. The paper presents the development of a boundary layer displacement method to be included in the CFD icing model using ANSYS Fluent.

Keywords: ice accretion; surface boundary displacement, Computational Fluid Dynamics, dynamic-mesh, cold climate

E.1 Introduction

Icing on wind turbines has been studied over the last 20 years and modelling of icing is a discipline, which has been approached by different methods and for different applications. Nevertheless, utility companies wish to improve and develop new and more precise turbine icing tools and production loss assessment models. The need for solving the energy and mass balance for droplets impinging on an object and to obtain the mass of accumulated ice over time is common for most of the tools. Within the wind power industry the model by Makkonen [1], originally developed for power line icing, has been widely used and is part of the iso standard iso-12494:2001 [2]. In recent work by Davis [3] the impact of icing on wind turbines was studied using Numerical Weather Prediction (WRF[1]) in combination with an icing model based on Makkonen's model [1], to forecast production losses due to icing. The original model [1] is empirically tuned for a cylinder but not a

[1] Weather Research and Forecasting

wind turbine. Thus, to improve on this fact [3] represents the turbine by a 1m long blade segment represented as a cylinder with a diameter based on the leading-edge radius of the given airfoil, and this showed promising results [4].

The power of the methodology by Davis [3] is the ability to study icing on an annual basis and the forecasting application provided by using the numerical weather models. However, details of a smaller time-scale from each individual icing event might be lost or not available. For future improvements of the methodology, a 3D CFD icing model specifically designed for wind turbines is put forward as a solution [3]. The methodology used by Vattenfall is similar to the overall approach seen in [3], but without any modifications to the Makkonen model. Similar to the conclusions from [3] experience have shown that changes to the ice model are essential to improve the overall production loss assessment methodology. Thus, this work aims to clarify whether a detailed CFD model can bring value into the current methodology for production loss assessment.

CFD models have met resistance in the wind power industry because of the computation time, the use of constant meteorological conditions and finally it has been questioned, if the accuracy gained from the micro-physics of a CFD simulations is necessary. In [5] an icing event of 17 hours was modelled using FENSAP-ICE based on data collected at a wind farm in Gaspé, Québec, Canada. The computational time was reduced by using a multi-shot approach of 34 steady-state simulations of 0.5 hours of icing, dividing the turbine blade into 9 stations and running the simulation in 2D. FENSAP-ICE is an commercial CFD code, which was originally developed for aircraft icing and is based on Messinger's model from 1953 [6]. The simulations were fed with observed values of temperature and wind speed and to obtain the power output a BEM-code was included. Another example of FENSAP-ICE being used for wind turbine application is seen in [7] and the [8], where performance degradation and power losses were studied and the possibilities of the design of an anti-icing system was proposed. The drawback of FENSAP-ICE is the strong link to the aircraft industry and that the model does not include shedding, which allows exaggerated ice horns to form [3]. Production loss assessment methods driven by numerical weather models [3] are typically fed with 1 hour based data. Such data can also be used in CFD simulations, as well as data of a much smaller time-scale. Furthermore, distributions of the Median Volumetric Diameter (MVD) can be included, which completely eliminates the issue of constant meteorological conditions.

A challenge when studying icing is the accessibility to observed and measured data. One problem is the reliability of the measurement equipment, as

pointed out in [9]. Another is the complexity related to measuring and observing icing directly on the turbine itself, as seen at the TechnoCentre éolien, Quebec, Canada [10]. Thus, to circumvent the issue an ice sensor, installed at Vattenfall's Swedish wind farm, Stor-Rotliden, has been chosen as the foundation of the development of an CFD-based icing model for wind turbines. The ice sensor is combitec IceMonitor, which is a 0.5m long freely rotating cylinder with a diameter of 3cm. It is installed on a met mast together with other measurement equipment, as seen in Figure E.1. From the CFD model development based on the IceMonitor, including testing and validation, the approach will be applicable to any geometry such as a turbine blade or a blade section. As the numerical platform of the study ANSYS Fluent has been used.

(a) (b)

Figure E.1: The IceMonitor to the left in the pictures at Stor-Rotliden wind farm with limited ice (a) and fully iced (b).

Other studies using ANSYS Fluent for icing applications are seen in [11] and [12]. In [11] the flow field around three different iced airfoils based on the airfoil (NACA 63-415) are simulated. The three geometries were obtained from experiments using in-fog icing conditions in a refrigerated wind tunnel. The k-ω SST turbulence model was used to study and compare numerical and experimental values of the lift, drag and pressure coefficients. A similar study was carried out in [12]. Another icing related study carried out using ANSYS Fluent is presented in [13], where the droplet collection efficiency (β) was calculated using an Eulerian frame, by employing the User-Defined-Scalar-Transport framework in ANSYS Fluent. In the Eulerian frame the collection efficiency was defined as:

$$\beta = \frac{\alpha_n(\boldsymbol{u} \cdot \boldsymbol{n})}{U_\infty} \tag{E.1}$$

where $\boldsymbol{n}$ is the unit surface normal vector, $\alpha_{\boldsymbol{n}}$ is the normalised droplet volume fraction on the surface and U_∞ is the free-stream velocity. This approach, of calculating the collection efficiency, is equivalent to the approach by FENSAP-ICE presented in [14]. Common for the previous work carried out using ANSYS Fluent is:

- decoupling of the iced geometry obtained and studying the aerodynamic changes of the iced geometry
- decoupling of the impingement model and ice model with the geometry change of the iced object

However, this study aims to combine the entire process into a full icing model capable of:

1. Impingement model (multiphase flow and collection efficiency)
2. Ice model including runback
3. Generation of new geometry of iced object
4. Study of the aerodynamic changes and the ability to add a heat source for de-icing applications

This paper focuses on the generation of the new geometry of the iced object. This is an essential step, which has to be robust and able to handle any kind of ice accumulation on the surface. From a CFD point of view, two approaches are suitable for this purpose:

- variable porosity
- surface boundary displacement

If taking a look at fouling deposition modelled in various CFD-combustion applications, the underlying methodology is similar to the accumulation of ice. An example is the work seen by Knudsen [15], where a porosity model is developed in ANSYS-CFX to account for the geometry change due to ash deposition. Using porosity approach in CFD simply means prescribing a porosity to each cell and updating the porosity according to the accumulated mass. Thus, if the given cell is completely covered by mass of for example ash slag, the cell will be included as completely blocked in the CFD flow solution. In this way, the geometry change is taken into account. The advantage of this approach is that a complex mesh-update algorithm is avoided and the computational time is kept low. The drawback could be the need for a very fine mesh to account for smaller-scale geometry changes, which might be interesting to include in an ice accretion model.

The other way to account for the accumulated mass is to update the surface boundary mesh and generate a new iced geometry. In [16] a method to predict ice on an airfoil is presented using a 2D panel method and Messinger's model as the thermodynamic model. From the calculated mass of accumulated ice, the ice thickness is found as $h = \dot{m}_{ice}\Delta t/\rho_{ice}\Delta s$ (m), where ρ_{ice} is the ice density [16] [17]. The new surface is generated by first placing the new nodes at the corresponding thickness in a perpendicular direction to the old surface followed by connecting the nodes by average points between the nodes. To account for shape distortion and twisting of the grid, for example, glaze ice conditions, a smoothing algorithm is included, which can delete and renumber nodes. In [18] heat and mass transfer is studied with in improved roughness model for aircraft applications using a the 2D CIRAMIL code, which is a combination of a 2D potential flow solver and a thermodynamic solver. The panels are updated by using the bisection-method, which insures that the ice grows continuously in the normal direction to the surface. The panels are calculated based on the old nodes and the ice sections are limited by the bisection of angles with adjacent neighbouring panels. In FENSAP-ICE the mesh is updated similar to [16] by a surface displacement vector $\Delta h = \dot{m}_{ice}\Delta t/\rho_{ice}$, which is obtained from the ice accretion speed vector normal to the surface [19]. The ice accretion speed vector is used as an input to an Arbitrary Lagrangian-Eulerian (ALE) formulation to displace the surface in time [19] [20].

E.2 Method

The model is set-up in the environment of ANSYS Fluent following a preliminary modelling study [21]. The Euler-Euler multiphase model [22] is employed to express the two-phase droplet laden flow of air and super-cooled water droplets in combination with the k-ω SST turbulence model [11], assuming no coalescence or break-up of particles and no heat or mass transfer between the phases. As mentioned previously two methods are suitable for taking the accumulated mass of ice into account. In this study it was chosen to use the surface boundary displacement method. The surface boundary displacement are addressed by employing User Defined Functions. The entire method is illustrated by the flow-diagram in Figure E.2.

E.2.1 Ice Model

In this study a simplified rime ice situation is modelled, since the surface boundary displacement is the main objective of the paper. Under rime ice accretion it is assumed, that all particles which hit the surface will freeze instantly and turn into ice. In fact, the complete model is based on a set of

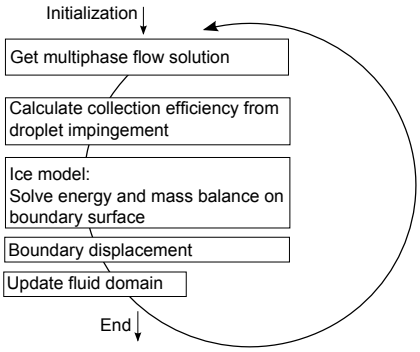

Figure E.2: Flow diagram of the modelling structure

partial differential equations (PDEs), originally presented in [6]. The PDEs will be integrated in the model frame by the User-Defined-Scaler-Transport framework in ANSYS Fluent [23]. The mass of ice $\dot{m}_{\text{ice}}$ initiates the mesh update algorithm and is explained in the following section.

E.2.2 Boundary Displacement

To insure a reliable and robust surface boundary displacement, the accumulated mass of ice has to be conserved, the ice growth is continuous and normal to surface and the displacement must be mesh independent. The surface boundary displacement is initialised by the Dynamic-mesh package by ANSYS Fluent [22], from where the DEFINE_GRID_MOTION macro is used, which is linked to an ANSYS Fluent node position algorithm. The macro is transient and by an iterative process the node points can be updated. The approach of this study is inspired by work using the ice height Δh_{ice} to displace the node points.

From the instantaneous accumulated mass of ice the mesh is updated by calculating a node displacement vector $\boldsymbol{v}_{\text{n,i}}$ giving the (x,y) coordinate of the new location of the node. The node displacement vector is obtained by a face-looping approach as follows:

1. Obtain face cell centre position displacement vector ($\mathbf{v}_{\text{f,i}}$), see Equation E.2
2. Relate/convert face cell centre position to new node positions
3. Move node point location by node displacement vector by an iterative mesh update process

$$\mathbf{v}_{\text{f,i}} = \frac{\dot{m}_{\text{ice}}}{\rho_{\text{ice}}} \boldsymbol{n} \tag{E.2}$$

where, ρ_{ice} is the density of ice and $\boldsymbol{n}$ is the surface normal. Figure E.3 illustrates the boundary displacement only based on the face centre displacement vectors. The shaded grey area is the area from each boundary cell, which is occupied by accumulated ice according to the face centre displacement vector. The red circle shows the inconsistent distribution of the accumulated mass of ice between the faces, which challenges the creation of the new surface boundary. To circumvent the issue illustrated in Figure E.3, corresponding node

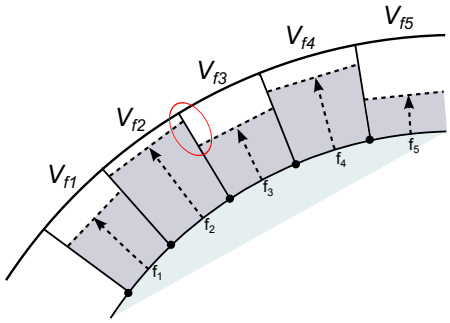

Figure E.3: Boundary displacement by face centre displacement vectors.

displacement vectors are found by liner interpolation, as illustrated in Figure E.4. From this method, the total accumulated mass of ice in each boundary cell will be distributed evenly to created the new surface boundary of the object, illustrated by the dashed line. By the linear interpolation the contri-

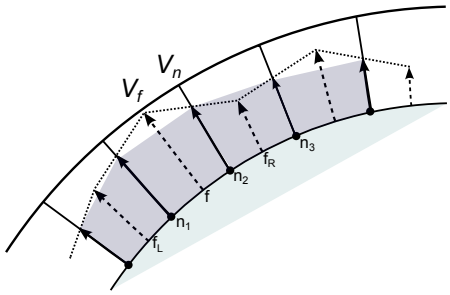

Figure E.4: Boundary displacement by converting face centre displacement vectors to node displacement vectors.

bution from the node neighbouring face, f_L and f_R , to the node displacement vector is enabled. The nodes are updated according to the following expression:

$$p_{n,i}^{t+\Delta t} = p_{n,i}^{t} + \mathbf{v}_{n,i}^{t}\Delta t \tag{E.3}$$

where $p_{n,i}$ is the current node positions, t is the current time and Δt the time step. The boundary layer displacement is fully transient, which means that

the mesh is updated every time step.

E.3 Results

Two 2D situations were studied, one with an angle of attack(aoa) of 0 ° and one with an aoa of 16 °. The C-grid topology was used to generate the grid, which consist of an outer unstructered part and an inner structured part surrounding the cylinder, as seen in Figure E.5. The conditions of the

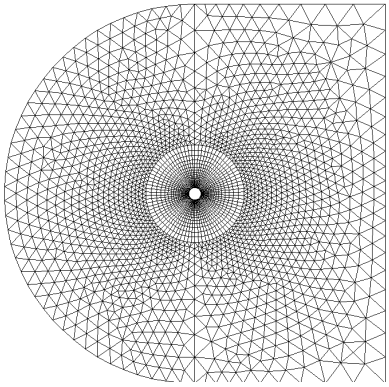

Figure E.5: Computational domain.

simulations are shown in Table F.1.

Parameter:		
Total no. cells	5013	mixed cells
BC cells*	82	no. cells
Time step size	0.01	s
Simulation time	15	min
aoa	0, 16	°
U_∞	20	m/s
T_∞	-10	°C
$\alpha_{d,\infty}$	$3.33{\cdot}10^{-7}$	−
LWC	0.3	g/m^3
MVD	10	µm

Table E.1: Test case settings. * = number of cells at boundary

In the simulation it is assumed that $\dot{m}_{\text{ice}} \approx \dot{m}_{\text{imp}} = U_\infty \text{LWC} \beta$. This implies that all mass, which hit the object will freeze and accumulate on the boundary. The assumption is close to assuming rime ice accretion. The collection efficiency (β) at t = 0 min, for the two cases are seen in Figure E.6. As expected the maximum collection is shifted to the left for the case of aoa = 16

°.

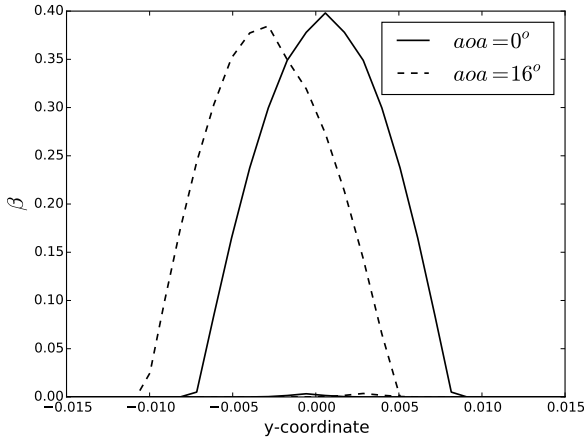

Figure E.6: Collection efficiency before ice accretion.

Figure E.7 and Figure E.8 shows the geometry change over 15 minutes of ice accretion, divided into intervals of 5 minutes. The ice growth is seen on the front of the cylinder around the stagnation point, which seems reasonable because of small MVD which results in the particles following the airflow and being deflecting around the object.

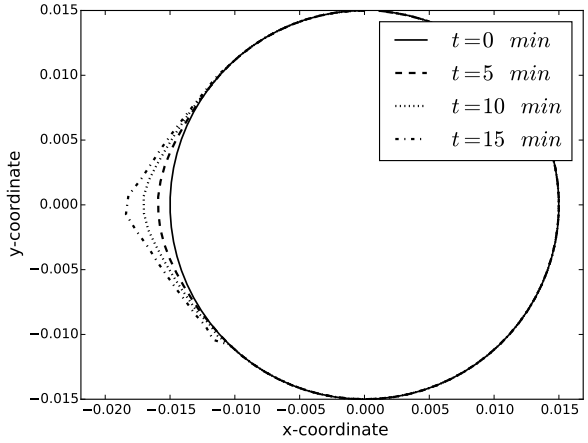

Figure E.7: Ice accretion shapes during 15 minutes of ice accretion at aoa of 0º.

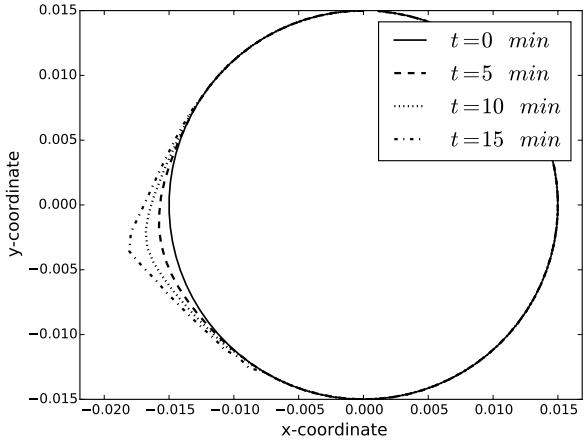

Figure E.8: Ice accretion shapes during 15 minutes of ice accretion at aoa of 16°.

E.4 Discussion and Conclusion

In this study it was found, that updating the mesh using the dynamic-mesh frame in ANSYS Fluent by applying a node displacement algorithm was feasible. A test case of 15 minutes of ice accretion was simulated successfully. To improve the mesh update a higher order discretisation scheme will be tested, such as the spline method. Furthermore, since the mesh update is fully transient it is time consuming especially for more dense mesh. Thus, for simulating longer icing events it is considered to let the model run in a so-called *quasi-steady* mode, similar to the 17 hours icing event in [24]. To improve on the ice model, a thermodynamic model will be included, which enables the study of glaze ice accretion and, for example, de-icing conditions.

E.5 Acknowledgement

Marie Cecilie Pedersen would like to thank Vattenfall R&D in Kolding and the Danish Agency for Science, Technology and Innovation for their financial support of the industrial PhD project.

References

[1] L. Makkonen, "Models for the Growth of Rime , Glaze , Icicles and Wet Snow on Structures," *Philosophical Transactions: Mathematical, Physical and Engineering Sciences*, vol. 358, no. 1776, pp. 2913–2939, 2000.

[2] T. S. S. Institute, "Athmospheric Icing on strutures, SS-ISO 12494," The Swedish Standards Institute, Tech. Rep., 2001, technical report.

[3] N. Davis, "Icing Impacts on Wind Energy Production," *PhD diss., Vestas Wind Systems A/S and The Technical University of Denmark, DTU Wind Energy*, 2014.

[4] N. Davis, A. N. Hahmann, N.-E. Clausen, and M. Žagar, "Forecast of Icing Events at a Wind Farm in Sweden," *Journal of Applied Meteorology and Climatology*, vol. 53, no. 2, pp. 262–281, 2014.

[5] D. Switchenko, W. G. Habashi, G. Baruzzi, and I. Ozcer, "FENSAP-ICE Simulation of Complex Wind Turbine Icing Events, and Comparison to Observed Performance Data," in *32nd ASME Wind Energy Symposium*, 2014.

[6] B. L. Messinger, "Equilibrium Temperature of an Unheated Icing Surface as a Function of Air Speed," *Journal of the Aeronautical Sciences (Institute of the Aeronautical Sciences)*, vol. 20, no. 1, pp. 29–42, 1953.

[7] T. Reid, G. Baruzzi, I. Ozcer, D. Switchenko, and W. Habashi, "FENSAP-ICE Simulation of Icing on Wind Turbine Blades, Part 1: Performance Degradation," in *51st AIAA Aerospace Sciences Meeting including the New Horizons Forum and Aerospace Exposition 07-10 January 2013, Grapevine (Dallas/Ft. Worth Region), Texas*, 2013.

[8] T. Reid, G. Baruzzi, I. Ozcer, D. Switchenko, and W. Habashi, "FENSAP-ICE Simulation of Icing on Wind Turbine Blades, Part 2: Ice Protection System Design," in *51st AIAA Aerospace Sciences Meeting including the New Horizons Forum and Aerospace Exposition*, 2013.

[9] H. Wickman, "Evaluation of Field Tests of Different Ice Measurement Methods for Wind Power," Uppsala University, Sweden, Tech. Rep., 2013, master Thesis.

[10] M. Wadham-Gagnon, "Wind Energy in Cold Climate," TechnoCentre éolien, Gaspe, Quebec, Canada, Tech. Rep., 2015, internal presentation at Vattenfall.

[11] F. Villalpando, M. Reggio, and A. Ilinca, "Numerical study of flow around iced wind turbine airfoil," *Engineering Applications of Computational Fluid Mechanics*, vol. 6, no. 1, pp. 39–45, 2012.

[12] X. Chi, B. Zhu, T. Shih, H. Addy, and Y. Choo, "CFD analysis of the aerodynamics of a business-jet airfoil with leading-edge ice accretion," *AIAA Paper*, vol. 560, 2004.

[13] S. Wirogo and S. Srirambhatla, "An Eulerian Method to Calculate the Collection Efficiency on Two and Three Dimensional Bodies," *AIAA paper*, vol. 1073, 2003.

[14] Y. Bourgault, Z. Boutanios, and W. G. Habashi, "Three-Dimensional Eulerian Approach to Droplet Impingement Simulation Using FENSAP-ICE, Part 1: Model, Algorithm, and Validation," *Journal of Aircraft*, vol. 37, no. 1, pp. 95–103, 2000.

[15] S. K. Kær, "Numerical Investigation of Deposit Formation in Straw-fired Boilers," *PhD diss., Aalborg University*, 2001.

[16] C. Son, S. Oh, and K. Yee, "Quantitative analysis of a two-dimensional ice accretion on airfoils," *Journal of Mechanical Science and Technology*, vol. 26, no. 4, pp. 1059–1071, 2012.

[17] Y. Cao, C. Ma, Q. Zhang, and J. Sheridan, "Numerical simulation of ice accretions on an aircraft wing," *Aerospace Science and Technology*, vol. 23, no. 1, pp. 296–304, 2012. [Online]. Available: `http://dx.doi.org/10.1016/j.ast.2011.08.004`

[18] G. Fortin, J.-L. Laforte, and A. Ilinca, "Heat and mass transfer during ice accretion on aircraft wings with an improved roughness model," *International Journal of Thermal Sciences*, vol. 45, no. 6, pp. 595–606, 2006.

[19] NTI, "User Manual FENSAP-ICE, Version 2012 release 1.1," Newmerical Technologies International, Montreal, Quebec, Canada, Tech. Rep., 2012, manual.

[20] W. Habashi, J. Dompierre, Y. Bourgault, M. Fortin, and M.-G. Vallet, "Certifiable computational fluid dynamics through mesh optimization," *AIAA journal*, vol. 36, no. 5, pp. 703–711, 1998.

[21] M. C. Pedersen and C. Yin, Preliminary modelling study of ice accretion on wind turbines, *Energy Procedia*, 2014. [Online]. Available: `http://dx.doi.org/10.1016/j.egypro.2014.11.1102`

[22] ANSYS Inc, "ANSYS Fluent Theory Guide," ANSYS, Tech. Rep. Relaese 15.0, November 2013.

[23] Ansys Inc, "ANSYS Fluent UDF Manual," ANSYS, Tech. Rep. Relaese 15.0, November 2013.

[24] C. N. Aliaga, M. S. Aubé, G. S. Baruzzi, and W. G. Habashi, "FENSAP-ICE-UNSTEADY: Unified In-Flight Icing Simulation Methodology for Aircraft, Rotorcraft, and Jet Engines," *Journal of Aircraft*, vol. 48, no. 1, pp. 119–126, 2011.

Paper F

Towards a CFD Model for Prediction of Wind Turbine Power Losses due to Icing in Cold Climate

Marie Cecilie Pedersen and Henrik Sørensen

The paper has been published in the *International Symposium on Transport Phenomena and Dynamics of Rotating Machinery (ISROMAC)*, Honolulu, Hawaii's O'ahu, USA, April 9-15, 2016.

The layout has been revised.

Towards a CFD Model for Prediction of Wind Turbine Power Losses due to Icing in Cold Climate

M. C. Pedersen [a,b] and H. Sørensen[b]

[a] *Vattenfall Vindkraft A/S, Jupitervej 6, DK-6000 Kolding, Denmark*
[b] *Aalborg University, Department of Energy Technology, Pontoppidanstræde 111, DK-9220 Aalborg, Denmark*

Abstract

Icing induced power losses is an important issue when operating wind turbines in cold climate. This paper presents a concept of modelling ice accretion on wind turbines using Computational Fluid Dynamics (CFD). The modelling concept works towards unifying the processes of modelling ice accretion and the aerodynamic analysis of the iced object into one CFD-based icing model. Modelling of icing and obtaining ice shapes in combination with mesh update by surface boundary displacement was demonstrated in the paper. It has been done by expressing in-cloud icing in CFD by an Eulerian multiphase model, implementing an icing module into the CFD solution and finally by surface boundary displacement also included in the CFD solution. The model has been developed using ANSYS Fluent and user-defined functions. The naca profile, NACA64618, has been used to illustrate the functionality of the model. Running ice accretion for different meteorological boundary conditions has illustrated the capabilities of the model and the generated ice shapes showed agreement with the literature.

Keywords: Ice accretion; Surface boundary displacement; CFD

F.1 Introduction

Wind power in cold climate has become more common especially in Nordic countries, such as Sweden, Finland, Norway and Canada. The current total installed capacity of wind power in cold climate is approximately 70 GW, which is expected to increase up to 70% towards the end of 2017 [1]. Cold climate areas are defined by experiencing temperatures below the operating limits of standard wind turbines and by the presence of icing events. Cold climate is attractive for wind energy extraction due to the low air density,

remote location and most likely sparse population. Nevertheless, producing electricity in cold climate regions is challenging due to icing related risks, such as ice being shed from the turbine blade, blade fatigue due to additional ice load and finally production losses due to icing. In remote cold climate areas the most severe risk is the production losses, which can have tremendous impact on the profitability of a wind farm.

Production losses in cold climate happens during atmospheric icing, by the impact of moisture on a surface at temperatures below 0^oC resulting in ice accretion. The interest of this work is periods where the conditions are in favour of building up, which is called meteorological icing. Ice building up during meteorological icing is referred to as *ice accretion*. Opposite, periods where the accreted ice remains on the structure is called instrumental icing [2]. Atmospheric icing can be divided into 3 main categories; in-cloud icing, freezing rain and wet snow icing. During in-cloud icing super-cooled droplets are present in a cloud or fog at cold temperatures resulting in the formation of hard rime, soft rime or glaze ice depending on the temperature [2]. In this work in-cloud icing at cold temperatures and thereby the formation of rime ice has been modelled.

Modelling of icing has been studied for power lines, within aeronautics, for structures and objects and more recently also for wind turbines. Within wind power, the aeronautic icing models such as Messinger's thermodynamic model from 1953 [3] and the panel based code LEWICE [4] have been widely used and accepted. Also the CFD code FENSAP-ICE originally developed for the aircraft industry has been applied to wind turbine applications, as seen in [5] where performance degradation and power losses were studied. Other icing models highly used within wind power are the empirical tuned cylinder based model by Makkonen [6] [2] and the panel based code TURBICE designed for de-icing applications [7]. Recent studies by [8] has managed to advancing Makkonen's cylinder based model to be more representative for a wind turbine. Common for LEWICE, TURBICE and Makkonen's cylinder based model is that the codes generate ice shapes. To study aerodynamic response of wind turbines during or after icing conditions the ice shape could be obtained of one of the latter mentioned methods followed by the use of CFD to study the aerodynamic changes. This was seen in [9] where LEWICE was used to generate icing shapes for a variation of meteorological conditions followed by a aerodynamic study using ANSYS Fluent. Thus, obtaining the ice shape was separated from the aerodynamic analysis, which was also seen in recent studies by [10]. In [11] and [12] the ice shapes were obtained from experiments followed by CFD analysis of the aerodynamic response. The objectives of this work is to develop a concept, which unifies the ice accretion process and the aerodynamic analysis into one CFD-

based ice accretion model.

F.2 Methods

The aim of the ice accretion model is to mimic an icing event in the best possible way by employing a CFD-based frame and to make the model as generic as possible. The Eulerian multiphase flow model has been used to imitate icing conditions in various CFD-based icing models. This is seen by the commercial code FENSAP-ICE, originally developed for the aircraft industry [13], which has recently been applied for wind turbine applications [14] and [5]. In other studies using ANSYS Fluent the Eulerian multiphase flow model has also been applied to imitate in-cloud icing conditions for ice accretion [15] and [16]. From the droplet solution of the Eulerian multiphase model, the variables of velocity, volume fractions, density and temperature for the phases will be available everywhere in the computational domain at any time.

The ice accretion model used in this study was inspired by Messiger's model [3], which has been applied for other CFD icing applications especially for aircraft purposes [13]. Nevertheless, the model in combination with an Eulerian multiphase flow model has also shown reasonable results and applications for wind turbines [10] and [14]. The modelling approach is structured as illustrated by Figure F.1, which consists of 3 main modules; 1) obtain multiphase flow solution, 2) ice accretion model and 3) surface boundary displacement.

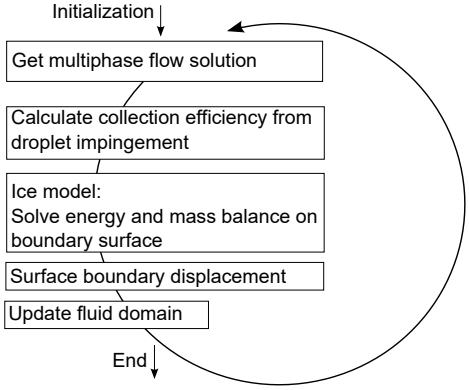

Figure F.1: Modelling structure.

The ice accretion model and the surface boundary displacement is included in the ANSYS Fluent solver by using user-defined functions. Unique for the

proposed modelling structure in Figure F.1 is that the three modules are updated every time-step adding a high accuracy to the model. Updating the multiphase flow solution after every surface boundary displacement ensures the changes in geometry to be reflected in the flow solution.

Other icing models, such as FENSAP-ICE [13] either uses an initial particle flow solution over the entire ice accretion time or uses a so-called quasi-steady approach, where the droplet solution are updated a given number of times during the ice accretion time [13]. Since the droplet solution and collection efficiency (β) will change over time, see example in Figure F.2, it is found necessary to update the Eulerian flow solution every time-step to ensure a reliable representation of the actual multiphase flow of air and particles at the given time of the ice accretion period. Figure F.2 shows the change in collection efficiency (β, Equation F.4) over time and the corresponding shape of the airfoil exposed to icing over time.

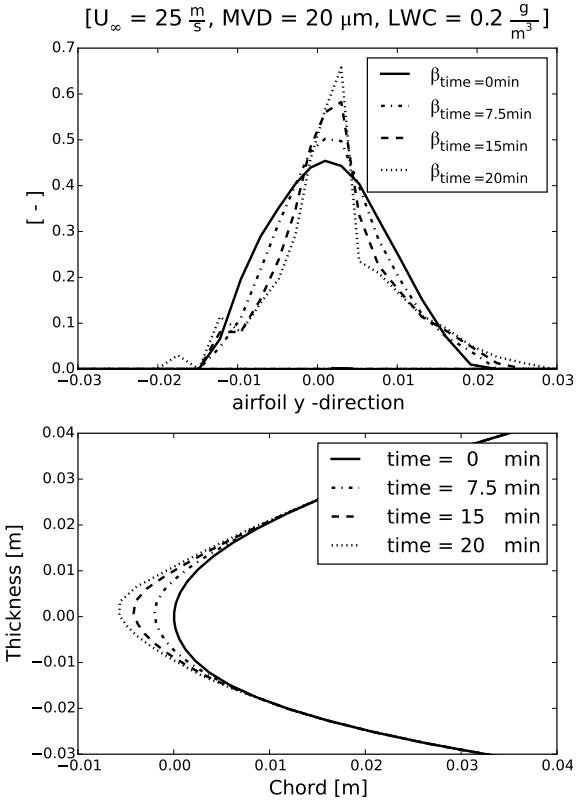

Figure F.2: Top: variation in collection efficiency (β) over 20 minutes of ice accretion. Bottom: corresponding ice shapes during 20 minutes of ice accretion.

Multiphase flow modelling The Eulerian description of a multiphase flow involves the concept of phasic volume fractions, α_q, which describes the space occupied by each phase. The laws of conservation of mass and momentum are satisfied by each phase individually [17]. The sum of all phases equals to one:

$$\sum_{q=1}^{n} \alpha_q = 1 \tag{F.1}$$

The volume fraction of each phase of the two-phase flow is solved by the continuity equation, shown here for phase q

$$\frac{\partial}{\partial t}(\alpha_q \rho_q) + \nabla \cdot (\alpha_q \rho_q \boldsymbol{v}_q) = \sum_{p=1}^{n} \left(\dot{m}_{pq} - \dot{m}_{qp}\right) + \mathrm{S}_q \tag{F.2}$$

where $\boldsymbol{v}_q$ is the velocity vector of phase q and $m_{pq,qp}$ characterize the mass transfer between the p^{th} and q^{th}phase. There is no mass exchange between the phases and no mass source are added for the phases, leaving the right hand side of Equation F.2 to zero. The solution of Equation F.2 for the secondary phase together with the conditions of Equation F.1 allows for the calculation of the primary-phase volume fraction. The conservation of momentum for the fluid phase q is given as:

$$\begin{aligned} \frac{\partial(\alpha_q \rho_q \boldsymbol{v}_q)}{\partial t} + \nabla \cdot (\alpha_q \rho_q \boldsymbol{v}_q \boldsymbol{v}_q) &= -\alpha_q \Delta \mathrm{p} \\ &+ \Delta \cdot \bar{\bar{\tau}}_q + \alpha_q \rho_q \boldsymbol{g} + \\ &+ \sum_{p=1}^{n} (K_{pq}(\boldsymbol{v}_p - \boldsymbol{v}_q)) \\ &+ (\vec{F}_q + \vec{F}_{\mathrm{lift},q} + \vec{F}_{\mathrm{wl},q} + \vec{F}_{\mathrm{td},q}) \end{aligned} \tag{F.3}$$

where $\boldsymbol{g}$ is the acceleration due to gravity, and K_{pq} is the momentum exchange coefficient between the phases, Δp, $\bar{\bar{\tau}}_q$, $\vec{F}_q$, $\vec{F}_{\mathrm{lift},q}$, $\vec{F}_{\mathrm{wl},q}$, $\vec{F}_{\mathrm{td},q}$ are the pressure gradient, stress-strain tensor, external body force, lift force, wall lubrication force and the turbulent dispersion force respectively. The energy conservation for the Eulerian multiphase model is solved by a separate enthalpy equation for each phase of the flow [17]. The k-ω SST turbulence is applied to the multiphase flow based on a preliminary study [16].

Ice accretion model For the simulation of ice accretion only rime ice has been considered. Figure F.3 illustrates the mass balance of rime ice accretion on the surface boundary of an object, where m_{imp} is the mass of droplets impinging on the object, m_{subl} is sublimation of ice mass from solid to vapor and

m_{ice} is the accumulated ice mass. It is assumed that all mass which impinge on the body will freeze instantaneously and turn into ice, see Equation F.5. In the model, the accreted ice mass becomes part of the object by applying a surface boundary displacement algorithm. Enclosing the accumulated mass of ice into the object geometry allows for studying the aerodynamic changes due to ice accretion.

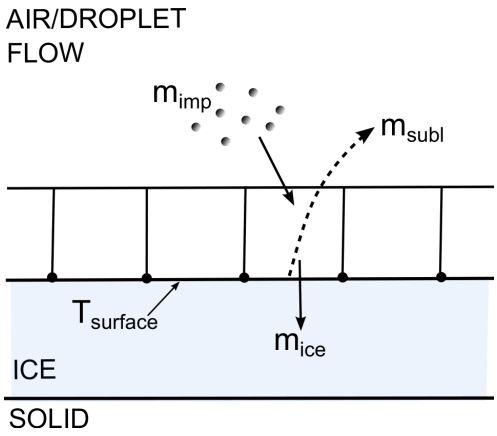

Figure F.3: Mass balance of rime ice accretion on surface boundary.

The mass of accumulated ice m_{ice}, is found instantaneously over time based on the collection efficiency (β):

$$\beta = \frac{\alpha_{\boldsymbol{n}}(\boldsymbol{u}_{\text{d}} \cdot \boldsymbol{n})}{U_\infty} \tag{F.4}$$

$$m_{\text{imp}} \approx m_{\text{ice}} = \beta U_\infty LWC \tag{F.5}$$

where α_n is the normalised droplet volume fraction $\left(\frac{\alpha_{d,\text{imp}}}{\alpha_\infty}\right)$, $\boldsymbol{u}_d$ is the droplet impact velocity, $\boldsymbol{n}$ is the unit surface normal and U_∞ is the free-stream velocity. The normalised velocity $\boldsymbol{u}_{\mathbf{n}}$ is given as $\left(\frac{\boldsymbol{u}_{\text{d}}}{u_\infty}\right)$. Thus the amount of accumulated ice mass is a function of the collection efficiency, the liquid water content in the cloud and the free-stream velocity.

Surface boundary displacement The mass of instantaneously accumulated ice (m_{ice}) initiates the surface boundary displacement. The surface boundary displacement is constructed around the Dynamic-mesh package available in ANSYS Fluent [17], from where the DEFINE_GRID_MOTION macro has been used. The macro is transient and by an iterative process the node point of the surface can be updated. This means, that the mesh will be updated at every time step. The mesh is updated by a node displacement vector $\mathbf{v}_{\text{n,i}}$:

$$\mathbf{v}_{n,i} = \frac{m_{ice}}{\rho_{ice}} \boldsymbol{n} \tag{F.6}$$

where ρ_{ice} is the density of ice. The node displacement vector gives a set of coordinates of the new location of the node. The process is obtained by a face-looping and node-looping approach as illustrated in Figure F.4.

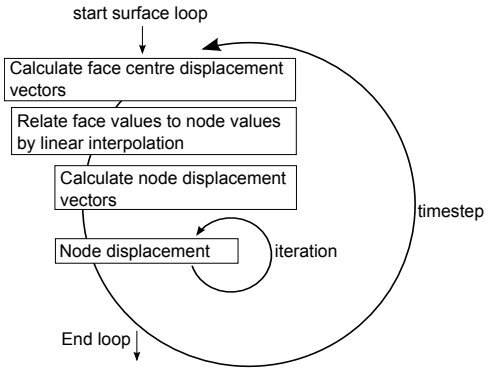

Figure F.4: Surface boundary displacement.

The instantaneously mass of ice and the boundary displacement vector is calculated at each face (f) of the surface boundary as illustrated in Figure F.5. By linear interpolation the contribution from the node neighbouring faces (f_L, f_R) to the node displacement vector at node i (n,i) is enabled. The node

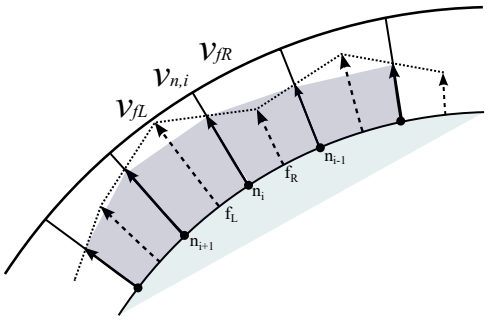

Figure F.5: Surface boundary displacement by surface displacement vectors.

positions are updated according to the following expression:

$$p_{n,i}^{t+\Delta t} = p_{n,i}^{t} + \mathbf{v}_{n,i}^{t} \Delta t \tag{F.7}$$

where $p_{n,i}$ is the current node positions, t is the current time and Δt the time step.

F.2.1 Model Setup

A set of simulations have been carried out to illustrate the capabilities of the CFD icing model. The NACA64618 profile with a sharp trailing edge has been used for the simulation in a computational domain consisting of 4050 cells, in a C-grid shape, as seen in Figure F.6. The NACA64618 profile was used, since it is part of the 5MW virtual NREL wind turbine also used for other icing studies [5] and [9]. The model inputs are presented in the following by specifying the conditions for the secondary phase (the super-cooled droplets) and for the primary phase (the airflow).

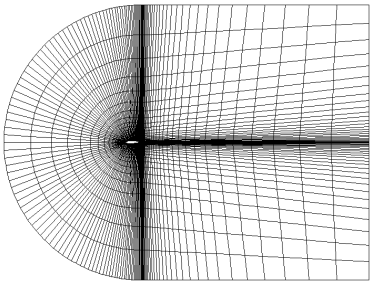

Figure F.6: Computational domain.

Secondary phase inputs From the liquid water content and density the volume fraction of the secondary phase have been specified as:

$$\alpha_{\mathrm{d}} = \frac{\mathrm{LWC}}{\rho_{\mathrm{d}}} \tag{F.8}$$

where ρ_{d} is the density of the super-cooled droplets. Simulations of ice accretion have been carried out for the different cases of secondary phase settings presented in Table F.1.

Meteorological inputs The meteorological conditions of the rime ice events are inspired by [9] and presented in Table F.2. The droplet size allows for a one-way coupling to exist between the airflow and the droplets.

Secondary phase conditions

LWC (g/m^3)	MVD (µm)	U_∞ (m/s)
0.05	6, 8, 10, 12, 14, 16, 18	13
0.10	6, 8, 10, 12, 14, 16, 18	13
0.20	6, 8, 10, 12, 14, 16, 18	13

Table F.1: Table of CFD model inputs: secondary phase.

Meteorological boundary conditions

Phases:	primary (airflow)	dispersed (droplets)	unit
U_∞	25	25	m/s
T_∞	-10	-10	^{o}C

Table F.2: Table of CFD model inputs: meteorological inputs.

Surface roughness The surface roughness is a significant parameter to include in an ice model since it determines the transition location of the airflow from laminar to turbulent over the rough surface. The sand grain roughness depends on the actual icing condition seen by the iced object. A way to take roughness into account is by employing a sand grain roughness (K_s) [7] and [18] based on empirical roughness parameters as:

$$K_s = \left(\frac{k_s^*}{k_{sb,\mathrm{LWC}}^*}\right)\left(\frac{k_s^*}{k_{sb,T_\infty}^*}\right)\left(\frac{k_s^*}{k_{sb,U_\infty}^*}\right)\left(\frac{k_s^*}{k_{sb,\mathrm{MVD}}^*}\right)k_{sb}^* c \tag{F.9}$$

where c is the cord length in meters. The empirical roughness parameters are defined as follows

$$\begin{aligned}
\left(\frac{k_s^*}{k_{sb,\mathrm{LWC}}^*}\right) &= (0.5714 + 0.2457(\mathrm{LWC}) \\
&\quad + 1.2571(\mathrm{LWC})^2) \\
\left(\frac{k_s^*}{k_{sb,T_\infty}^*}\right) &= (0.047T_\infty - 11.27) \\
\left(\frac{k_s^*}{k_{sb,U_\infty}^*}\right) &= (0.4286 + 0.0044139U_\infty) \\
\left(\frac{k_s^*}{k_{sb,\mathrm{MVD}}^*}\right) &= \left(\frac{1, \quad \mathrm{MVD} \leq 20}{1.667 - 0.0333(\mathrm{MVD}),\ \mathrm{MVD} > 20}\right) \\
k_{sB}^* &= (0.001177)
\end{aligned}$$

During ice accretion the sand-grain roughness will change affecting the transitions area and flow field at the boundary of the iced object. In [7] the time dependence of the surface roughness height is taken into account by multiplying by a factor depending on the freezing fraction (f), the fraction of particles which actually freeze at impact and the number of ice layers simulated. The freezing fraction is a number between 0-1, where 1 correspond to rime ice and $0 < f > 1$ is glaze ice conditions, [19]. For f close to or equal to 1 the sand grain roughness is multiplied with 1 as soon as a reasonable rime ice layer is obtained. Thus, since only rime ice accretion is simulated in this

study it is found reasonable to apply a constant sand-grain roughness based on Equation F.9 from time equal to zero, even though this will enhance the ice accretion at the initial stage.

F.3 Results and Discussion

The focus of this study has been on developing and testing the functionality of the presented CFD ice accretion model on the NACA64618 airfoil. The generated ice shapes have been compared to ice shapes presented in the work by Etemaddar et al. 2014 [9], where ice accretion has been simulated on the NACA64618 airfoil using the panel-based code LEWICE [4]. From [9] it was shown, that increasing LWC would increase ice accretion, especially in the direction of the chord. Likewise, increasing MVD would increase ice accretion but more severe along the thickness of the airfoil. In this study, ice accretion has been simulated for 20 minutes with a time-step size of 0.01 second for all cases of secondary phase settings presented in Table F.1 with the meteorological boundary conditions given in Table F.2. Furthermore a constant density of ice of 650 kg/m^3 has been used an angle of attack of 0 ^{o}. The generated ice shapes is seen for the cases of LWC of 0.05 g/m^3, 0.10 g/m^3 and 0.15 g/m^3 in Figure F.7 for cases with LWC of 0.20 g/m^3 and 0.25 g/m^3 in Figure F.8. Figure F.7 and F.8 illustrate how the total amount of ice accretion increased with an increasing LWC. Furthermore, the figures illustrates that increasing MVD will result in more ice accretion, which was most severe for the high numbers of LWC. This can be seen in Figure F.8. The results from the simulations was in agreement with the conclusions regarding LWC and MVD found in [9] and [20].

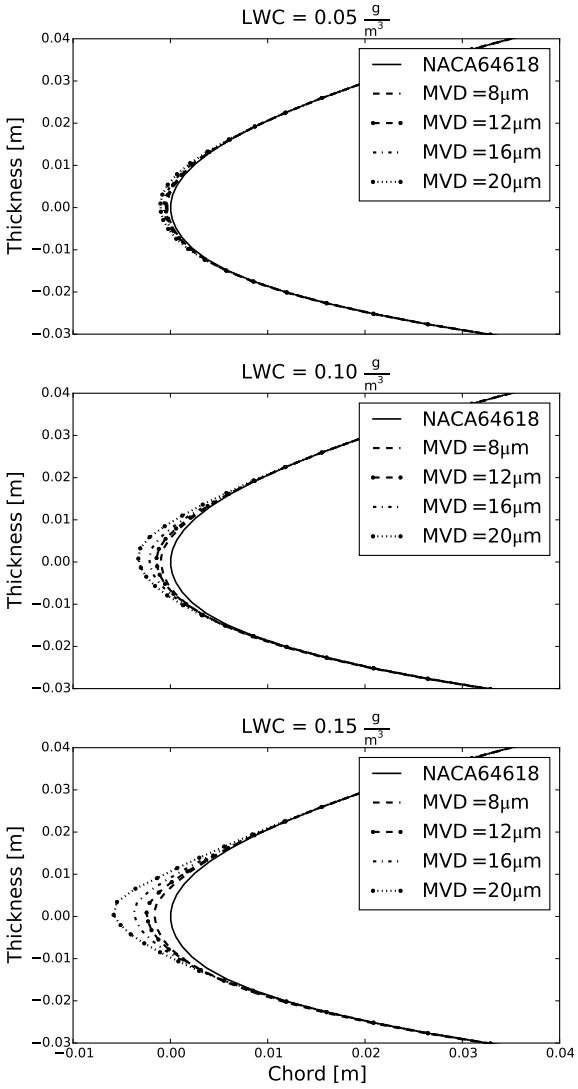

Figure F.7: Generated ice shapes after 20 minutes of ice accretion using surface boundary displacement for U_∞ = 25 m/s, T_∞ = -10 ºC and LWC of 0.05 g/m^3, 0.10 g/m^3 and 0.15 g/m^3.

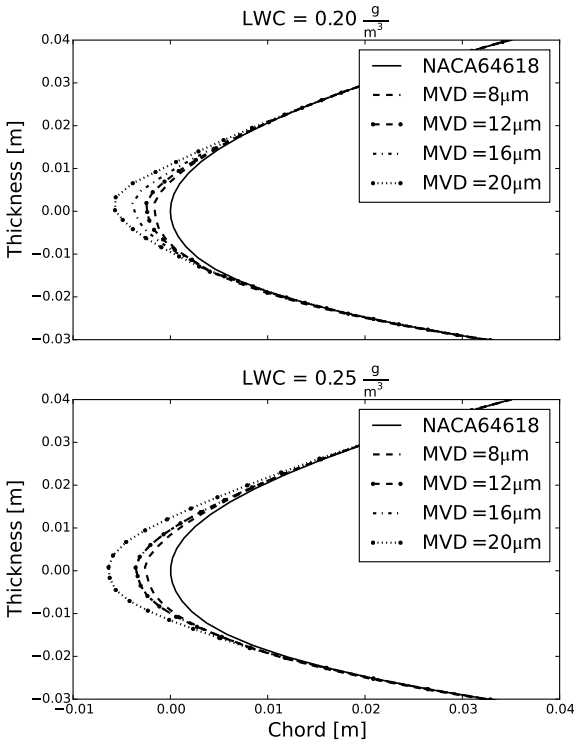

Figure F.8: Generated ice shapes after 20 minutes of ice accretion using surface boundary displacement for U_∞ = 25 m/s, T_∞ = -10 °C and LWC of 0.20 g/m^3 and 0.25 g/m^3.

F.3.1 Conclusions

From the study a promising concept towards a complete CFD model for prediction of wind turbine power losses due to icing in cold climate was established. The study has illustrated that it was possible to unify the ice accretion process with the aerodynamic analysis in one CFD ice accretion model. The concept has demonstrated the ability to model rime ice accretion and perform surface boundary displacement per time step for an icing period of 20 minutes. Furthermore, the simulated ice accretion cases showed agreement with the literature and the model was able to include the influence of droplet variation and variation in of the liquid water content. Future work is to extend the icing time and include varying meteorological input conditions and finally to compare the model with site-measurements or data from a climatic wind tunnel, as seen by [21]. Furthermore, changes in lift and draft forces for a variation of angle of attacks should be studied.

F.4 Acknowledgement

Marie Cecilie Pedersen would like to thank Vattenfall Vindkraft A/S for hosting and partly granting the Industrial PhD program and the Innovation Fund Denmark from the Danish Ministry of Higher education and Science for partly granting the program.

References

[1] Timo Wallenius. Special Theme: Cold Climate Turbines("CCTs"). *BTM World Market Update, BTM-Consult*, pages 29–42, 2013.

[2] iso. Athmospheric Icing on strutures, ISO 12494:2001(E). Technical report, ISO, Geneva, Switzerland, 2001.

[3] Bernard L Messinger. Equilibrium Temperature of an Unheated Icing Surface as a Function of Air Speed. *Journal of the Aeronautical Sciences (Institute of the Aeronautical Sciences)*, 20(1):29–42, 1953.

[4] William Wright. User's Manual for LEWICE Version 3.2. Technical report, NASA, National Aeronautics and Space Administration, Glenn Research Center, Cleveland, Ohio, USA, 2008.

[5] Thomas Reid, Guido Baruzzi, Isik Ozcer, David Switchenko, and Wagdi Habashi. FENSAP-ICE Simulation of Icing on Wind Turbine Blades, Part 1: Performance Degradation. In *51st AIAA Aerospace Sciences Meeting including the New Horizons Forum and Aerospace Exposition 07-10 January 2013, Grapevine (Dallas Ft. Worth Region), Texas*, 2013.

[6] Lasse Makkonen. Models for the Growth of Rime, Glaze, Icicles and Wet Snow on Structures. *Philosophical Transactions: Mathematical, Physical and Engineering Sciences*, 358(1776):2913–2939, 2000.

[7] Lasse Makkonen, Timo Laakso, Mauri Marjaniemi, and Karen Finstad. Modelling and prevention of ice accretion on wind turbines. *Wind Engineering*, 25(1):3–21, 2001.

[8] Neil Davis. Icing Impacts on Wind Energy Production. *PhD diss., Vestas Wind Systems A/S and The Technical University of Denmark, DTU Wind Energy*, 2014.

[9] M. Etemaddar, M. O. L. Hansen, and T. Moan. Wind turbine aerodynamic response under atmospheric icing conditions. *Wind Energy*, 17(2):241–265, 2014.

[10] M Ali and N Sankar Lakshmi. In-Cloud Ice Accretion Modeling on Wind Turbine Blades Using Extended Messinger Model. In *13th International Energy Conversion Engineering Conference*, 2015.

[11] Fernando Villalpando, Marcelo Reggio, and Adrian Ilinca. Numerical study of flow around iced wind turbine airfoil. *Engineering Applications of Computational Fluid Mechanics*, 6(1):39–45, 2012.

[12] X Chi, Bin Zhu, T.I.P Shih, H.E. Addy, and Y.K. Choo. CFD analysis of the aerodynamics of a business-jet airfoil with leading-edge ice accretion. *AIAA Paper*, 560, 2004.

[13] NTI. User Manual FENSAP-ICE, Version 2012 release 1.1. Technical report, Newmerical Technologies International, Montreal, Quebec, Canada, 2012. Manual.

[14] David Switchenko, Wagdi G. Habashi, Guido Baruzzi, and Isik Ozcer. FENSAP-ICE Simulation of Complex Wind Turbine Icing Events, and Comparison to Observed Performance Data. In *32nd ASME Wind Energy Symposium*, 2014.

[15] Sutikno Wirogo and Shashidhar Srirambhatla. An Eulerian Method to Calculate the Collection Efficiency on Two and Three Dimensional Bodies. *AIAA paper*, 1073, 2003.

[16] Mare Cecilie Pedersen and Chungen Yin. Preliminary modelling study of ice accretion on wind turbines. *Energy Procedia*, 2014.

[17] ANSYS Inc. ANSYS Fluent Theory Guide. Technical Report Relaese 15.0, ANSYS, November 2013.

[18] Jaiwon Shin and Brian Berkowitz. Prediction of ice shapes and their effect on airfoil drag. *Journal of aircraft*, 31(2):263–270, 1994.

[19] Lorenzo Battisti. *Wind Turbines in Cold Climate*. Springer, Springer International Publishing Switzerland 2015, 1 edition, 2015.

[20] Matthew C Homola, Muhammad S Virk, Tomas Wallenius, Per J Nicklasson, and Per A Sundsbø. Effect of atmospheric temperature and droplet size variation on ice accretion of wind turbine blades. *Journal of wind engineering and industrial aerodynamics*, 98(12):724–729, 2010.

[21] Peter M Blasco, Jose Palacios, and Sven Schmitz. Investigation of Wind Turbine Power Generation During Atmospheric Icing by Multi-Disciplinary Experimentation. In *33rd Wind Energy Symposium*, 2015.

ISSN (online): 2446-1636
ISBN (online): 978-87-7210-218-4

AALBORG UNIVERSITY PRESS